



**A
F
F
T
C**

**An Investigation Relating Longitudinal
Pilot-induced Oscillation Tendency Ratings to
Describing Function Predictions for Rate-limited Actuators
(Project MAX GAP)**

**Joel B. Witte, Maj, USAF
Project Manager / Project Test Pilot**

**Svend E. Monsen, Capt, RNoAF
Project Test Pilot**

**Thomas A. Washington, Capt, USAF
Project Test Pilot**

**Karl K. Cowart, Capt, USAF
Project Flight Test Engineer**

**Richard M. Salasovich, Capt, USAF
Project Flight Test Engineer**

DECEMBER 2003

FINAL TECHNICAL INFORMATION MEMORANDUM

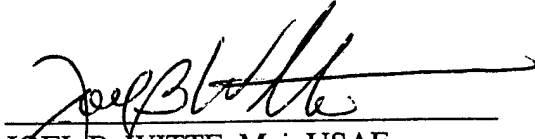
20040317 181

Approved for public release; distribution is unlimited.

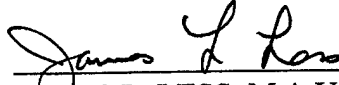
**AIR FORCE FLIGHT TEST CENTER
EDWARDS AIR FORCE BASE, CALIFORNIA
AIR FORCE MATERIEL COMMAND
UNITED STATES AIR FORCE**

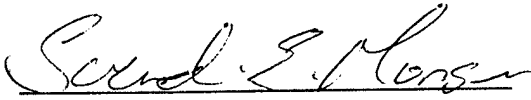
This Technical Information Memorandum (AFFTC-TIM-03-08, *An Investigation Relating Longitudinal Pilot-induced Oscillation Tendency Ratings to Describing Function Predictions for Rate-limited Actuators (Project MAX GAP)*) was prepared and submitted under Job Order Number: M03C1300 by the Commandant, US Air Force Test Pilot School (USAF TPS), Edwards Air Force Base, CA 93524-6485.

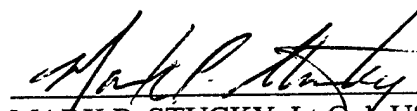
Prepared by:

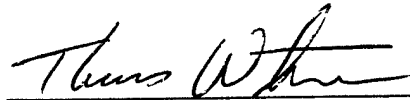

JOEL B. WITTE, Maj, USAF
Project Manager/Project Test Pilot

Reviewed by:

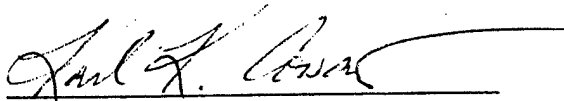

JAMES L. LESS, Maj, USAF
Staff Monitor



SVEND E. MONSEN, Capt, RNoAF
Project Test Pilot



MARK P. STUCKY, Lt Col, USAF
Chief, Test Management


THOMAS A. WASHINGTON, Capt, USAF
Project Test Pilot

Approved by:


KARL K. COWART, Capt, USAF
Project Flight Test Engineer


ERNIE H. HAENDSCHKE, Col, USAF
Commandant, USAF Test Pilots School


RICHARD M. SALASOVICH, Capt, USAF
Project Flight Test Engineer

REPORT DOCUMENTATION PAGE*Form Approved*
OMB No. 0704-0188

Public reporting burden for this collection of information is estimated to average 1 hour per response, including the time for reviewing instructions, searching existing data sources, gathering and maintaining the data needed, and completing and reviewing this collection of information. Send comments regarding this burden estimate or any other aspect of this collection of information, including suggestions for reducing this burden to Department of Defense, Washington Headquarters Services, Directorate for Information Operations and Reports (0704-0188), 1215 Jefferson Davis Highway, Suite 1204, Arlington, VA 22202-4302. Respondents should be aware that notwithstanding any other provision of law, no person shall be subject to any penalty for failing to comply with a collection of information if it does not display a currently valid OMB control number. **PLEASE DO NOT RETURN YOUR FORM TO THE ABOVE ADDRESS.**

1. REPORT DATE (DD-MM-YYYY)

12-12-2003

2. REPORT TYPE

Final Technical Information Memorandum

3. DATES COVERED (From - To)

16 to 22 Oct 2003

4. TITLE AND SUBTITLE

An Investigation Relating Longitudinal Pilot-induced Oscillation
Tendency Ratings to Describing Function Predictions for Rate-limited
Actuators (Project MAX GAP)

5a. CONTRACT NUMBER**5b. GRANT NUMBER****5c. PROGRAM ELEMENT NUMBER****6. AUTHOR(S)**

Witte, Joel, Maj, USAF
Monsen, Svend, Capt, RNoAF
Washington, Thomas, Capt, USAF
Cowart, Kris, Capt, USAF
Salasovich, Rich Capt, USAF

5d. PROJECT NUMBER**5e. TASK NUMBER****5f. WORK UNIT NUMBER****7. PERFORMING ORGANIZATION NAME(S) AND ADDRESS(ES)**

Air Force Flight Test Center
412th Test Wing
USAF Test Pilot School
220 South Wolfe Ave
Edwards AFB CA 93524-6485

8. PERFORMING ORGANIZATION REPORT NUMBER

AFFTC-TIM-03-08

9. SPONSORING / MONITORING AGENCY NAME(S) AND ADDRESS(ES)

Dr. Brad Liebst
AFIT/ENY
Bldg 640 2950 P St
Wright-Patterson AFB OH 45433-7521

10. SPONSOR/MONITOR'S ACRONYM(S)**11. SPONSOR/MONITOR'S REPORT NUMBER(S)****12. DISTRIBUTION / AVAILABILITY STATEMENT**

Approved for public release; distribution is unlimited.

13. SUPPLEMENTARY NOTES

CA: Air Force Flight Test Center Edwards AFB CA

CC: 012100

14. ABSTRACT

This report presents the results of Project MAX GAP, a method of predicting pilot-induced oscillations (PIO) caused by actuator rate limiting. The overall test objective was to correlate, if possible, Pilot-induced Oscillation Tendency Ratings with a new preflight calculation called the *Gap Criterion*. The Air Force Institute of Technology, Engineering Department (AFIT/ENY) requested this testing. The USAF Test Pilot School (TPS), Class 03A, conducted 8 flight tests totaling 10.8 hours at Edwards AFB, California, from 16 to 22 October 2003.

15. SUBJECT TERMS

handling qualities (PIO) pilot-induced oscillation PIO prediction rate limiting flight controls

16. SECURITY CLASSIFICATION OF:**a. REPORT**
UNCLASSIFIED**b. ABSTRACT**
UNCLASSIFIED**c. THIS PAGE**
UNCLASSIFIED**17. LIMITATION OF ABSTRACT**SAME AS
REPORT**18. NUMBER OF PAGES**

133

19a. NAME OF RESPONSIBLE PERSON

Dr. Brad Liebst

19b. TELEPHONE NUMBER (include area code)

(937) 255-3636 ext: 4636

THIS PAGE INTENTIONALLY LEFT BLANK

PREFACE

This technical report presents the evaluation procedures, concepts, and results from the MAX GAP test project. The United States Air Force Test Pilot School (USAF TPS) MAX GAP Test Team conducted tests at Wright Patterson Air Force Base, Ohio and the Air Force Flight Test Center, Edwards Air Force Base, California. Both the USAF TPS and the Air Force Institute of Technology (AFIT) sponsored this project.

The MAX GAP Test Team would like to thank Mr. Curt Clark and Mr. Jeff Slutz of AFRL/VACD who worked diligently to ensure our success in the LAMARS simulator. We would also like to thank Mr. Andy Markofski and Mr. Mike Steen of Veridian Flight Research for their outstanding contributions. Additionally, we would like to thank the entire NF-16D VISTA maintenance team for their dedication to ensuring our program success.

THIS PAGE INTENTIONALLY LEFT BLANK

EXECUTIVE SUMMARY

This Technical Report presents the results of the flight test of the MAX GAP project. The objectives of the project were to correlate, if possible, Pilot-induced Oscillation Tendency Ratings with a new preflight calculation called the *Gap Criterion* and to collect and analyze historical simulator and flight test data as well as to compile new simulator and flight test data to augment this database.

The responsible Test Organization was the 412th Test Wing. The MAX GAP Test Team, members of the United States Air Force Test Pilot School (USAF TPS) Class 03A, accomplished all test and evaluation sorties.

Pilot-induced Oscillations (PIO) are an unwanted pilot plus aircraft oscillation. There are many causes for this unwanted motion, one of which is actuator rate limiting. Actuator rate limiting is a non-linear phenomenon caused by the pilot and/or flight control system (FCS) demanding more actuator performance than the actuator can produce. The result is a reduction in magnitude of the output and a phase shift between the pilot/FCS input and the actuator output. This interaction can drive the system toward a limit cycle of PIO.

The *Gap Criterion* is a preflight calculation based on a linear representation of the bare airframe aircraft dynamics and a Neal-Smith pilot model and a non-linear representation of a simple rate-limited actuator model. This simple non-linear model can be represented by a describing function. Using these tools, a new criterion called the *Gap Criterion* can be computed which may relate to PIO tendency rating.

The MAX GAP Test Team applied the *Gap Criterion* to historical simulator and flight test data and to data gathered during this project. The Large Amplitude Multimode Aerospace Simulator (LAMARS) at Wright-Patterson AFB, OH and the NF-16D Variable In-flight Simulator Test Aircraft (VISTA) operated by the USAF Test Pilot School at Edwards AFB, CA were used to collect this data.

Overall results confirmed a correlation between *Gap Criterion* and PIO Tendency Rating. All four Phase 2 Handling Qualities unaltered datasets and five out of seven Phase 3 datasets showed correlation with at least 95% confidence.

THIS PAGE INTENTIONALLY LEFT BLANK

TABLE OF CONTENTS

<u>Description</u>	<u>Page</u>
REPORT DOCUMENTATION PAGE.....	iii
Preface.....	v
Executive Summary	vii
Table of Contents	ix
List of Illustrations	xi
List of Tables	xvii
Introduction.....	1
Background.....	1
Program Chronology.....	2
Test Item Description.....	2
Test Objectives.....	3
Overall Objective	3
Specific Test Objectives	3
Test and Evaluation.....	5
Historical data	5
Historical data procedures.....	5
Historical data results.....	5
Simulator data	6
Simulator procedures	6
Simulator Results	7
Flight data	9
Flight test procedures.....	9
Flight test results	9
Conclusions and Recommendations	13
References.....	15
Appendix A: Derivation of the <i>Gap Criterion</i>	17
Appendix B: Data Analysis	37
Appendix C: PIO Rating Scales.....	41

TABLE OF CONTENTS (CONCLUDED)

<u>Description</u>	<u>Page</u>
Appendix D: Test Point Configurations	43
Appendix E: Tracking Tasks	47
Appendix F: Historical Data Figures	49
Appendix G: LAMARS Data Figures.....	55
Appendix H: VISTA Data Figures	63
Appendix I: LAMARS Simulator Histograms	73
Appendix J: VISTA Flight Histograms	93
Appendix K: Lessons Learned.....	113
List of Acronyms	115
Distribution	117

LIST OF ILLUSTRATIONS

<u>Description</u>	<u>Page</u>
Figure 1. Example of Elevator Rate limiting	1
Figure A1. F-15E PIO Sequence (Reference 6).....	17
Figure A2. Example of a Nonlinear System	18
Figure A3. Saturation Nonlinearity and the Corresponding Input-output Relationship	20
Figure A4 Actuator Model Development	21
Figure A5. Closed Loop Actuator Transfer Function Diagram	23
Figure A6. Rate limiting Input and Output.....	25
Figure A7. Describing Function Phase Angle Comparison.....	29
Figure A8. Pitch Tracking Closed Loop System	29
Figure A9. Simplified Pitch Tracking Closed Loop System	30
Figure A10. Resulting Cases.....	32
Figure A11. Nichols Chart of the Example Problem.....	35
Figure C1: Pilot-Induced Oscillation (PIO) Rating Scales	41
Figure C2: PIO Tendency Classification Scale	42
Figure E1 Example Heads Up Display	47
Figure E2: Sum-of-sines Pitch Tracking Task.....	47
Figure E3: MIL-HDBK-1797 Pitch Tracking Task.....	48
Figure F1A: HAVE PREVENT Phase 2 Sum-of-Sines Task LAMARS Data (2D).....	50
Figure F1B: HAVE PREVENT Phase 2 Sum-of-Sines Task LAMARS Data (3D)	50
Figure F2A: HAVE PREVENT Phase 3 Discrete HUD Tracking Task LAMARS Data (2D)	51
Figure F2B: HAVE PREVENT Phase 3 Discrete HUD Tracking Task LAMARS Data (3D)	51
Figure F3A: HAVE PREVENT Phase 3 Target Task LAMARS Data (2D)	52

Figure F3B: HAVE PREVENT Phase 3 Target Task LAMARS Data (3D).....	52
Figure F4A: HAVE OLOP Phase 2 Sum-of-Sines Task Flight Data (2D).....	53
Figure F4B: HAVE OLOP Phase 2 Sum-of-Sines Task Flight Data (3D).....	53
Figure F5A: HAVE OLOP Phase 3 Discrete HUD Tracking Task Flight Data (2D)	54
Figure F5B: HAVE OLOP Phase 3 Discrete HUD Tracking Task Flight Data (3D)	54
Figure G1A: MAX GAP Phase 2 Sum-of-Sines Task LAMARS Data (2D)	56
Figure G2B: MAX GAP Phase 2 Sum-of-Sines Task LAMARS Data (3D)	56
Figure G2A: MAX GAP Phase 3 HUD Discrete Tracking Task LAMARS Data (2D).....	57
Figure G2B: MAX GAP Phase 3 HUD Discrete Tracking Task LAMARS Data (3D).....	57
Figure G3A: MAX GAP Phase 3 Target Tracking Task LAMARS Data (2D)	58
Figure G3B: MAX GAP Phase 3 HUD Target Tracking Task LAMARS Data (3D).....	58
Figure G4: Phase 2 Sum-of-Sines, PIOR: 5	59
Figure G5: Phase 2 Sum-of-Sines, PIOR: 1.....	60
Figure G6A: MAX GAP Phase 2 Sum-of-Sines Tracking Task LAMARS Data Reduced (2D)	61
Figure G6B: MAX GAP Phase 2 Sum-of-Sines Tracking Task LAMARS Data Reduced (3D)	61
Figure G7A: MAX GAP Phase 3 Discrete Tracking Task LAMARS Data Reduced (2D) ...	62
Figure G7B: MAX GAP Phase 3 Discrete Tracking Task LAMARS Data Reduced (3D) ...	62
Figure H1A: MAX GAP Phase 2 Sum-of-Sines Task Flight Data (2D)	64
Figure H1B: MAX GAP Phase 2 Sum-of-Sines Task Flight Data (3D)	64
Figure H2A: MAX GAP Phase 3 Discrete HUD Tracking Task Flight Data (2D).....	65
Figure H2B: MAX GAP Phase 3 Discrete HUD Tracking Task Flight Data (3D).....	65
Figure H3A: MAX GAP Phase 3 Target Task Flight Data (2D).....	66
Figure H3B: MAX GAP Phase 3 Target Task Flight Data (3D).....	66
Figure H4: Phase 2 Sum-of-Sines, PIOR: 5.....	67

Figure H5: Phase 2 Sum-of-Sines, PIOR: 1.....	68
Figure H6A: MAX GAP Phase 2 Sum-of-Sines Task Flight Data Reduced (2D)	69
Figure H6B: MAX GAP Phase 2 Sum-of-Sines Task Flight Data Reduced (3D)	69
Figure H7A: MAX GAP Phase 3 Discrete HUD Tracking Task Flight Data Reduced (2D). 70	
Figure H7B: MAX GAP Phase 3 Discrete HUD Tracking Task Flight Data Reduced (3D). 70	
Figure H8A: MAX GAP Phase 3 Target Task Flight Data Reduced (2D).....	71
Figure H8B: MAX GAP Phase 3 Target Task Flight Data Reduced (3D).....	71
Figure I1 LAMARS Data, Case B, 15 deg/sec	74
Figure I2 LAMARS Data, Case B, 30 deg/sec	74
Figure I3 LAMARS Data, Case B, 60 deg/sec	75
Figure I4 LAMARS Data, Case N, 15 deg/sec	75
Figure I5 LAMARS Data, Case N, 30 deg/sec	76
Figure I6 LAMARS Data, Case N, 60 deg/sec	76
Figure I7 LAMARS Data, Case W, 15 deg/sec	77
Figure I8 LAMARS Data, Case W, 30 deg/sec	77
Figure I9 LAMARS Data, Case W, 60 deg/sec	78
Figure I10 LAMARS Data, Case Y, 15 deg/sec	78
Figure I11 LAMARS Data, Case Y, 30 deg/sec	79
Figure I12 LAMARS Data, Case Y, 60 deg/sec	79
Figure I13 LAMARS Data, Case B, 15 deg/sec	80
Figure I14 LAMARS Data, Case B, 30 deg/sec	80
Figure I15 LAMARS Data, Case B, 60 deg/sec	81
Figure I16 LAMARS Data, Case N, 15 deg/sec	81
Figure I17 LAMARS Data, Case N, 30 deg/sec	82
Figure I18 LAMARS Data, Case N, 60 deg/sec	82

Figure I19 LAMARS Data, Case W, 15 deg/sec	83
Figure I20 LAMARS Data, Case W, 30 deg/sec	83
Figure I21 LAMARS Data, Case W, 60 deg/sec	84
Figure I22 LAMARS Data, Case Y, 15 deg/sec	84
Figure I23 LAMARS Data, Case Y, 30 deg/sec	85
Figure I24 LAMARS Data, Case Y, 60 deg/sec	85
Figure I25 LAMARS Data, Case B, 15 deg/sec	86
Figure I26 LAMARS Data, Case B, 30 deg/sec	86
Figure I27 LAMARS Data, Case B, 60 deg/sec	87
Figure I28 LAMARS Data, Case N, 15 deg/sec	87
Figure I29 LAMARS Data, Case N, 30 deg/sec	88
Figure I30 LAMARS Data, Case N, 60 deg/sec	88
Figure I31 LAMARS Data, Case W, 15 deg/sec	89
Figure I32 LAMARS Data, Case W, 30 deg/sec	89
Figure I33 LAMARS Data, Case W, 60 deg/sec	90
Figure I34 LAMARS Data, Case Y, 15 deg/sec	90
Figure I35 LAMARS Data, Case Y, 30 deg/sec	91
Figure I36 LAMARS Data, Case Y, 60 deg/sec	91
Figure J1 Flight Test Data, Case B, 15 deg/sec	94
Figure J2 Flight Test Data, Case B, 30 deg/sec	94
Figure J3 Flight Test Data, Case B, 60 deg/sec	95
Figure J4 Flight Test Data, Case N, 15 deg/sec	95
Figure J5 Flight Test Data, Case N, 30 deg/sec	96
Figure J6 Flight Test Data, Case N, 60 deg/sec	96
Figure J7 Flight Test Data, Case W, 15 deg/sec	97

Figure J8 Flight Test Data, Case W, 30 deg/sec	97
Figure J9 Flight Test Data, Case W, 60 deg/sec	98
Figure J10 Flight Test Data, Case Y, 15 deg/sec	98
Figure J11 Flight Test Data, Case Y, 30 deg/sec	99
Figure J12 Flight Test Data, Case Y, 60 deg/sec	99
Figure J13 Flight Test Data, Case B, 15 deg/sec	100
Figure J14 Flight Test Data, Case B, 30 deg/sec	100
Figure J15 Flight Test Data, Case B, 30 deg/sec	101
Figure J16 Flight Test Data, Case N, 15 deg/sec	101
Figure J17 Flight Test Data, Case N, 30 deg/sec	102
Figure J18 Flight test Data, Case N, 60 deg/sec	102
Figure J19 Flight Test Data, Case W, 15 deg/sec	103
Figure J20 Flight Test Data, Case W, 30 deg/sec	103
Figure J21 Flight Test Data, Case W, 60 deg/sec	104
Figure J22 Flight Test Data, Case Y, 15 deg/sec	104
Figure J23 Flight Test Data, Case Y, 30 deg/sec	105
Figure J24 Flight Test Data, Case Y, 60 deg/sec	105
Figure J25 Flight Test Data, Case B, 15 deg/sec	106
Figure J26 Flight Test Data, Case B, 30 deg/sec	106
Figure J27 Flight Test Data, Case B, 60 deg/sec	107
Figure J28 Flight Test Data, Case N, 15 deg/sec	107
Figure J29 Flight Test Data, Case N, 30 deg/sec	108
Figure J30 Flight Test Data, Case N, 60 deg/sec	108
Figure J31 Flight Test Data, Case W, 15 deg/sec	109
Figure J32 Flight Test Data, Case W, 30 deg/sec	109

Figure J33 Flight Test Data, Case W, 60 deg/sec	110
Figure J34 Flight Test Data, Case Y, 15 deg/sec	110
Figure J35 Flight Test Data, Case Y, 30 deg/sec	111
Figure J36 Flight Test Data, Case Y, 60 deg/sec	111

LIST OF TABLES

<u>Description</u>	<u>Page</u>
Table 1: Evaluation Criteria.....	5
Table 2: Summary of Historical data results.....	6
Table 3: Summary of LAMARS results	7
Table 4: Summary of Recalculated LAMARS Simulation Results.....	8
Table 5: Summary of flight test results.....	9
Table 6: Summary of Recalculated Flight Test Results.....	11
Table A1: Neal-Smith Pilot Models	31
Table B1: MAX GAP Test Data.....	37
Table D1: HAVE PREVENT Bare Airframe Test Cases	43
Table D2: HAVE PREVENT Test Case <i>Gap Criterion</i> Values.....	43
Table D3: HAVE OLOP Bare Airframe Test Cases	44
Table D4: HAVE OLOP Test Case <i>Gap Criterion</i> Values	44
Table D5: MAX GAP LAMARS Bare Airframe Test Cases	44
Table D6: MAX GAP LAMARS Test Case <i>Gap Criterion</i> Values.....	45
Table D7: MAX GAP VISTA Bare Airframe Test Cases	45
Table D8: MAX GAP VISTA Test Case <i>Gap Criterion</i> Values.....	45
Table D9: Test Configuration Matrix	46

THIS PAGE INTENTIONALLY LEFT BLANK

INTRODUCTION

A newly developed metric called the *Gap Criterion* was compared to Pilot-induced Oscillation (PIO) tendency ratings to determine if any correlation exists. The United States Air Force Test Pilot School (USAF TPS) Class 03A MAX GAP Test Team analyzed historical simulator and flight test data from Projects HAVE OLOP (Reference 1) and HAVE PREVENT (Reference 2). The test team gathered additional simulator data using the Large Amplitude Multimode Aerospace Research Simulator (LAMARS) located at Wright-Patterson AFB, OH. Flight test data were collected using the NF-16D Variable In-flight Simulator Test Aircraft (VISTA) at the Air Force Flight Test Center (AFFTC), Edwards AFB, CA.

Background

Pilot-induced Oscillations are an unwanted pilot plus aircraft oscillation. There are many causes for this unwanted motion, one of which is actuator rate limiting. Actuator rate limiting is a non-linear phenomenon caused by the pilot and/or flight control system (FCS) demanding more actuator performance than the actuator can produce. The result is a reduction in magnitude of the output and a phase lag between the pilot/FCS input and the actuator output. This interaction can drive the system toward a limit cycle. These effects are shown by the triangular elevator response depicted in Figure 1.

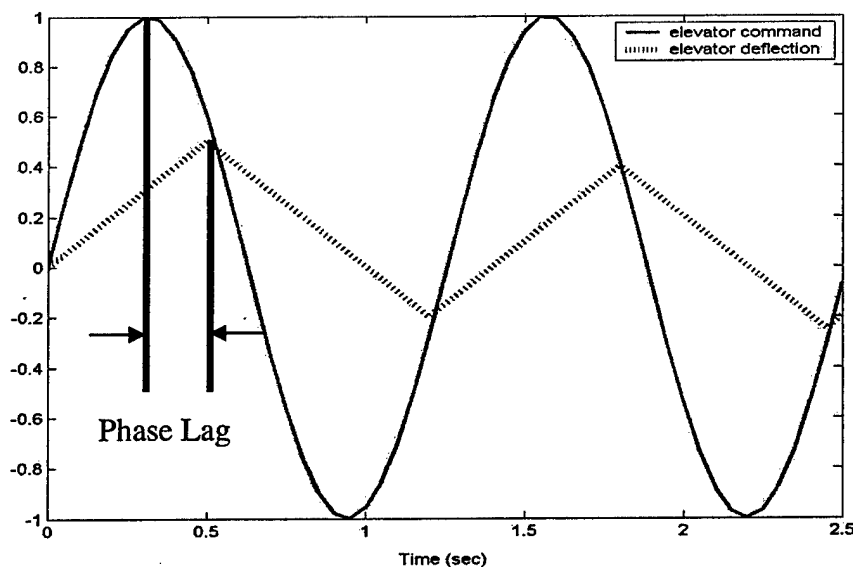


Figure 1. Example of Elevator Rate limiting

The *Gap Criterion* is a preflight calculation based on a linear representation of the augmented and bare airframe aircraft dynamics and a Neal-Smith pilot model, MIL-HDBK-1797 (Reference 3) and a non-linear representation of a simple rate-limited actuator model.

This simple model can be represented by a describing function. For a limit cycle to exist, the magnitude and phase of the frequency response of the combined linear dynamics must equal the negative inverse of the magnitude and phase of the describing function in at least one intersection. Most sets of stable aircraft dynamics convolved with their optimum Neal-Smith pilot model do not ordinarily intersect with the describing function. Therefore, the pilot gain is artificially inflated to cause the intersection. At this intersection, the amplitude and frequency of the PIO input can be determined. The *Gap Criterion* is the product of the inflated gain and the input amplitude normalized by the maximum available actuator deflection. A detailed derivation of the *Gap Criterion* is shown in Appendix A.

The PIO Tendency Classification scale of MIL-HDBK-1797 (Reference 3) shown in Figure C1 of Appendix C was used in this test. This decision tree was augmented with the additional MIL-HDBK-1797 descriptors shown in Appendix C.

This project performed a PIO investigation for various combinations of bare airframe dynamics and actuator rate limits. This investigation was divided into three parts: Phase 1, 2, and 3. The Phase 1 investigation consisted of open loop and gentle tracking maneuvers to evaluate low (pilot) gain, low-bandwidth handling qualities. Some example maneuvers included doublets, step inputs, and pitch angle captures. Phase 2 testing is an evaluation of high gain, high bandwidth handling qualities. It uses a specialized technique, called Handling Qualities During Tracking (HQDT), requiring the pilot to, "track a precision aim point on a target as aggressively and assiduously as possible, always striving to correct even the smallest tracking errors as rapidly as possible." (Reference 4) HQDT is the most reliable method of determining PIO susceptibility. A Sum-of-sines HUD tracking task was used for Phase 2. During Phase 3 testing, the test pilot performed an operational evaluation of the aircraft's PIO susceptibility. For this project, the Phase 3 evaluation alternated between a discrete pitch-tracking task with the HUD symbology shown in Figure 3 and an aircraft target tracking task.

PROGRAM CHRONOLOGY

The MAX GAP Test Team began with applying the *Gap Criterion* to historical simulator and flight test data from similar PIO studies HAVE PREVENT (DEC 2002) and HAVE OLOP (DEC 2000). Next, the test team gathered PIO tendency rating data using the Large Amplitude Multimode Aerospace Simulator (LAMARS), Wright-Patterson AFB, OH on 21-22 August 2003. Following the LAMARS testing, flight tests were conducted in the NF-16D Variable In-flight Simulator Test Aircraft (VISTA) at the Air Force Flight Test Center (AFFTC) at Edwards AFB, CA from 17-22 October 2003. In total, one calibration sortie, eight test sorties and five target sorties were executed, totaling 17.7 hours.

TEST ITEM DESCRIPTION

The test item evaluated was the *Gap Criterion* and its possible correlation to PIO tendency ratings. The maximum elevator deflection rates selected were 15, 30 and 60 deg/sec. A cross-section of bare airframe short period natural frequencies and damping ratios

using these maximum elevator deflection rates were selected to determine a range of *Gap Criteria*. Subsequently, four bare airframe test cases with different short period properties were selected which yielded a distributed range of *Gap Criteria*. For specific details on the derivation of the *Gap Criterion* and rate limit/airframe dynamics combinations see Appendices A and D.

TEST OBJECTIVES

Overall Objective

To determine if there is a correlation between computed *Gap Criterion* values and the resultant PIO Tendency Rating assigned to the combination of bare airframe dynamics and maximum elevator deflection rates.

Specific Test Objectives

To achieve the overall test objective, a three phase program was developed with each phase having specific objectives:

Test Objective 1: Determine the correlation between PIO tendency rating and *Gap Criterion* using historical PIO data.

Test Objective 2: Determine the correlation between PIO tendency rating and *Gap Criterion* using the LAMARS simulator.

Test Objective 3: Determine the correlation between PIO tendency rating and *Gap Criterion* using the NF-16 VISTA.

All specific test objectives were met.

THIS PAGE INTENTIONALLY LEFT BLANK

TEST AND EVALUATION

The objective of this program was to evaluate a new criterion for predicting PIO Tendency Rating for rate-limited actuators. This criterion was called the *Gap Criterion* and was based on describing function techniques. The project compared assigned PIO tendency ratings for various combinations of bare aircraft dynamics and actuator rate limits. These combinations are described in detail in Appendix D. The evaluation criteria used in this test to determine quality of the correlation are shown in Table 1

Table 1: Evaluation Criteria

Confidence Level	Rating
< 80%	UNSATISFACTORY
80% - 95%	MARGINAL
> 95%	SATISFACTORY

Historical data

The first objective was to determine the correlation between PIO tendency rating and *Gap Criterion* using historical PIO data

Historical data procedures

The *Gap Criterion* was computed based on the selected bare airframe dynamics of Projects HAVE PREVENT and HAVE OLOP (see Appendix D). These values were matched with the assigned PIO tendency ratings. The correlation coefficient between the assigned PIO tendency rating and the computed *Gap Criterion* was determined as described in Appendix B.

Historical data results

The recorded PIO tendency ratings for each task were plotted against the corresponding *Gap Criterion* value (Appendix F). A linear curve fit was applied to the data to determine the correlation coefficient. This correlation coefficient was compared to the minimum correlation coefficient needed to indicate if a relationship between the assigned PIO tendency ratings and the *Gap Criterion* existed. Both 80% and 95% confidence level minimum correlation coefficients were computed based on dataset size. For purposes of this evaluation, an actual correlation coefficient greater than the 95% confidence minimum correlation coefficient was considered satisfactory, greater than the 80% confidence minimum correlation coefficient was considered marginal and less than 80% confidence was unsatisfactory. Table 2 shows a summary of these historical results.

Table 2: Summary of Historical data results

	TASK	Sample Size	r_{\min}		r_{actual}	Correlation	Evaluation
			80%	95%			
Project Have Prevent	Phase 2 Sum of Sines	30	0.241	0.361	0.585	YES	SATISFACTORY
	Phase 3 Discrete	19	0.308	0.456	0.596	YES	SATISFACTORY
	Phase 3 Target Tracking	12	0.398	0.576	0.394	MINOR	UNSATISFACTORY
Project HAVE OLOP	Phase 2 Sum of Sines	72	0.153	0.232	0.477	YES	SATISFACTORY
	Phase 3 Discrete	77	0.148	0.224	0.460	YES	SATISFACTORY
The values for r_{\min} represent the minimum required value of the correlation coefficient for the stated level of confidence							

The results listed in Table 2 demonstrate that four out of five historical datasets indicate a correlation exists between *Gap Criterion* and PIO Tendency Rating with at least 95% confidence. The r_{actual} result from the Phase 3 Target Tracking data of Project Have Prevent equates to a 79.5% confidence level that a correlation exists, just barely missing a marginal rating.

Simulator data

The second objective was to determine the correlation between PIO tendency rating and *Gap Criterion* using the LAMARS.

Simulator procedures

PIO tendency ratings for each combination of bare airframe dynamics/FCS and actuator rate limit listed in Appendix D were collected using a sum-of-sines HUD pitch-tracking task during Phase 2 evaluation and either a discrete HUD pitch-tracking task or an aircraft target-tracking task during Phase 3 evaluations. These tasks were performed in the LAMARS ground simulator. The simulated conditions were 15,000 ft pressure altitude and 300 KIAS. The test points were randomly ordered and the test pilot was unaware of the configuration being flown. Graphical descriptions of the sum-of-sines and discrete HUD pitch-tracking task are shown in Appendix E. The gain of the pitch angle MIL-HDBK-1797 pitch tracking task was increased 250% to increase pilot workload and bandwidth. The aircraft target-tracking task consisted of a simulated aircraft at constant speed, 3g turn with preprogrammed reversals. Several gross acquisition captures were conducted during the duration of the task to determine PIO tendency rating. Differing PIO tendency ratings were expected due to differing pilot opinion. What was not expected or desired was variability in ratings from the same test pilot, on the same test case, performing the same task. Prior to the LAMARS sorties, in an effort to reduce this type of variability, the test pilots "calibrated" themselves using a fixed-base simulator located at the USAF Test Pilot School conducting Phase 1 and Phase 2 evaluations on known good and bad aircraft configurations. This

calibration proved useful in identifying the indications of PIO and increasing proficiency in the use of PIO tendency rating scales. See Appendix K for lessons learned.

Simulator Results

The recorded PIO tendency ratings for each task were plotted against the corresponding *Gap Criterion* values. A correlation coefficient was computed (Appendix B) to determine if a correlation exists between the two values. Table 3 shows a summary of the LAMARS simulation results.

Table 3: Summary of LAMARS results

TASK	Sample Size	r_{\min}		r_{actual}	Correlation	Evaluation
		80%	95%			
Phase 2 Sum of Sines	66	0.160	0.242	0.337	YES	SATISFACTORY
Phase 3 Discrete	49	0.186	0.281	0.327	YES	SATISFACTORY
Phase 3 Target Tracking	44	0.197	0.297	0.469	YES	SATISFACTORY

The values for r_{\min} represent the minimum required value of the correlation coefficient for the stated level of confidence

From the results in Table 3 it can be stated, with 95% confidence that a correlation exists between PIO tendency rating and the corresponding *Gap Criterion* values. This evaluation was true for all three tasks evaluated.

Figures in Appendix G show the PIO tendency rating vs. *Gap Criterion* raw data for each task completed in the LAMARS. There were numerous instances where identical PIO tendency ratings were given for a specific *Gap Criterion* value. Looking specifically at Figure G1, which shows the LAMARS data for a Phase 2 Sum-of-Sines task, there are several data points that support the *Gap Criterion* theory. The first example is a data point with a small *Gap Criterion* value. For this data point during Phase 2 evaluations there were five instances where test pilots assigned a PIO tendency rating of 5. Looking at the associated stripcharts (Figure G4), in all cases the aircraft response was out of phase with pilot's inputs and rate limiting was present. The second example is a data point with a large *Gap Criterion* value. The PIO tendency ratings assigned for this *Gap Criterion* varied from 1-6. There were two occurrences where a PIO tendency rating of 1 was assigned along with one 2, 4, 5 and 6. Looking at the associated stripcharts (Figure G5), rate limiting was present in this example, but the aircraft and pilot were still in phase. The evaluation pilot found the handling qualities of the simulated aircraft favorable and assigned a PIO tendency rating of 1. The occurrences of PIO tendency ratings of 4, 5, and 6 given for this example were unexpected and did not match theory. Further investigation of these unexpected ratings found that rate limiting was present for all three evaluations, but the pilot and the aircraft were still in phase. These unexpected findings led to the issue of data quality.

Data quality of points where LAMARS results did not fall in line with the predicted *Gap Criterion* theory were questioned. Specifically, for low *Gap Criterion* values where

PIO was predicted, there were instances where favorable PIO tendency ratings (1-3) were given when rate limiting occurred and the aircraft response was 180 degrees out of phase with the inputs of the pilot (classic PIO). Also, there were examples when non-favorable PIO tendency ratings (4-6) were assigned for high *Gap Criterion* values where no rate limiting occurred and no PIO was predicted. It was concluded that the occurrences of favorable PIO ratings given when "classic" PIO was present were the result of the pilot failing to interpret PIO cues correctly. It was also concluded that non-favorable PIO ratings given without the presence of rate limiting were attributable to some other phenomenon other than rate limiting. The Gap Criterion was not extended to include analysis of non rate limited PIO. Therefore from this analysis the data were screened and points were removed according to the following criteria:

- (1) Cases employing a 15 deg/sec rate limit where rate limiting was present and the aircraft response was approximately 180 degrees out of phase with the pilot's inputs and a favorable PIO tendency rating was assigned; and
- (2) Cases employing a 60 deg/sec rate limit where the aircraft and pilot were in or out phase, but no rate limiting occurred and a non-favorable PIO tendency rating was assigned.

Data were not eliminated from the 30 deg/sec rate limit cases because of ambiguities in determining the cause of a possible PIO from aircraft dynamics or rate limiting.

New correlation factors were calculated once the data were screened and are shown in Table 4. In total, six data points were removed from the Phase 2 Sum-of-Sines task and two samples were removed from the Phase 3 Discrete HUD tracking task. As a result of the data screening the minimum correlation coefficient values for 80% and 95% confidence increased due to the reduction in sample size but, the computed correlation coefficients for the linear models also increased resulting in better correlation. Figures in Appendix G also include the screened LAMARS data sets.

Table 4: Summary of Recalculated LAMARS Simulation Results

Task	Sample Size	$r_{80\%}$	$r_{90\%}$	$r_{95\%}$	Required	Conclusion
Phase 2 Sum of Sines	60	0.168	0.254	0.581	YES	SATISFACTORY
Phase 3 Discrete	47	0.190	0.288	0.501	YES	SATISFACTORY
Phase 3 Target Tracking	44	0.197	0.297	0.469	YES	SATISFACTORY

The values for r_{min} represent the minimum required value of the correlation coefficient for the stated level of confidence

It is evident that a correlation exists between assigned PIO tendency ratings and the associated *Gap Criteria*. This program did not take the next step to determine the amount of

correlation between these two values. **Conduct further evaluations to determine the level of correlation between PIO tendency ratings and *Gap Criterion* values. (R1)¹**

Flight data

The final objective was to determine the correlation between PIO tendency rating and *Gap Criterion* using the NF-16 VISTA.

Flight test procedures

PIO tendency ratings for each combination of bare airframe dynamics and actuator rate limit listed in Appendix D were evaluated using a sum-of-sines tracking task during Phase 2 evaluation and either a discrete tracking task or target tracking evaluation during Phase 3 evaluation. These tasks were performed in the NF-16D VISTA. The test conditions were 15,000 ft pressure altitude and 300 KIAS. The test points of were randomly ordered and the test pilot was unaware of the configuration being flown. Phase 1, 2 and 3 evaluations were conducted on each test point. Graphical descriptions of the sum-of-sines and discrete HUD pitch-tracking task are shown in Appendix E. The gain of the pitch angle MIL-HDBK-1797 pitch tracking task was increased 150% to increase pilot workload and bandwidth. The aircraft target-tracking task was conducted using a T-38 target aircraft. VISTA flew approximately 2,000 ft in trail of the target and, on command, the target aircraft began a 3g constant airspeed turn. Altitude was used to maintain g and airspeed constant. The VISTA evaluation pilot delayed and then attempted a gross acquisition capture of the target. Multiple capture attempts per test point were used to determine PIO tendency rating.

Flight test results

The recorded PIO tendency ratings for each task were plotted against the corresponding *Gap Criterion* values. A correlation coefficient was computed (Appendix B) to determine if a correlation exists between the two values. Table 5 shows a summary of the LAMARS simulation results.

Table 5: Summary of flight test results

Task	Sample Size	r_{min}	$r_{0.95}$	$r_{0.99}$	Correlation	Result
Phase 2 Sum-of-sines	81	0.144	0.219	0.301	YES	SATISFACTORY
Phase 3 Discrete	48	0.188	0.284	0.327	YES	SATISFACTORY
Phase 3 Target Tracking	27	0.255	0.331	0.008	NO	UNSATISFACTORY

The values for r_{min} represent the minimum required value of the correlation coefficient for the stated level of confidence

¹ Numerals preceded by an R within parentheses at the end of a paragraph correspond to the recommendation numbers tabulated in the Conclusions and Recommendations section of this report.

From Table 5 it can be stated, with 95% confidence that a correlation exists between PIO tendency rating and the corresponding *Gap Criterion* values. This evaluation was true for both the Phase 2 and Phase 3 Discrete tracking task. The Phase 3 target tracking task showed no correlation.

Figures in Appendix H show the PIO tendency rating vs. *Gap Criterion* raw data for each task completed in the VISTA. As with the LAMARS data, there were numerous instances where identical PIO tendency ratings were given for a specific *Gap Criterion* value. Looking specifically at Figure H1A and H1B, which show the VISTA data for a Phase 2 sum-of-sines task, there are several data points that support the *Gap Criterion* theory. The first example of such is a data point with a small *Gap Criterion* value. For this data point during Phase 2 evaluations there were eight instances where test pilots assigned a PIO tendency rating of 4 or 5. Looking at the associated stripcharts for one of these instances, (Figure H4) the aircraft's response was clearly out of phase with pilot's inputs with rate limiting present. The second example is a data point with a large *Gap Criterion* value. The six PIO tendency ratings assigned for this *Gap Criterion* varied from 1-3. Looking at the associated stripcharts for one instance, (Figure H5) rate limiting was not present, but there was a slight amount of phase lag. Even with a little phase lag, the evaluation pilot found the handling qualities of the simulated aircraft favorable.

As with the LAMARS data, VISTA flight tests generated some data points which did not fall in line with the predicted theory. As a result the data were screened and points were removed according to the same criteria:

- (1) Cases employing a 15 deg/sec rate limit where rate limiting was present and the aircraft response was approximately 180 degrees out of phase with the pilot's inputs and a favorable PIO tendency rating was assigned; and
- (2) Cases employing a 60 deg/sec rate limit where the aircraft and pilot were in or out phase, but no rate limiting occurred and a non-favorable PIO tendency rating was assigned.

Data were not eliminated from the 30 deg/sec rate limit cases because of ambiguities in determining the cause of a possible PIO from aircraft dynamics or rate limiting.

New correlation factors were calculated once the data were screened and are shown in Table 6. In total, ten data points were removed from the Phase 2 Sum-of-Sines task, two samples were removed from the Phase 3 Discrete HUD tracking task and one data point was removed from the Phase 3 Target tracking task. As a result of the data screening, the minimum correlation coefficient values for 80% and 95% confidence increased due to the reduction in sample size, but the computed correlation coefficients for the linear models also increased resulting in better correlation. Figures in Appendix H also show the screened VISTA data sets.

Table 6: Summary of Recalculated Flight Test Results

TASK	Sample Size	r_{min}		r_{actual}	Correlation	Evaluation
		80%	95%			
Phase 2 Sum of Sines	71	0.154	0.233	0.400	YES	SATISFACTORY
Phase 3 Discrete	46	0.193	0.291	0.3308	YES	SATISFACTORY
Phase 3 Target Tracking	26	0.260	0.388	0.0945	NO	UNSATISFACTORY

The values for r_{min} represent the minimum required value of the correlation coefficient for the stated level of confidence

In all cases of flight test, the Phase 3 Target Tracking task yielded the worst results in terms of correlation. This poor performance was attributed to two major factors: (1) The low steady state turn rate and lower than expected maximum load factor or "g" of the VISTA at the test conditions (15,000 ft MSL, 300 KCAS) and (2) the repeatability of the tracking task. Depending on how long the test pilot delayed before attempting the gross acquisition determined the aircraft response. If the delay was short, the VISTA was still "ramping-up" in turn rate and g when the capture was attempted. This capture usually required a high-gain input to stop the turn rate at the desired level. If the delay was too long, the VISTA reached a steady state turn rate and g which made the capture task extremely predictable and only required the pilot to make low-gain inputs to achieve the desired rates. In retrospect, the target tracking task procedure was poorly defined and the conditions chosen were not selected to elicit the desired, high-gain pilot response. See Appendix K for lessons learned.

THIS PAGE INTENTIONALLY LEFT BLANK

CONCLUSIONS AND RECOMMENDATIONS

A new metric called the *Gap Criterion* was developed and compared to Pilot-induced Oscillation (PIO) tendency ratings. The objective of this program was to evaluate the utility of the new criterion for predicting PIO Tendency Rating for rate-limited actuators. *Gap Criterion* values were compared to assigned PIO tendency ratings from four sets of aircraft dynamics at three different elevator rate limits using historical data, the Large Amplitude Multimode Aerospace Simulator (LAMARS) and the NF-16D Variable In-flight Simulator Test Aircraft (VISTA).

The results of historical data, LAMARS data and VISTA flight data positively demonstrated that there was a correlation between the *Gap Criterion* and assigned PIO tendency rating. In general, small *Gap Criterion* values corresponded to large or poor PIO tendency ratings and vice versa. This program established that there was a correlation but did not explore the significance of the correlation.

R1 Conduct further evaluations to determine the level of correlation between PIO tendency ratings and *Gap Criterion* values. (Page 9)

THIS PAGE INTENTIONALLY LEFT BLANK

REFERENCES

1. Gilbreath, Greg. and others. A Limited Evaluation of a Pilot-Induced Oscillation Prediction Criterion (HAVE OLOP). AFFTC, Edwards AFB, CA, December 2000.
2. Hanley, James and others. Comparison of Nonlinear Algorithms in the Prevention of Pilot-Induced Oscillation Caused by Actuator Rate Limiting (Project HAVE PREVENT). AFFTC, Edwards AFB, CA, December 2002.
3. Department of Defense. Military Standard, Flying Qualities of Piloted Aircraft. MIL-HDBK-1797, 19 December 1997.
4. Flying Qualities Testing, Air Force Flight Test Center, Edwards Air Force Base, 20 February 2002
5. NF-16D 86-0048 Partial Flight Manual (VISTA), Secretary of the Air Force, WL/FIIA, Wright-Patterson AFB, OH, January, 1998.
6. Klyde, David H. and others, *Unified Pilot-Induced Oscillation Theory, Volume 1: PIO Analysis with Linear and Nonlinear Effective Vehicle Characteristics, Including Rate Limiting*, WL-TR-96-3028, Air Force Research Laboratories, Wright-Patterson AFB, Ohio, December 1995.
7. Slotine, Jean-Jacques and Li, Weiping, *Applied Nonlinear Control*, Prentice Hall, Upper Saddle River, New Jersey, 1991.
8. Mitchell, David G. and Klyde, David H., *A Critical Examination of PIO Prediction Criteria*, AIAA-98-4335, American Institute of Aeronautics and Astronautics, 1998.
9. Gilbreath, Greg., *Prediction of Pilot-Induced Oscillations (PIO) Due to Actuator Rate Limiting Using the Open-Loop Onset Point (OLOP) Criterion*, MS Thesis, AFIT/GAE/ENY/01M-02, School of Aeronautical Engineering, Air Force Institute of Technology (AU), Wright-Patterson AFB, OH, March 2002.
10. Doman, David B. and Foringer, Lori Ann, *Interactive Flying Qualities Toolbox for Matlab*, USAF Wright Laboratory, Flight Dynamics Directorate, Flight Control Division, Flying Qualities Section, Wright- Patterson AFB, Ohio, August 1996.
11. Wheeler, Anthony J., *Introduction to Engineering Experimentation*, Prentice Hall, Upper Saddle River, New Jersey, 1996.

THIS PAGE INTENTIONALLY LEFT BLANK

APPENDIX A: DERIVATION OF THE *GAP CRITERION*

Theory

This appendix will discuss describing functions and how they can be used to understand and predict PIO onset when considered in the context of rate-limited actuators. Further, the Neal-Smith pilot model will be explained followed by an example integrating all of these concepts. The basis of the *Gap Criterion* will then be covered.

Describing Function Development

Observing the time history of an F-15E PIO from Figure A-1, it can be seen that the pilot input is approximately sinusoidal. This is true in general of all PIO incidents (Reference 6). The describing function technique can be used for limit cycle analysis due to the fact that the form of the signals in a limit-cycling system, such as a PIO, is usually approximately sinusoidal (Reference 7).

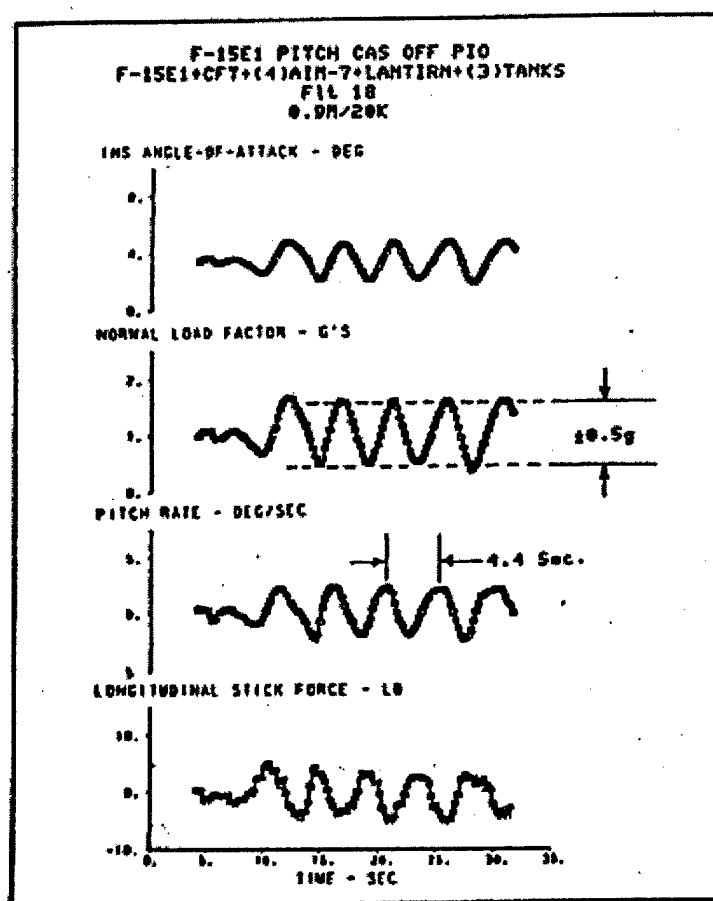


Figure A1. F-15E PIO Sequence (Reference 6)

Any system, which can be rearranged into the form shown in Figure A-2, can be studied using describing functions (Reference 7). Examples of nonlinear elements include dead-zones, hysteresis or saturations. Saturations are the focus of this study.

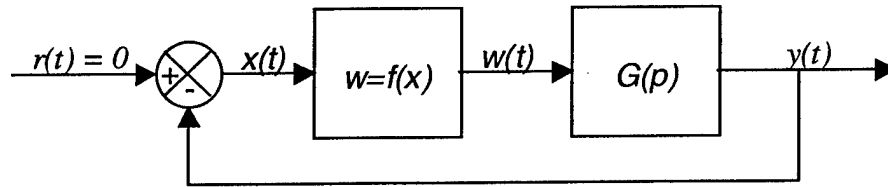


Figure A2. Example of a Nonlinear System

For the basic version of the describing function method, the system has to satisfy the following four conditions (Reference 7):

- 1) There is only a single nonlinear component
- 2) The nonlinear component is time-invariant
- 3) Corresponding to a sinusoidal input $x = A \sin(\omega t)$, only the fundamental component $w_1(t)$ in the output $w(t)$ has to be considered
- 4) The nonlinearity is odd

Consider a sinusoidal input into the nonlinear element of the system shown in Figure 2-1 of the form $x(t) = A \sin(\omega t)$. Due to nonlinear effects, the output $w(t)$ is often a periodic though non-sinusoidal function. The output function $w(t)$ can be expanded using Fourier series as seen in Eqn 1 and the derivation which follows (Reference 7):

$$w(t) = \frac{a_0}{2} + \sum_{n=1}^{\infty} [a_n \cos(n\omega t) + b_n \sin(n\omega t)] \quad (A1)$$

where:

$$a_0 = \frac{1}{\pi} \int_{-\pi}^{\pi} w(t) d(\omega t) \quad (A2)$$

$$a_n = \frac{1}{\pi} \int_{-\pi}^{\pi} w(t) \cos(n\omega t) d(\omega t) \quad (A3)$$

$$b_n = \frac{1}{\pi} \int_{-\pi}^{\pi} w(t) \sin(n\omega t) d(\omega t) \quad (A4)$$

Applying condition four from above, $a_0 = 0$ for all odd functions. Further, applying the third assumption means discarding all other terms except $n = 1$ (Reference 7). This leaves:

$$w(t) \approx w_1(t) = a_1 \cos(\omega t) + b_1 \sin(\omega t) \quad (A5)$$

which can be rewritten as:

$$w_1(t) = M \sin(\omega t + \phi) \quad (A6)$$

Where

$$M = \sqrt{a_1^2 + b_1^2} \quad (A7)$$

$$\phi = \tan^{-1} \left(\frac{a_1}{b_1} \right) \quad (A8)$$

Rewritten in complex notation leads to:

$$w_1(t) = M e^{j(\omega t + \phi)} = (b_1 + ja_1) e^{j(\omega t)} \quad (A9)$$

Finally, the describing function, $N(A, \omega)$, is defined to be the complex ratio of the fundamental component of the nonlinear element to the input sinusoid. This is shown in Eqn 9:

$$N(A, \omega) = \frac{M e^{j(ax+\phi)}}{A e^{j(ax)}} = \frac{M}{A} e^{j\phi} = \frac{1}{A} (b_1 + ja_1) \quad (A10)$$

Now consider the saturation input-output relationship shown in Figure A-3 below:

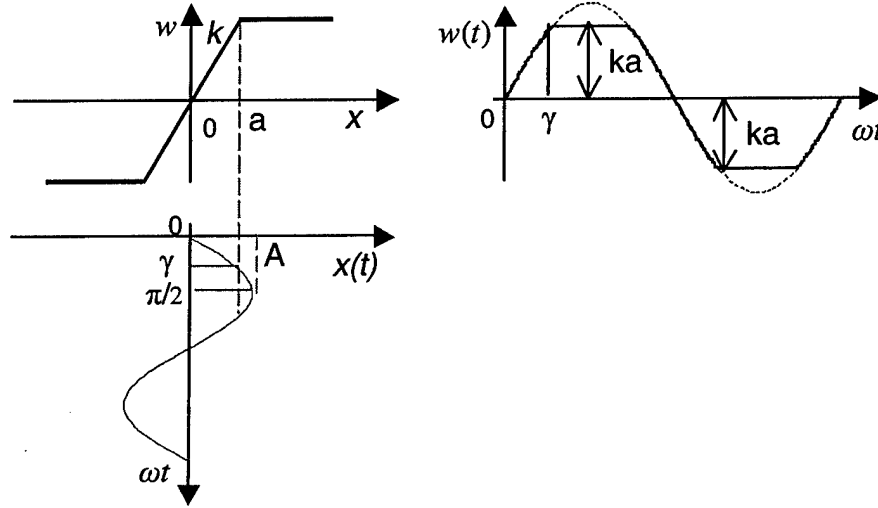


Figure A3. Saturation Nonlinearity and the Corresponding Input-output Relationship

From the figure, it is apparent that if our input, $x(t) = A \sin(\omega t)$, has a maximum amplitude $A \leq a$ then the input remains in the linear range and the output is just $w(t) = kA \sin(\omega t)$. But if the maximum amplitude, A , is greater than a , clipping occurs and the value of $w(t)$ can be split up into two sets over the first quarter of the symmetric output:

$$w(t) = \begin{cases} kA \sin(\omega t) & 0 \leq \omega t \leq \gamma \\ ka & \gamma < \omega t \leq \pi/2 \end{cases}$$

where $\gamma = \sin^{-1}(a/A)$

The output $w(t)$ is an odd function, implying $a_1 = 0$ in Eqn 5. Further, dividing the output into four quarters yields a new equation for b_1 :

$$b_1 = \frac{4}{\pi} \int_0^{\pi/2} w(t) \sin(\omega t) d(\omega t) \quad (A11)$$

$$b_1 = \frac{4}{\pi} \int_0^{\gamma} kA \sin^2(\omega t) d(\omega t) + \frac{4}{\pi} \int_{\gamma}^{\pi/2} ka \sin(\omega t) d(\omega t) \quad (A12)$$

$$b_1 = \frac{2ka}{\pi} \left[\gamma + \frac{a}{A} \sqrt{1 - \frac{a^2}{A^2}} \right] \quad (A13)$$

Substituting $a_1 = 0$ and Eqn 13 into Eqn 10 leaves:

$$N(A, \omega) = \frac{b_1}{A} = \frac{2k}{\pi} \left[\gamma + \frac{a}{A} \sqrt{1 - \frac{a^2}{A^2}} \right] = \frac{2k}{\pi} \left[\sin^{-1} \left(\frac{a}{A} \right) + \frac{a}{A} \sqrt{1 - \frac{a^2}{A^2}} \right] \quad (A14)$$

Sinusoidal Input Describing Function Approximation

Now, consider the block diagram in Figure A-4 of a first order actuator system and the derivations which follow (Reference 6).

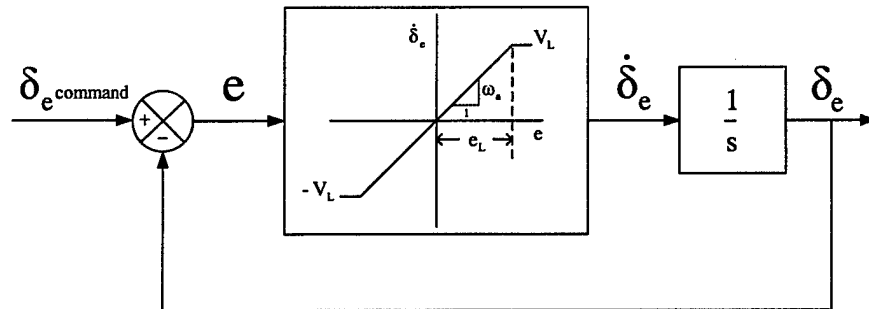


Figure A4 Actuator Model Development

The nonlinear portion of this model is exactly the same as the saturation nonlinearity discussed previously. Substituting the appropriate new nomenclature and letting $e(t) = E \sin(\omega t + \varphi)$ replace $x(t)$, leads to the following describing function for the nonlinear element:

$$N(A, \omega) = \frac{2\omega_a}{\pi} \left[\sin^{-1} \left(\frac{e_L}{E} \right) + \frac{e_L}{E} \sqrt{1 - \frac{e_L^2}{E^2}} \right] \quad (\text{A15})$$

Further, by using series expansions for both the arcsine term and the square root the describing function can be approximated by:

$$N(A, \omega) = \frac{2\omega_a}{\pi} \left[\left(\frac{e_L}{E} + \frac{1}{6} \left(\frac{e_L}{E} \right)^3 + \dots \right) + \frac{e_L}{E} \left(1 - \frac{1}{2} \frac{e_L^2}{E^2} - \dots \right) \right] \quad (\text{A16})$$

Keeping only the first order linear terms yields:

$$N(A, \omega) = \frac{2\omega_a}{\pi} \left[\frac{e_L}{E} + \frac{e_L}{E} \right] = \frac{4\omega_a}{\pi} \frac{e_L}{E} \quad (\text{A17})$$

Substituting $V_L = \omega_a e_L$ leads to:

$$N(A, \omega) = \frac{4}{\pi} \frac{V_L}{E} \quad (\text{A18})$$

Next, consider the revised block diagram shown in Figure A-5 and determine the closed loop transfer function, treating N as a constant.

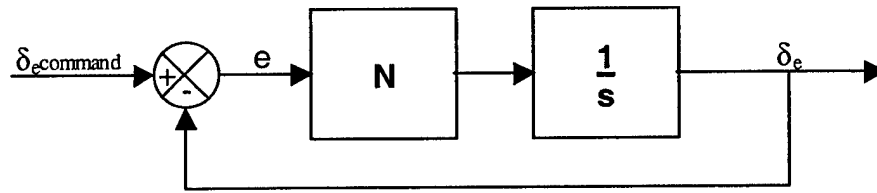


Figure A5. Closed Loop Actuator Transfer Function Diagram

Treating N as a constant and utilizing standard block diagram transfer function techniques, the relationship of e to $\delta_{e\text{command}}$ is:

$$\frac{e(s)}{\delta_{e\text{command}}(s)} = \frac{1}{1 + \frac{N}{s}} \quad (\text{A19})$$

Assuming $\delta_{e\text{command}}(t) = A \sin(\omega t)$ and $e(t) = E \sin(\omega t + \phi)$ and substituting $j\omega$ for s , the equation for the magnitude of this transfer function becomes:

$$\left| \frac{e(s)}{\delta_{e\text{command}}(s)} \right| = \frac{1}{\sqrt{1 + \frac{N^2}{\omega^2}}} = \left| \frac{E \sin(\omega t + \phi)}{A \sin(\omega t)} \right| = \frac{E}{A} \quad (\text{A20})$$

Rearranging Eqn 18 in terms of E gives:

$$E = \frac{4 V_L}{\pi N} \quad (\text{A21})$$

Substituting Eqn 21 into Eqn 20 and rearranging terms yields:

$$N = \frac{\omega}{\sqrt{\left(\frac{\pi A \omega}{4 V_L}\right)^2 - 1}} \quad (\text{A22})$$

Now, still treating N as a constant and utilizing standard block diagram transfer function techniques, the relationship of δ_e to $\delta_{e\text{command}}$ is:

$$\frac{\delta_e(s)}{\delta_{e\text{command}}(s)} = \frac{1}{\frac{s}{N} + 1} = \frac{N}{s + N} \quad (\text{A23})$$

and its magnitude is:

$$\left| \frac{\delta_e(j\omega)}{\delta_{e\text{command}}(j\omega)} \right| = \frac{\sqrt{N^2}}{\sqrt{\omega^2 + N^2}} \quad (\text{A24})$$

and substituting Eqn 22 into Eqn 24 gives:

$$\left| \frac{\delta_e(j\omega)}{\delta_{e\text{command}}(j\omega)} \right| = \frac{4 V_L}{\pi A \omega} \quad (\text{A25})$$

Solving for the phase angle of Eqn 21 yields:

$$\angle \frac{\delta_e(j\omega)}{\delta_{e\text{command}}(j\omega)} = \tan^{-1} \left(\frac{-\omega}{N} \right) \quad (\text{A26})$$

And substituting Eqn 20 yields:

$$\angle \frac{\delta_e(j\omega)}{\delta_{e\text{command}}(j\omega)} = -\tan^{-1} \left(\sqrt{\left(\frac{\pi A \omega}{4 V_L} \right)^2 - 1} \right) \quad (\text{A27})$$

Sinusoidal Input/Triangle Output Describing Function Approximation

Another describing function approximation can be made by utilizing the observed characteristics of a saturated actuator. The input, $x_i(t)$, is sinusoidal in nature and the output, $x_o(t)$, takes on the familiar saw tooth triangle shape as shown in Fig 2-5:

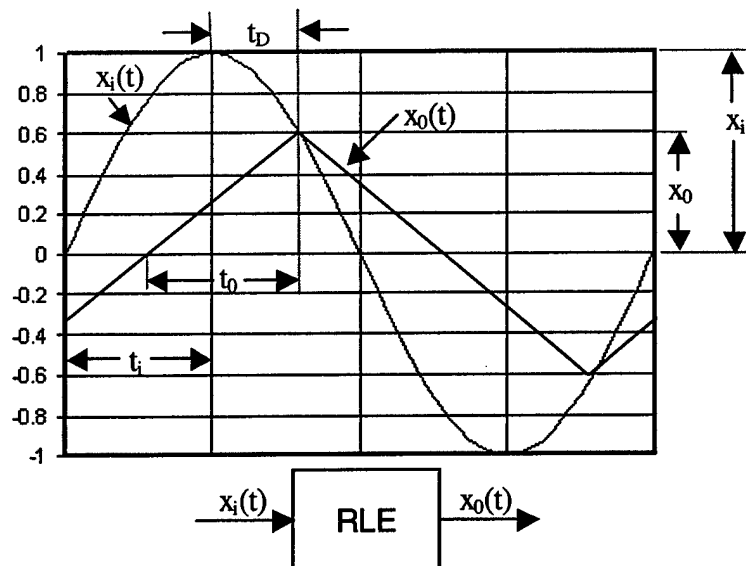


Figure A6. Rate limiting Input and Output

As before, let the input be sinusoidal as shown in Eqn 28:

$$x_i(t) = x_{i \max} \sin(\omega t) \quad (\text{A28})$$

and the derivative or input rate is:

$$\dot{x}_i(t) = x_{i \max} \omega \cos(\omega t) \quad (\text{A29})$$

Now, let $\omega = 2\pi/T$ where $T = 4t_i$. Then the maximum input rate is:

$$\dot{x}_{i \max} = \frac{\pi x_{i \max}}{2 t_i} \quad (\text{A30})$$

The rate of the output, \dot{x}_0 , is equal to the slope of the output and is given by:

$$\dot{x}_0 = \pm \frac{x_0}{t_0} \quad (\text{A31})$$

Now, take the relationship of the output rate to the input rate in the range of t_0 and solve for the ratio of output to input magnitude as:

$$\frac{\dot{x}_0}{\dot{x}_{i \max}} = \left(\frac{x_0}{t_0} \right) / \left(\frac{\pi x_{i \max}}{2 t_i} \right) = \frac{x_0}{t_0} \frac{2 t_i}{x_{i \max} \pi} \quad (\text{A32})$$

Recognizing t_0 equals t_i , and rearranging terms gives:

$$\frac{x_0}{x_{i \max}} = \frac{\pi}{2} \frac{x_0}{x_{i \max}} = K^* \quad (\text{A33})$$

Rewriting this expression in terms of the Figure 2-3 variables and recognizing that the output rate when saturated is V_L and the maximum input rate is $A\omega$ leaves

$$K^* = \frac{\pi}{2} \frac{V_L}{A\omega} \quad (\text{A34})$$

The describing function magnitude is then expressed using the K^* value multiplied by the Fourier fundamental of the triangle wave as seen in Eqn 35 (Reference 6).

$$\left| \frac{\delta_e(j\omega)}{\delta_{e \text{ command}}(j\omega)} \right| = \frac{8}{\pi^2} K^* = \frac{4}{\pi} \frac{V_L}{A\omega} \quad (\text{A35})$$

This is exactly the same expression derived earlier for the closed loop actuator describing function magnitude. To obtain the phase angle of the input/output relationship, the term t_D as shown in Figure A-6 must be determined. The input and output amplitudes are equal when $t = t_i + t_D$. Substituting this into Eqn 26 yields:

$$x_{i \max} \sin[\omega(t_i + t_D)] = x_0 \quad (\text{A36})$$

Simplifying this expression by substituting $K^* = x_0/x_{i \max}$, expanding $\sin[\omega(t_i + t_D)]$, and substituting $\omega t_i = \pi/2$ results in (Reference 6):

$$\cos(\Delta\phi) = K^* \quad (\text{A37})$$

Where $\Delta\phi = \omega t_D$ is the phase angle between the input and output. Solving for $\Delta\phi$ and noting that it is a phase lag leads to Eqn 38:

$$-\Delta\phi = -\cos^{-1}(K^*) = \angle \frac{\delta_e(j\omega)}{\delta_{e\text{command}}(j\omega)} = -\tan^{-1} \left[\sqrt{\left(\frac{1}{K^*}\right)^2 - 1} \right] \quad (\text{A38})$$

Now to compare with the closed loop describing function phase angle, substitute $K^* = \frac{\pi V_L}{2 A\omega}$ into Eqn 38 as accomplished in Eqn 39:

$$\angle \frac{\delta_e(j\omega)}{\delta_{e\text{command}}(j\omega)} = -\tan^{-1} \left[\sqrt{\left(\frac{2A\omega}{\pi V_L}\right)^2 - 1} \right] \quad (\text{A39})$$

This is slightly different from the closed loop describing function phase angle. These differences are shown in Figure A-7:

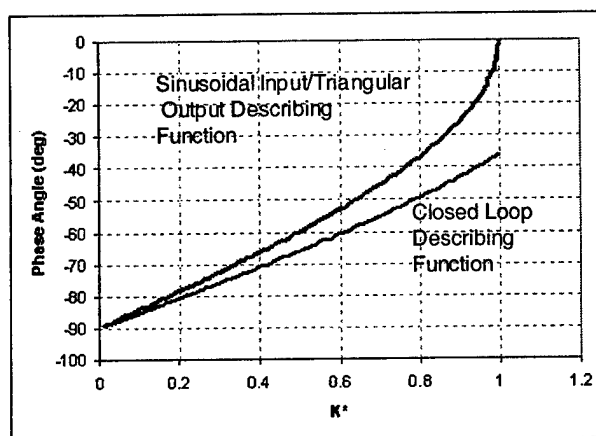


Figure A7. Describing Function Phase Angle Comparison

The more accurate of these two describing function approximations for application to Category II PIO is the sinusoidal input/triangle output solution (Reference 6).

Applying Describing Function Results to Predict PIO

Consider the longitudinal closed loop system shown in Figure A-8. $G_p(s)$ represents a model of the pilot and $G_c(s)$ represents a model of the bare airframe. The remaining elements are equivalent to the rate limited actuator model previously discussed in Figure A-4.

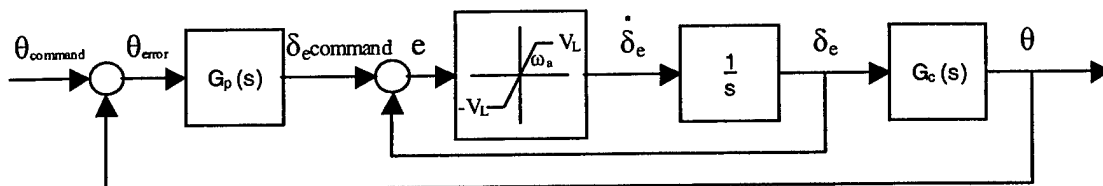


Figure A8. Pitch Tracking Closed Loop System

The linear elements $G_p(s)$ and $G_c(s)$ can be combined into one linear element, $G(s)$ and the nonlinear element, $N(A, \omega)$, remains separate as shown in Figure A-9.

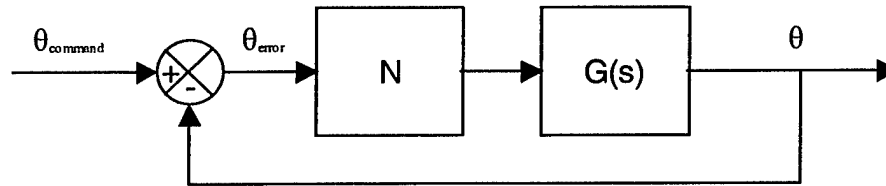


Figure A9. Simplified Pitch Tracking Closed Loop System

The requirement for a neutrally damped oscillation is simply that the open-loop amplitude ratio equal 1.0 and for the phase to be -180° (Reference 6). In order for a PIO to persist, the system shown in Fig A-9 must satisfy the Nyquist criteria shown in the following equation (Reference 6):

$$G(j\omega)N(j\omega, A) = -1 \quad (\text{A40a})$$

or

$$G(j\omega) = \frac{-1}{N(j\omega, A)} \quad (\text{A40b})$$

The easiest way to view the application of this equation is to plot the open-loop magnitude and phase values of the negative inverse describing function $(-1/N(j\omega, A))$ using the K^* solutions from Eqns 35 and 37 as well as the open-loop magnitude and phase of $G(j\omega)$. If the two plots intersect, a PIO is predicted (Reference 6). This will be shown by means of an example later in this chapter. The K^* solutions for the negative inverse describing function are shown below in Eqns 41a and 41b:

$$\left| \frac{-1}{N(K^*)} \right| = -20 \text{Log} \left(\frac{8K^*}{\pi^2} \right) \text{ (dB)} \quad (\text{A41a})$$

$$\angle \frac{-1}{N(K^*)} = \frac{180}{\pi} \cos^{-1}(K^*) - 180 \text{ (deg)} \quad (\text{A41b})$$

Pilot Model

There are many pilot models to choose from in the literature. Some believe that a simple gain with no phase lag best represents the pilot in the PIO situation (Reference 6). Others believe structural models are better predictors (Reference 8). In another recent study, the Neal-Smith pilot model was judged to best represent the pilot model prior to the onset of rate limiting (Reference 9). In this study, the Neal-Smith pilot model will be utilized.

The Neal-Smith pilot model is useful for pilot-aircraft pitch attitude control loops with unity-feedback and has the following characteristics (Reference 3):

1. Adjustable Gain
2. Time delay
3. Ability to develop lead, or to operate on derivative or rate information
4. Ability to develop lag, or to smooth inputs
5. Ability to provide low-frequency integration

The Neal-Smith pilot model can take on one of two forms. This determination is based on the whether constant speed or two-degree-of-freedom equations are used to represent the bare aircraft dynamics. These are typified by noting whether or not a free integrator is contained in the denominator of the aircraft pitch transfer function. Otherwise, three-degree-of-freedom equations or flight control system utilizing attitude stabilization will require a different form. The following table shows the transfer functions of the Neal-Smith pilot models (Reference 3):

Table A1: Neal-Smith Pilot Models

Aircraft Transfer Function with a Free Integrator	Aircraft Transfer Function without a Free Integrator
$G_p(s) = K_p \frac{(T_{p1}s + 1)}{(T_{p2}s + 1)} e^{-0.25s}$	$G_p(s) = K_p \frac{(5s + 1)}{s} \frac{(T_{p1}s + 1)}{(T_{p2}s + 1)} e^{-0.25s}$

The theory states that the pilot chooses his gain, K_p , and his lead/lag time constants, T_{p1} and T_{p2} , to attain a certain bandwidth. This bandwidth varies with the flight phase category. For example, for Category A flight phases such as air-to-air dogfighting, the required bandwidth is 3.5 rad/sec. This is measured at a closed-loop phase of -90 degrees. Further, the pilot adjusts to minimize droop: no greater than 3 dB for Level 1 performance and no greater than 9 dB for Level 2 over the frequency range from 0 to 10 rad/sec while at the same time minimizing closed loop resonance (Reference 3). The phase lag term, $e^{-0.25s}$, represents delays in the pilot's neuromuscular system (Reference 3).

Gap Criterion

Utilizing the previous theoretical developments, a systematic process relating bare aircraft plant dynamics, augmented aircraft plant dynamics and actuator rate limits to predicted PIO tendency rating will be introduced. The procedure is to be called the *Gap Criterion*.

Computing the *Gap Criterion* consists of the following steps:

1. Determine the bare aircraft pitch-to-commanded actuator transfer function, $G_c(s) = \theta(s)/\delta_c(s)$
2. If the short period poles of $G_c(s)$ are unstable then *Gap Criterion* = 0. This is due to control amplitudes approaching zero causing an immediate departure due to dynamic instability.
3. Determine an appropriate optimized Neal-Smith pilot model, $G_p(s)$, for the bare aircraft transfer function $G_c(s)$ appended with the first order linear actuator model G_{act} shown below and then augmented with feedback.

$$G_{act}(s) = \frac{\omega_a}{s + \omega_a}, \text{ where } \omega_a = 20$$

4. Plot the open-loop magnitude and phase of $G(s) = G_c(s)G_p(s)$ on a Nichols chart
5. Plot the negative inverse describing function open-loop magnitude and phase on the same Nichols chart using the K^* equations A-41A and A-41B
6. Determine the resulting case by reference to Figure A-10 and then compute the *Gap Criterion* by following the steps of that case.

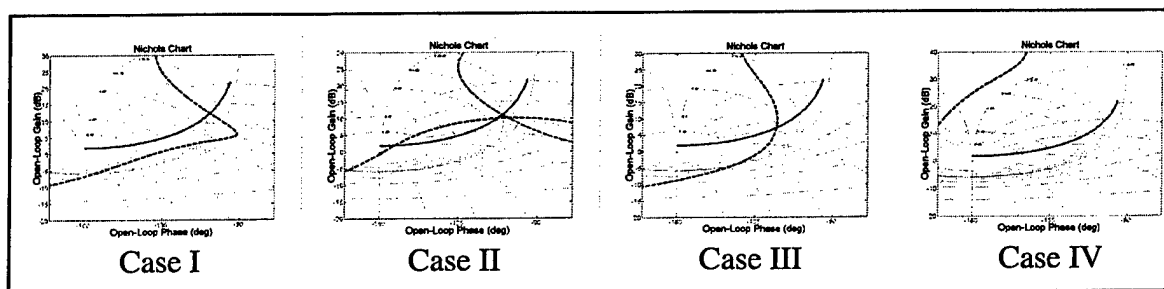


Figure A10. Resulting Cases

Case I

1. Determine the minimum amount by which the pilot would need to increase his gain, ΔK_p (dB), such that the two magnitude-phase lines just intersect at a frequency greater than the -3 dB Neal-Smith droop frequency
2. Determine the values of K^* and ω (rad/sec) at this intersection
3. Determine the amplitude, A , of the commanded actuator deflection utilizing the following equation where V_L is the known actuator rate limit in deg/sec:

$$K^* = \frac{\pi V_L}{2 A \omega}$$

4. Normalize this amplitude by dividing by the maximum available actuator deflection, A_{max}
5. The *Gap Criterion* is this normalized amplitude multiplied by ΔK_p .

$$\text{Gap Criterion} = (A/A_{max}) * 10^{(\Delta K_p/20)}$$

Case II

1. Determine the minimum amount by which the pilot would need to decrease his gain, ΔK_p (dB), such that the two magnitude-phase lines only intersect in one place at a frequency greater than the -3 dB Neal-Smith droop frequency
2. Determine the values of K^* and ω (rad/sec) at this intersection
3. Determine the amplitude, A , of the commanded actuator deflection utilizing the following equation where V_L is the known actuator rate limit in deg/sec:

$$K^* = \frac{\pi V_L}{2 A \omega}$$

4. Normalize this amplitude by dividing by the maximum available actuator deflection, A_{max}
5. The *Gap Criterion* is this normalized amplitude multiplied by ΔK_p .

$$\text{Gap Criterion} = (A/A_{max}) * 10^{(\Delta K_p/20)}$$

Case III

1. Determine the values of K^* and ω (rad/sec) at the intersection
2. Determine the amplitude, A , of the commanded actuator deflection utilizing the following equation where V_L is the known actuator rate limit in deg/sec:

$$K^* = \frac{\pi V_L}{2 A \omega}$$

3. Normalize this amplitude by dividing by the maximum available actuator deflection, A_{max}
4. The *Gap Criterion* is this normalized amplitude multiplied by ΔK_p .

$$\text{Gap Criterion} = (A/A_{max})$$

Case IV

1. No determination of Gap Criterion can be made. deg/sec:

Example of Gap Criterion Application

Reconsider the closed loop system of Figure A-8 with the following characteristics:

- $G_c(s) = \frac{(4.5)(s+1.5)}{s(s^2 + 3s + 6)}$
- $G_{act}(s) = \frac{20}{s + 20}$
- $V_L = 30 \text{ deg/sec}$
- Maximum actuator deflection: $\delta_{e \max} = 30 \text{ deg}$
- Category A flight phase

Utilizing the USAF Wright Laboratory Flight Dynamics Directorate's MATLAB® Interactive Flying Qualities Toolbox for Matlab (Reference 10), the Neal-Smith pilot model was found to be:

$$G_p(s) = 0.856(0.583s + 1)e^{-0.25s}$$

Noting that this is an improper transfer function and cannot be used with MATLAB®, the model was modified with a very small T_{p2} :

$$G_p(s) = 0.856 \frac{(0.583s + 1)}{(0.0001s + 1)} e^{-0.25s}$$

The open-loop magnitude and phase of $G(s) = G_p(s)G_c(s)$ are plotted in Figure A-11 as well as the open-loop magnitude and phase of the negative inverse describing function. This is a Case I result. It can be seen that a ΔK_p increase of 7.502 dB or 2.372 absolute is all that is needed for the two lines to meet. At this intersection, the values for K^* and ω are 0.7635 and 3.9418 rad/sec, respectively. After calculating the amplitude, $A = 15.66 \text{ deg}$, the

result is normalized by dividing by 30 deg ($\delta_{e \max}$). This normalized result is multiplied by ΔK_p to yield the Gap Criterion. In this example the *Gap Criterion* equals 1.238.

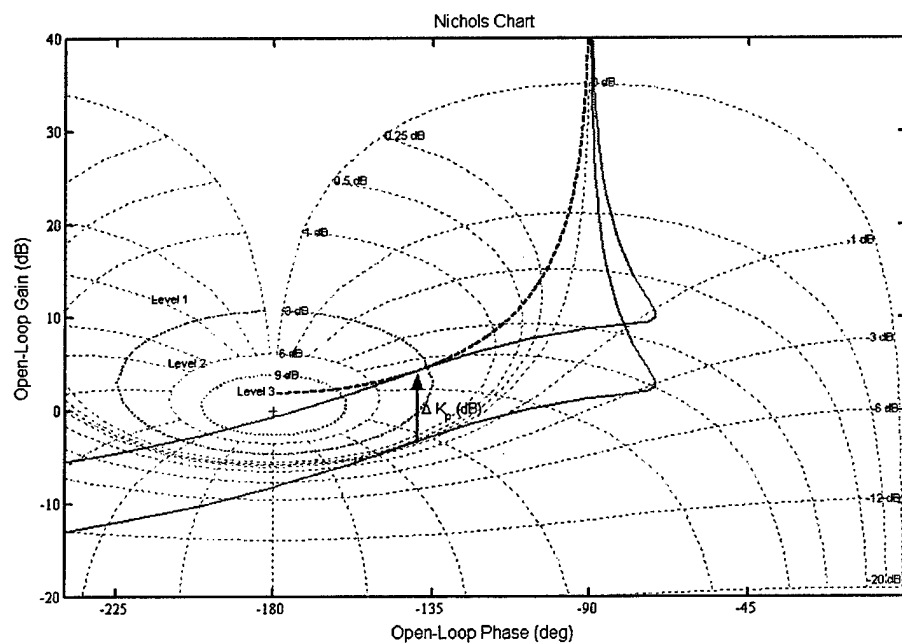


Figure A11. Nichols Chart of the Example Problem

THIS PAGE INTENTIONALLY LEFT BLANK

APPENDIX B: DATA ANALYSIS

OVERVIEW

This data analysis plan (DAP) appendix describes the test data that was required to meet the stated objectives and the associated data reduction techniques. The majority of the data collected was in the form of pilot assigned PIO tendency ratings and comments. Time history data was also collected as supporting data (to determine the presence of rate limiting, evaluate data quality, etc).

REQUIRED DATA

The following data from each test point were required for analysis:

- Pilot assigned PIO Rating
- Pilot Comments
- Time history of flight data

The test team used three sources of data: digital data from the VISTA Data Acquisition System (DAS) in Matlab® format recorded electronically, pilot audio and HUD video recorded on HI-8 tapes, and data recorded in the control room and in the test aircraft.

MEDIA AND DATA FORMAT

Table B.1: MAX GAP Test Data, identifies the time history data sources, the data media, and the format in which the data were recorded. These parameters will be recorded via the NF-16D VISTA data acquisition system. The data was converted to Matlab® format by Advanced Information Engineering Services, Inc.

Table B1: MAX GAP Test Data

Config	None	n/a	1 to 999
Act_Rate_Out	Deg/sec	64 Hz	-80 to 80
Act_Out	Degrees	64 Hz	-80 to 80
Pilot	Degrees	64 Hz	-40 to 40
θ_{task}	Degrees	64 Hz	-30 to 30
θ_{act}	Degrees	64 Hz	-30 to 30
V_c	KIAS	64 Hz	0 to 500
N_z	G's	64 Hz	-4 to 8
Mach	None	64 Hz	0 to 1
H_i	Ft	64 Hz	2000 to 22000
Rec No	None	64 Hz	1 to 100
VSS Engage	None	64 Hz	0 or 1
HUD_TR_D_S	Percent	64 Hz	0 to 100
HUD_TR_A_S	Percent	64 Hz	0 to 100
Total Fuel	Lbs	64 Hz	0 to 8000
Rate Flag		64 Hz	0 to 1

DATA REDUCTION

Time histories of flight data were reduced to Matlab[®] format by Advanced Information Engineering Services, Inc. after each flight and were provided electronically to the test team. HUD Hi-8 video, MFD video, pilot audio, written pilot comments and ratings, and time histories were used to review each test point to determine data quality.

DATA ANALYSIS

Test Objective 2: Determine the correlation between PIO tendency rating and *Gap Criterion* using the LAMARS simulator.

PIO Tendency Ratings were collected for selected bare airframe dynamics and rate limit combinations using the LAMARS simulator.

Data Requirements

- PIO Tendency Rating
- Pilot Comments
- MAX GAP Test Data time histories

Data Reduction and Analysis

The pre-computed *Gap Criterion* for the selected bare airframe and rate limit configuration was plotted versus the assigned PIO Tendency Rating. Pilot comments and MAX GAP test data were used to determine data quality and the presence of rate limiting. The significance of the data correlation was determined by computing a correlation coefficient, r , shown in equation B1 (Reference 11).

$$r_{xy} = \frac{\sum_{i=1}^n (x_i - \bar{x})(y_i - \bar{y})}{\left[\sum_{i=1}^n (x_i - \bar{x})^2 \sum_{i=1}^n (y_i - \bar{y})^2 \right]^{1/2}} \quad (\text{B1})$$

Where n is the number of data pairs and \bar{x} and \bar{y} are the mean values of x and y which were obtained experimentally (Eqn B2).

$$\bar{x} = \frac{\sum_{i=1}^n x_i}{n} \quad \bar{y} = \frac{\sum_{i=1}^n y_i}{n} \quad (\text{B2})$$

Test Objective 3: Determine the correlation between PIO tendency rating and *Gap Criterion* using the NF-16 VISTA.

PIO Tendency Ratings were collected for the selected bare airframe dynamics and rate limit combinations using the NF-16 VISTA

Data Requirements

- PIO Tendency Rating
- Pilot Comments
- MAX GAP Test Data time histories

Data Reduction and Analysis

The pre-computed *Gap Criterion* for the selected bare airframe and rate limit configuration was plotted versus the assigned PIO Tendency Rating. Pilot comments and MAX GAP test data were used to determine data quality and the presence of rate limiting. The significance of the data correlation was determined by computing a correlation coefficient as shown in equation B1 (Reference 11).

DATA ANALYSIS PRODUCTS

The Quick Look and In-Depth analysis were used to generate the final data products. The ultimate product was a plot of *Gap Criterion* versus PIO tendency rating. Supporting data were presented in the form of time history plots of MAX GAP test datasets.

HARDWARE AND SOFTWARE REQUIREMENTS

Advanced Information Engineering Services, Inc. provided their own hardware and software to reduce the VISTA DAS data from the instrumentation format on the aircraft to the digital Matlab[®] format. Desktop PC computers with Microsoft Excel, Matlab[®] and Simulink[®] were available at TPS to perform the data analysis. Hi-8 tape playback equipment was available at TPS for mission review.

THIS PAGE INTENTIONALLY LEFT BLANK

APPENDIX C: PIO RATING SCALES

<u>PIO RATING SCALE</u>		
Did I experience a PIO?		
No		
	Did I experience undesirable motion?	
 No	1
	Yes	
	Did undesirable motion <i>tend to occur</i> ?	2
	Was undesirable motion <i>easily induced</i> ?	3
Yes		
	While attempting maneuvers or tight control?	
	Was the PIO <i>bounded</i> ?.....	4
	Was the PIO <i>divergent</i> ?	5
	While exercising normal control?	6

DESCRIPTION	NUMERICAL RATING
No tendency for pilot to induce undesirable motions.	1
Undesirable motions tend to occur when pilot initiates abrupt maneuvers or attempts tight control. These motions can be prevented or eliminated by pilot technique.	2
Undesirable motions easily induced when pilot initiates abrupt maneuvers or attempts tight control. These motions can be prevented or eliminated but only at sacrifice to task performance or through considerable pilot attention and effort.	3
Oscillations tend to develop when pilot initiates abrupt maneuvers or attempts tight control. Pilot must reduce gain or abandon task to recover.	4
Divergent oscillations tend to develop when pilot initiates abrupt maneuvers or attempts tight control. Pilot must open loop by relasing or freezing the stick.	5
Disturbance or normal pilot control may cause divergent oscillation. Pilot must open control loop by releasing or freezing the stick.	6

Figure C1: Pilot-Induced Oscillation (PIO) Rating Scales

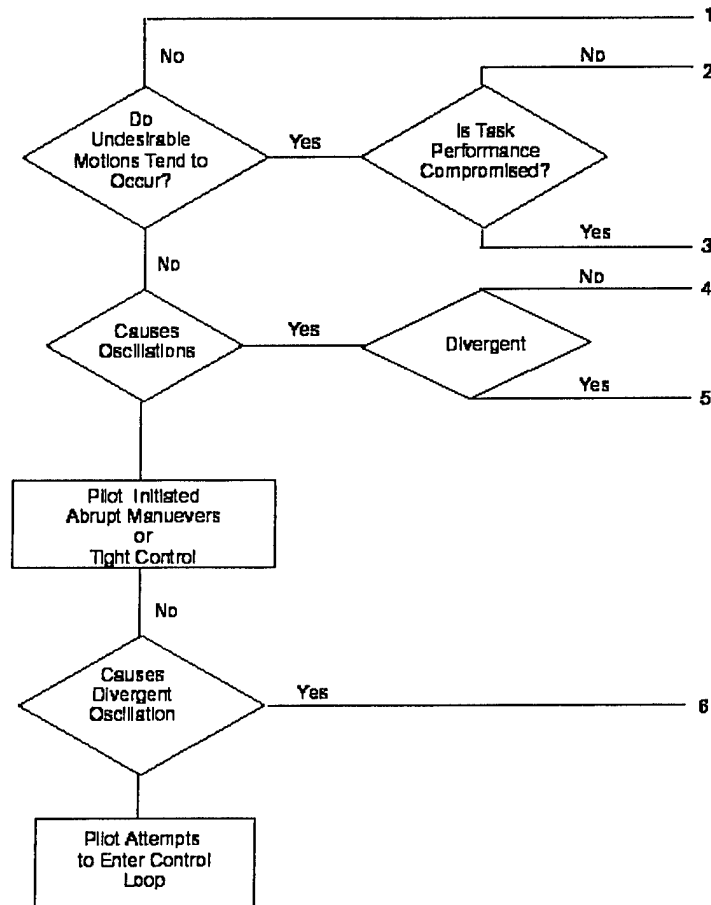


Figure C2: PIO Tendency Classification Scale

APPENDIX D: TEST POINT CONFIGURATIONS

Table D1 shows the system dynamics used for the Project HAVE PREVENT historical evaluation. The corresponding angle-of-attack (K_a) and pitch-rate (K_q) feedback gains used for the *Gap Criterion* analysis are included.

Table D1: HAVE PREVENT Bare Airframe Test Cases

Case	Bare Airframe Poles	ω_{ndp} (rad/s)	ζ_{sp}	K_a (approx.)	K_q (approx.)	Augmented Aircraft Poles
A	$-2.18 \pm 2.23j$ $-.017 \pm .074j$	3.12	0.70	0	0	$-2.18 \pm 2.23j$ $-.017 \pm .074j$
B	$-1.43 \pm 1.85j$ $-.016 \pm .079j$	2.34	0.61	0.21	0.14	$-2.27 \pm 2.35j$ $-.017 \pm .074j$
C	$-0.86 \pm .086j$ $-.009 \pm .097j$	0.86	0.995	0.51	0.24	$-2.24 \pm 2.52j$ $-.017 \pm .074j$
D	1.07, -1.67 $-.017 \pm .033j$	$T_2 = 2.31 \text{ sec}$		0.61	0.34	$-2.32 \pm 2.62j$ $-.017 \pm .074j$

Note: K_q and K_a are the feedback gains required to achieve the desired closed loop dynamics.

These test cases yielded the *Gap Criterion* values shown in Table D2, based on a maximum elevator deflection angle of ± 30 degrees.

Table D2: HAVE PREVENT Test Case *Gap Criterion* Values

Bare Airframe Case	Maximum Elevator Deflection Rate	<i>Gap Criterion</i>	Bare Airframe Case	Maximum Elevator Deflection Rate	<i>Gap Criterion</i>
A	15°/sec	0.555	C	15°/sec	0.300
A	30°/sec	1.109	C	30°/sec	0.600
A	45°/sec	1.664	C	45°/sec	0.900
A	60°/sec	2.218	C	60°/sec	1.201
B	15°/sec	0.556	D	15°/sec	0
B	30°/sec	1.111	D	30°/sec	0
B	45°/sec	1.667	D	45°/sec	0
B	60°/sec	2.223	D	60°/sec	0

Table D3 shows the system dynamics used for the Project HAVE OLOP historical evaluation. The corresponding angle-of-attack (K_a) and pitch-rate (K_q) feedback gains used for the *Gap Criterion* analysis are included.

Table D3: HAVE OLOP Bare Airframe Test Cases

Case	Bare Airframe Poles	ω_{nsp} (rad/s)	ζ_{sp}	K_α	K_q	Augmented Aircraft Poles
A	$-0.510 \pm 3.36j$ $-0.017 \pm 0.074j$	3.40	0.15	0.023	0.412	$-3.51 \pm 3.58j$ $-0.017 \pm 0.060j$
C	$-1.29 \pm 1.72j$ $-0.017 \pm 0.074j$	2.15	0.60	0.897	0.347	$-3.50 \pm 3.57j$ $-0.017 \pm 0.074j$
D	1.284, -2.13 $-0.017 \pm 0.074j$	$T_2 = 0.6 \text{ sec}$		1.218	0.487	$-3.55 \pm 3.62j$ $-0.017 \pm 0.074j$

Note: K_q and K_α are the feedback gains required to achieve the desired closed loop dynamics.

These test cases yielded the *Gap Criterion* values shown in Table D4, based on a maximum elevator deflection angle of ± 30 degrees.

Table D4: HAVE OLOP Test Case *Gap Criterion* Values

Bare Airframe Case	Maximum Elevator Deflection Rate	<i>Gap Criterion</i>	Bare Airframe Case	Maximum Elevator Deflection Rate	<i>Gap Criterion</i>
A	10°/sec	0.049	C	40°/sec	0.681
A	20°/sec	0.097	C	50°/sec	0.851
A	30°/sec	0.146	C	60°/sec	1.021
A	40°/sec	0.194	D	10°/sec	0
A	50°/sec	0.243	D	20°/sec	0
A	60°/sec	0.291	D	30°/sec	0
C	10°/sec	0.170	D	40°/sec	0
C	20°/sec	0.340	D	50°/sec	0
C	30°/sec	0.510	D	60°/sec	0

Table D5 shows the system dynamics used for the MAX GAP LAMARS evaluation. The corresponding angle-of-attack (K_α) and pitch-rate (K_q) feedback gains used for the *Gap Criterion* analysis and the LAMARS programming are included.

Table D5: MAX GAP LAMARS Bare Airframe Test Cases

Case	Bare Airframe Poles	ω_{nsp} (rad/s)	ζ_{sp}	K_α	K_q	Augmented Aircraft Poles
B	$-1.43 \pm 1.85j$ $-0.017 \pm 0.074j$	2.34	0.61	0.156	0.123	$-2.17 \pm 2.22j$ $-0.017 \pm 0.070j$
N	$-0.939 \pm 2.99j$ $-0.017 \pm 0.074j$	3.13	0.30	-0.335	0.177	$-2.18 \pm 2.22j$ $-0.018 \pm 0.050j$
W	$-4.24 \pm 2.05j$ $-0.017 \pm 0.074j$	4.71	0.90	-0.501	-0.345	$-2.18 \pm 2.24j$ $-0.017 \pm 0.081j$
Y	$-2.09 \pm 1.01j$ $-0.017 \pm 0.074j$	2.32	0.90	0.346	0.0334	$-2.19 \pm 2.24j$ $-0.017 \pm 0.080j$

Note: K_q and K_α are the feedback gains required to achieve the desired closed loop dynamics.

These test cases yielded the *Gap Criterion* values shown in Table D6, based on a maximum elevator deflection angle of ± 30 degrees.

Table D6: MAX GAP LAMARS Test Case *Gap Criterion* Values

Bare Airframe Case	Maximum Elevator Deflection Rate	<i>Gap Criterion</i>	Bare Airframe Case	Maximum Elevator Deflection Rate	<i>Gap Criterion</i>
B	15°/sec	0.595	W	15°/sec	0.488
B	30°/sec	1.191	W	30°/sec	0.976
B	60°/sec	2.381	W	60°/sec	1.952
N	15°/sec	0.319	Y	15°/sec	0.928
N	30°/sec	0.638	Y	30°/sec	1.855
N	60°/sec	1.275	Y	60°/sec	3.710

Table D7 shows the actual system dynamics used for MAX GAP VISTA flight test evaluation. The corresponding angle-of-attack (K_α) and pitch-rate (K_q) feedback gains used for the *Gap Criterion* analysis are included.

Table D7: MAX GAP VISTA Bare Airframe Test Cases

Case	Bare Airframe Poles	ω_{nsp} (rad/s)	ζ_p	K_α	K_q	Augmented Aircraft Poles
B	-1.42±1.85j -.017±.074j	2.33	0.61	-0.0212	0.0877	-1.98±-1.69j -.017±.065j
N	-.493±2.86j -.017±.074j	2.90	0.17	-0.408	0.254	-2.29±1.95j -.018±.031j
W	-3.26±1.77j -.017±.074j	3.70	0.88	-0.0946	-0.185	-2.10±2.14j -.017±.082j
Y	-3.02, -0.96 -.017±.074j	1.70	1.17	0.485	0.0400	-2.09±2.14j -.017±.083j

Note: K_q and K_α are the feedback gains required to achieve the desired closed loop dynamics.

These test cases yielded the *Gap Criterion* values shown in Table D8, based on a maximum elevator deflection angle of ±30 degrees.

Table D8: MAX GAP VISTA Test Case *Gap Criterion* Values

Bare Airframe Case	Maximum Elevator Deflection Rate	<i>Gap Criterion</i>	Bare Airframe Case	Maximum Elevator Deflection Rate	<i>Gap Criterion</i>
B	15°/sec	0.629	W	15°/sec	0.513
B	30°/sec	1.257	W	30°/sec	1.026
B	60°/sec	2.514	W	60°/sec	2.052
N	15°/sec	0.194	Y	15°/sec	1.347
N	30°/sec	0.388	Y	30°/sec	2.693
N	60°/sec	0.776	Y	60°/sec	5.387

Table D9: Test Configuration Matrix

Test Point	Bare Airframe Dynamics	Maximum Elevator Rate Limit	Phase, Task
1	B	60	Phase 2, Sum-of-sines
2	B	60	Phase 3, Discrete Tracking
3	B	60	Phase 3, Target Tracking
4	B	30	Phase 2, Sum-of-sines
5	B	30	Phase 3, Discrete Tracking
6	B	30	Phase 3, Target Tracking
7	B	15	Phase 2, Sum-of-sines
8	B	15	Phase 3, Discrete Tracking
9	B	15	Phase 3, Target Tracking
10	N	60	Phase 2, Sum-of-sines
11	N	60	Phase 3, Discrete Tracking
12	N	60	Phase 3, Target Tracking
13	N	30	Phase 2, Sum-of-sines
14	N	30	Phase 3, Discrete Tracking
15	N	30	Phase 3, Target Tracking
16	N	15	Phase 2, Sum-of-sines
17	N	15	Phase 3, Discrete Tracking
18	N	15	Phase 3, Target Tracking
19	W	60	Phase 2, Sum-of-sines
20	W	60	Phase 3, Discrete Tracking
21	W	60	Phase 3, Target Tracking
22	W	30	Phase 2, Sum-of-sines
23	W	30	Phase 3, Discrete Tracking
24	W	30	Phase 3, Target Tracking
25	W	15	Phase 2, Sum-of-sines
26	W	15	Phase 3, Discrete Tracking
27	B	60	Phase 2, Sum-of-sines
28	Y	60	Phase 2, Sum-of-sines
29	Y	60	Phase 3, Discrete Tracking
30	Y	60	Phase 3, Target Tracking
31	Y	30	Phase 2, Sum-of-sines
32	Y	30	Phase 3, Discrete Tracking
33	Y	30	Phase 3, Target Tracking
34	Y	15	Phase 2, Sum-of-sines
35	Y	15	Phase 3, Discrete Tracking
36	Y	15	Phase 3, Target Tracking

Notes:

1. All test points will be flown at 15,000 ft pressure altitude and 300 KIAS. The data bands are ± 5000 ft and ± 10 KIAS for entry.
2. The VSS automatically adjusts for fuel weight. The VSS gains are changed to preserve the same short period dynamics. Aircraft total weight does not have a data band.

APPENDIX E: TRACKING TASKS

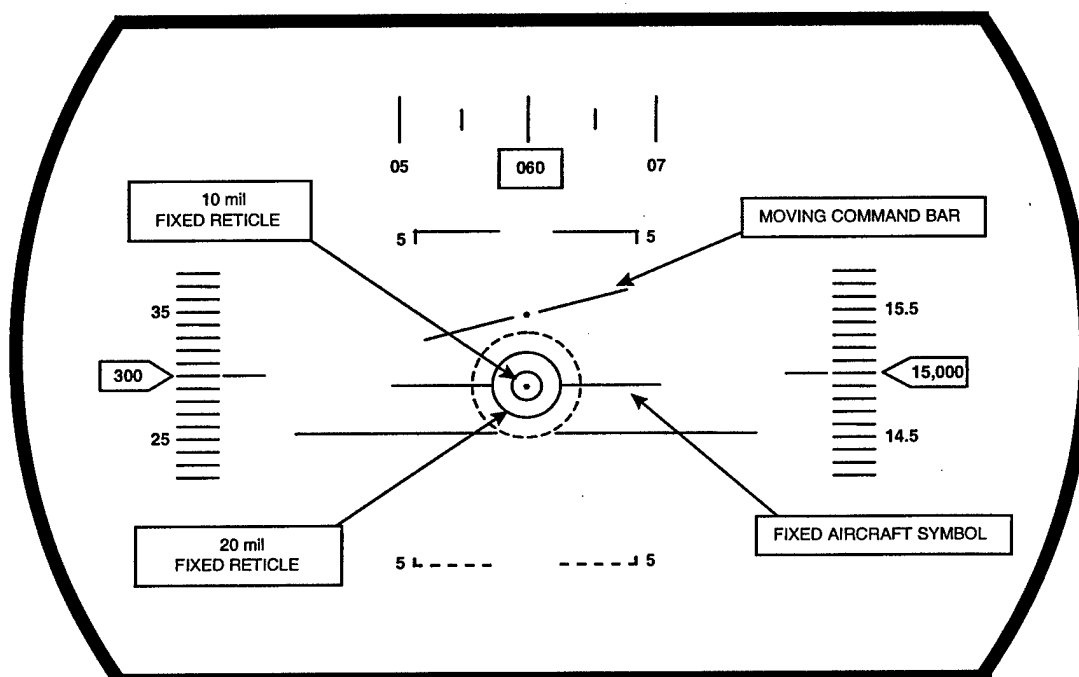


Figure E1 Example Heads Up Display

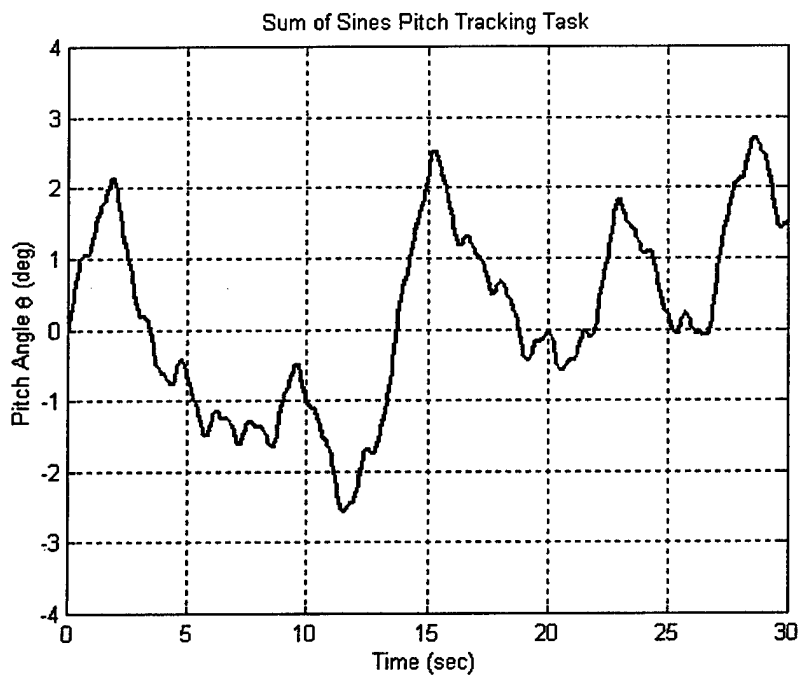


Figure E2: Sum-of-sines Pitch Tracking Task

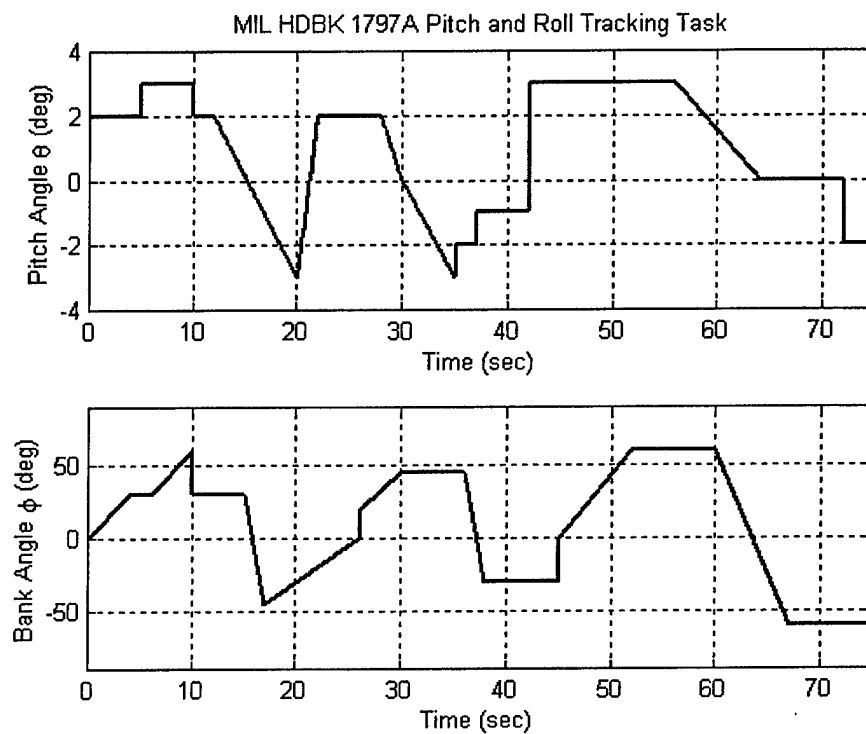


Figure E3: MIL-HDBK-1797 Pitch Tracking Task

APPENDIX F: HISTORICAL DATA FIGURES

The MAX GAP historical data figures are in this appendix. Data from two previous Test Management Projects (TMPs), HAVE PREVENT and HAVE OLOP, were investigated to see if a correlation between PIO tendency rating and the *Gap Criterion* existed. There are two types of charts shown. One is a 2D "bubble chart" of the PIO tendency rating versus the *Gap Criterion*. This "bubble chart" uses circles of different diameters to depict data density in terms of the number of times a similar PIO tendency rating is assigned to a single *Gap Criterion* value. Also, a linear curve fit with the corresponding equation, R^2 value, and correlation factor are shown on the 2D "bubble chart." The second type of figure is a 3D stem plot with the same data as the 2D "bubble chart" from a different perspective. The horizontal plane of the 3D chart contains the PIO tendency rating and the *Gap Criterion*. The vertical axis shows the number of occurrences for a single PIO tendency rating for a discrete *Gap Criterion*. An increasing height of the vertical bars corresponds to a greater number of occurrences. The same linear model from the 2D "bubble chart" is shown on the floor of the 3D view. This provides insight into how the data density drives to the model to match the Gap Criterion theory, which states that low Gap values should lead to the high PIO tendency ratings and vice versa.

HAVE PREVENT LAMARS Phase 2 Sum-of-Sines Task

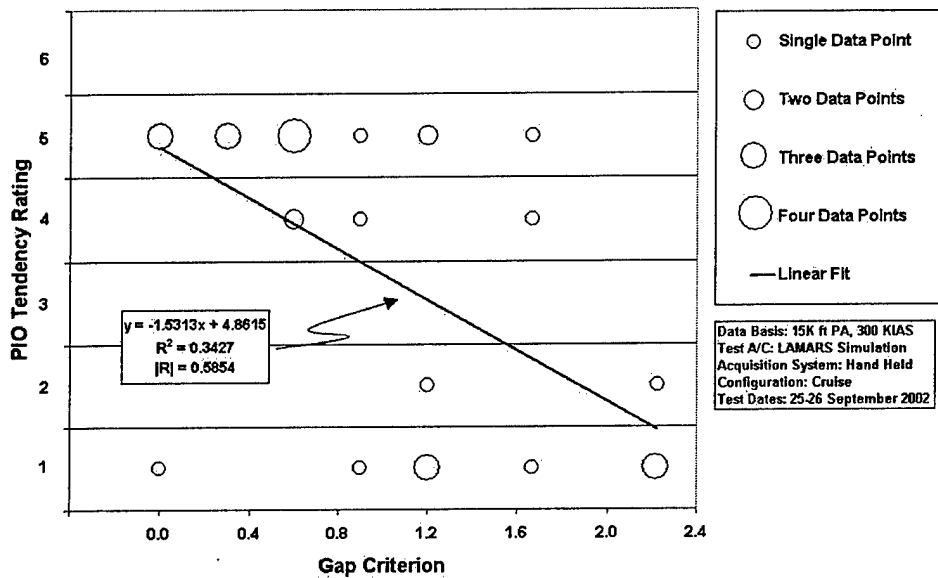


Figure F1A: HAVE PREVENT Phase 2 Sum-of-Sines Task LAMARS Data (2D)

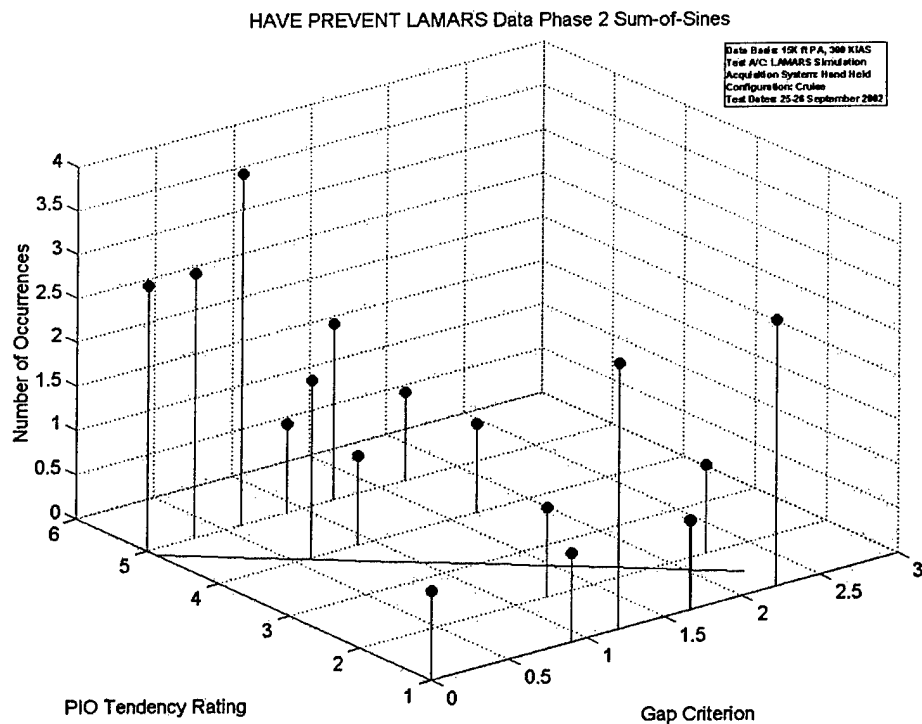


Figure F1B: HAVE PREVENT Phase 2 Sum-of-Sines Task LAMARS Data (3D)

HAVE PREVENT LAMARS Phase 3 Discrete HUD Pitch Tracking Task

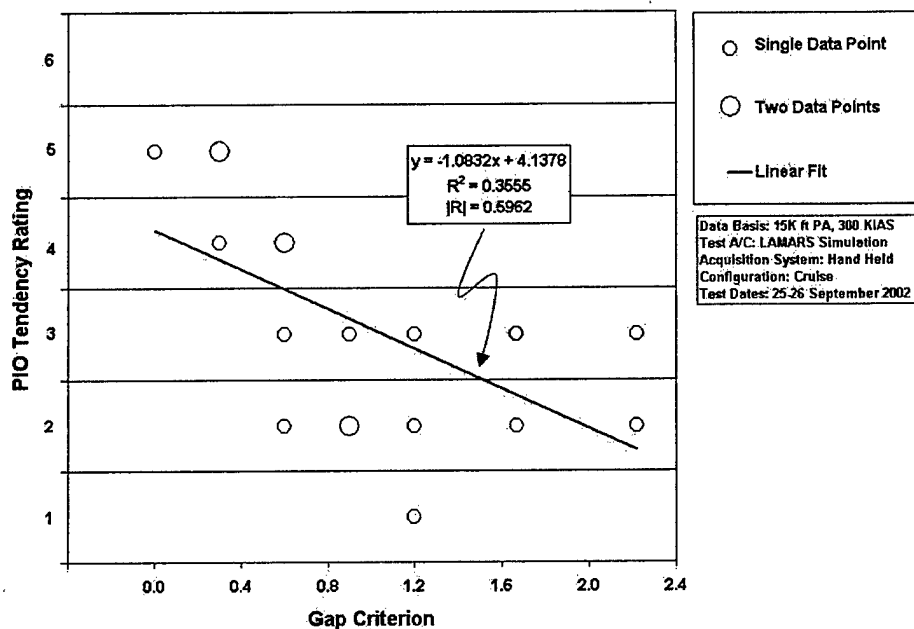


Figure F2A: HAVE PREVENT Phase 3 Discrete HUD Tracking Task LAMARS Data (2D)

HAVE PREVENT LAMARS Data Phase 3 HUD Discrete Task

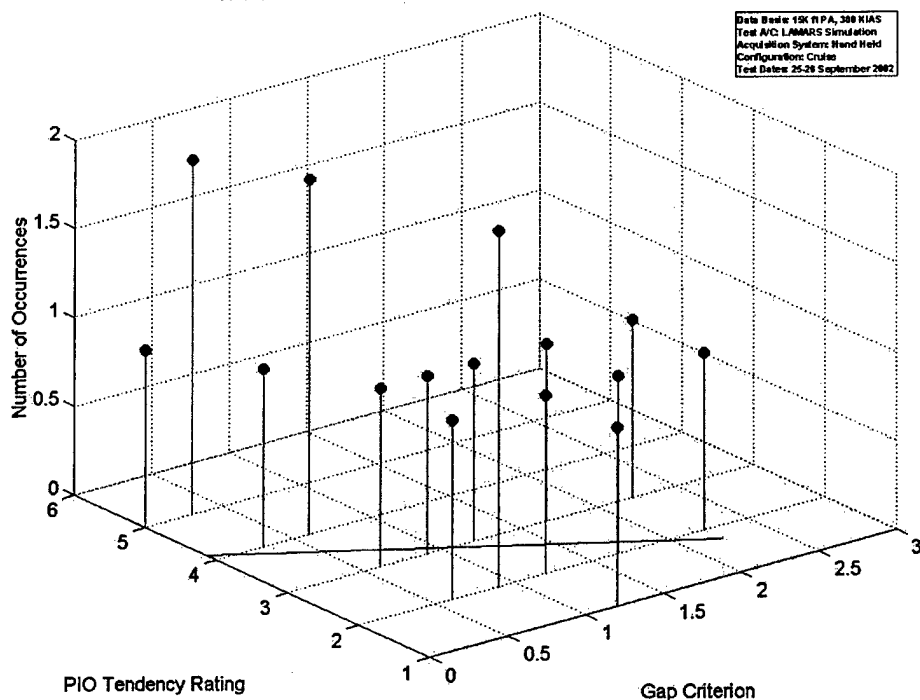


Figure F2B: HAVE PREVENT Phase 3 Discrete HUD Tracking Task LAMARS Data (3D)

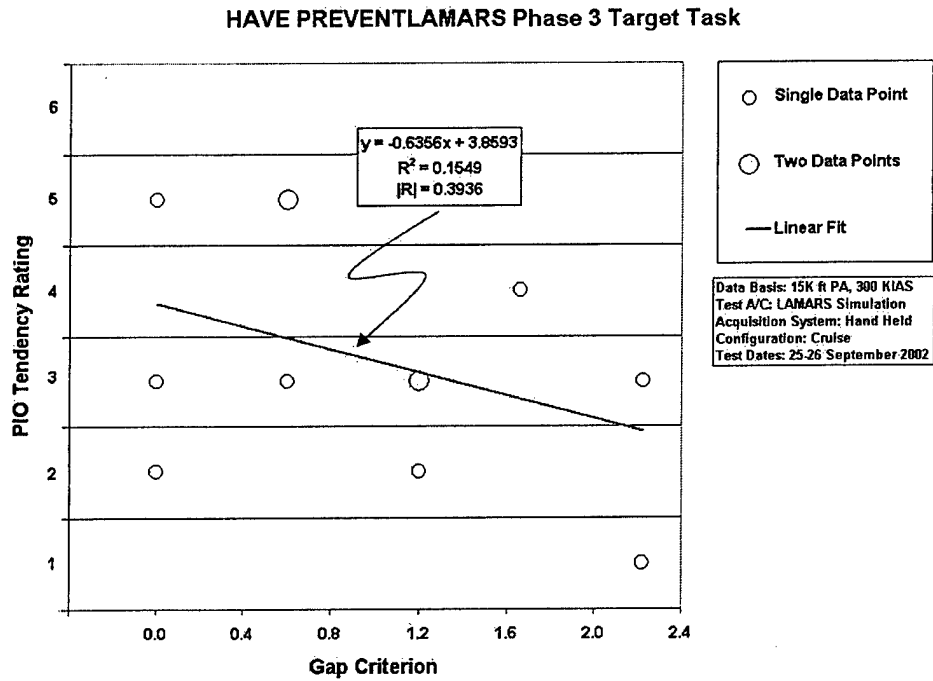


Figure F3A: HAVE PREVENT Phase 3 Target Task LAMARS Data (2D)

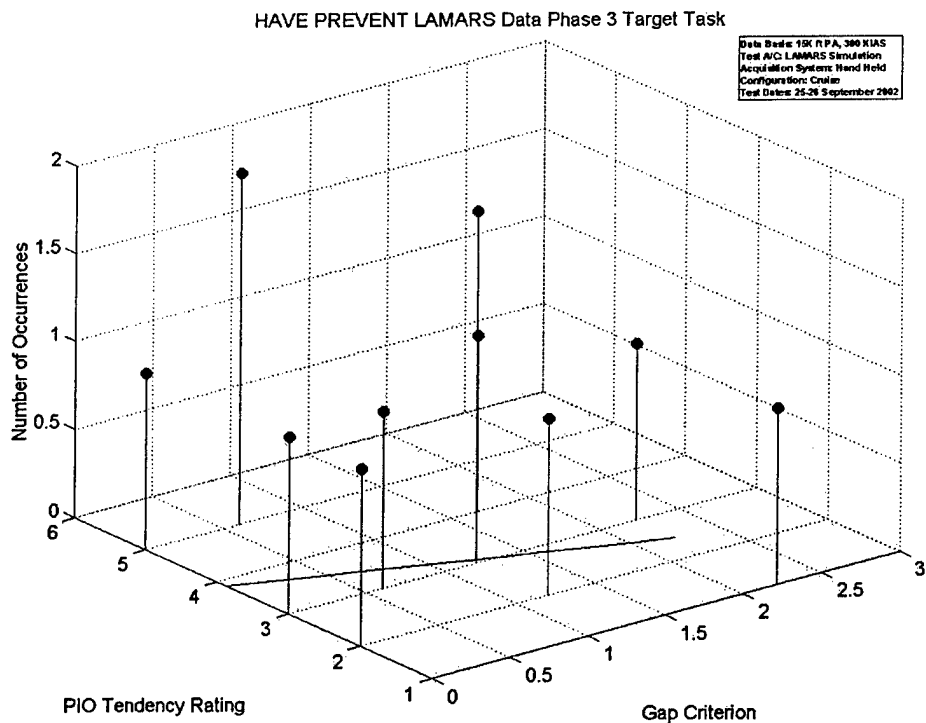


Figure F3B: HAVE PREVENT Phase 3 Target Task LAMARS Data (3D)

HAVE OLOP VISTA Phase 2 Sum-of-Sines Task

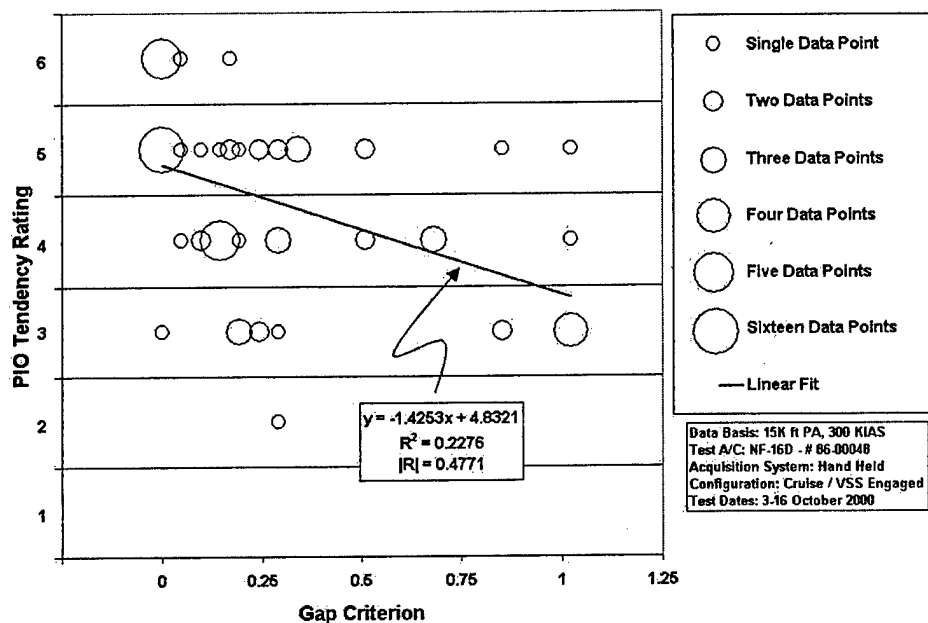


Figure F4A: HAVE OLOP Phase 2 Sum-of-Sines Task Flight Data (2D)

HAVE OLOP FLIGHT Data Phase 2 Sum-of-Sines

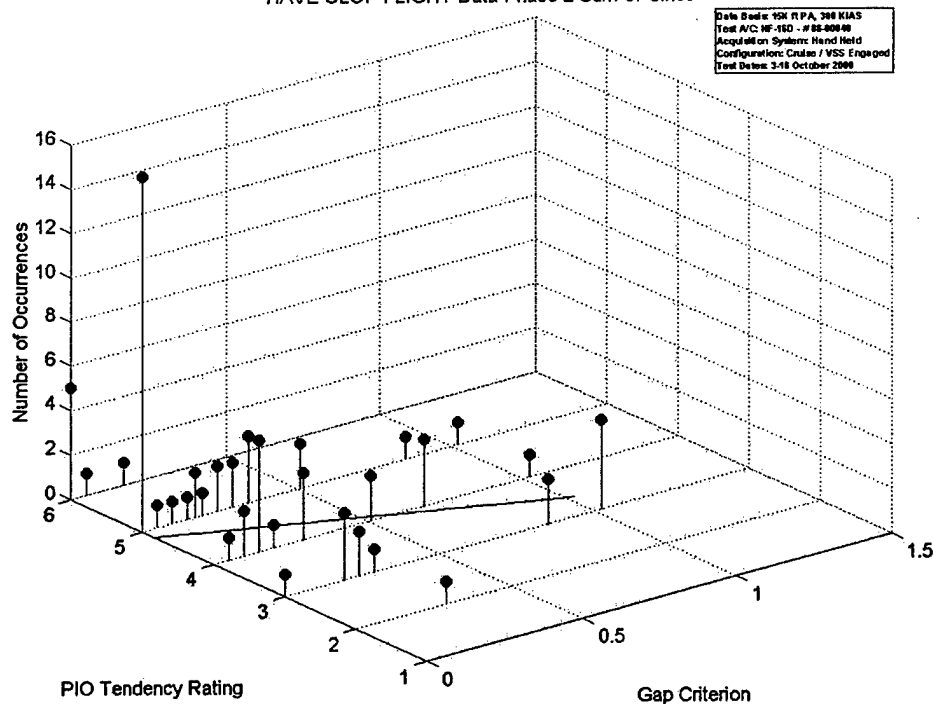


Figure F4B: HAVE OLOP Phase 2 Sum-of-Sines Task Flight Data (3D)

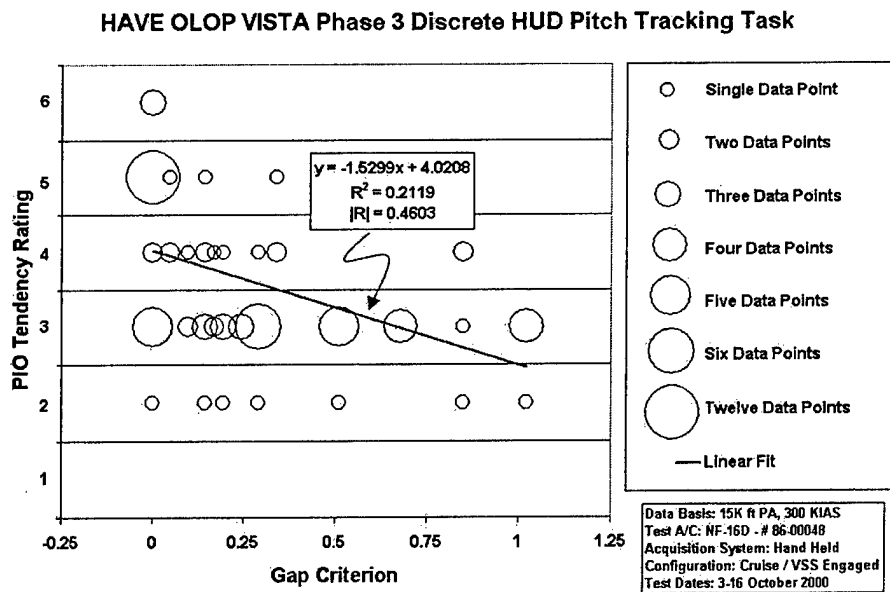


Figure F5A: HAVE OLOP Phase 3 Discrete HUD Tracking Task Flight Data (2D)

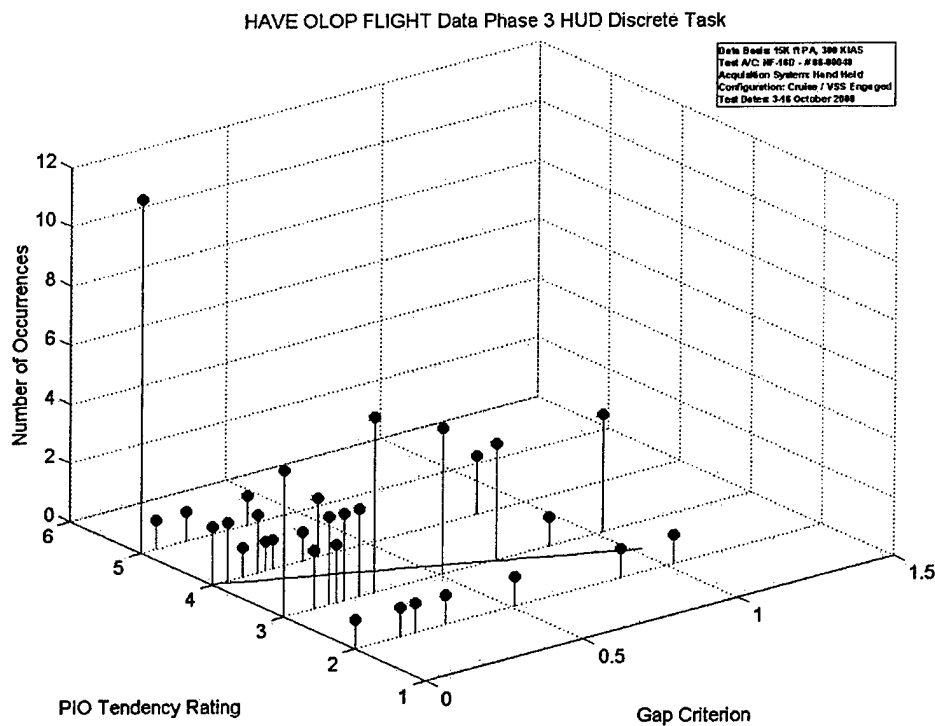


Figure F5B: HAVE OLOP Phase 3 Discrete HUD Tracking Task Flight Data (3D)

APPENDIX G: LAMARS DATA FIGURES

The MAX GAP LAMARS test data figures are in this appendix. There are three types of charts shown. One is a 2D "bubble chart" of the PIO tendency rating versus the *Gap Criterion*. This "bubble chart" uses circles of different diameters to depict data density in terms of the number of times a similar PIO tendency rating is assigned to a single *Gap Criterion* value. Also, a linear curve fit with the corresponding equation, R^2 value, and correlation factor are shown on the 2D "bubble chart." The second type of figure is a 3D stem plot with the same data as the 2D "bubble chart" from a different perspective. The horizontal plane of the 3D chart contains the PIO tendency rating and the *Gap Criterion*. The vertical axis shows the number of occurrences for a single PIO tendency rating for a discrete *Gap Criterion*. An increasing height of the vertical bars corresponds to a greater number of occurrences. The same linear model from the 2D "bubble chart" is shown on the floor of the 3D view. This provides insight into how the data density drives to the model to match the Gap Criterion theory, which states that low Gap values should lead to the high PIO tendency ratings and vice versa. The third chart shown contains stripchart time histories of the following: LAMARS longitudinal stick position; variation of pitch angle and HUD task pitch angle; variation of alpha; left and right elevator position; and actual actuator rate.

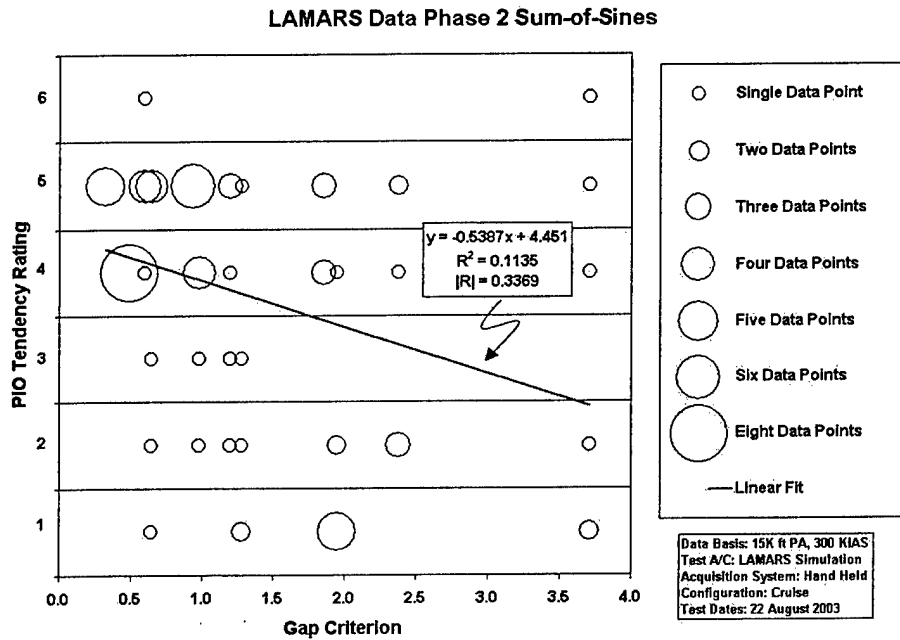


Figure G1A: MAX GAP Phase 2 Sum-of-Sines Task LAMARS Data (2D)

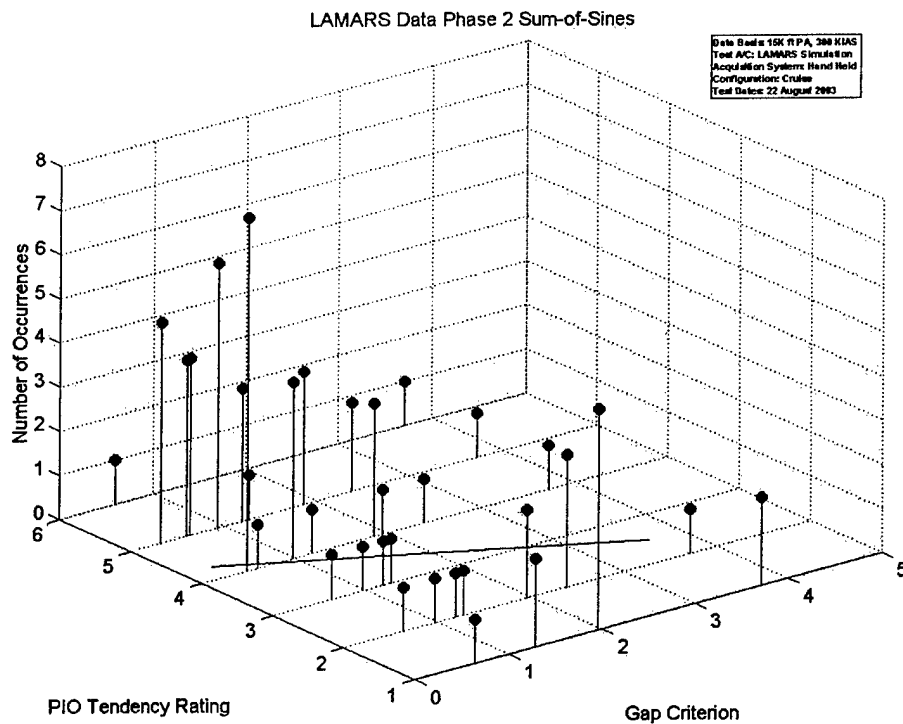


Figure G2B: MAX GAP Phase 2 Sum-of-Sines Task LAMARS Data (3D)

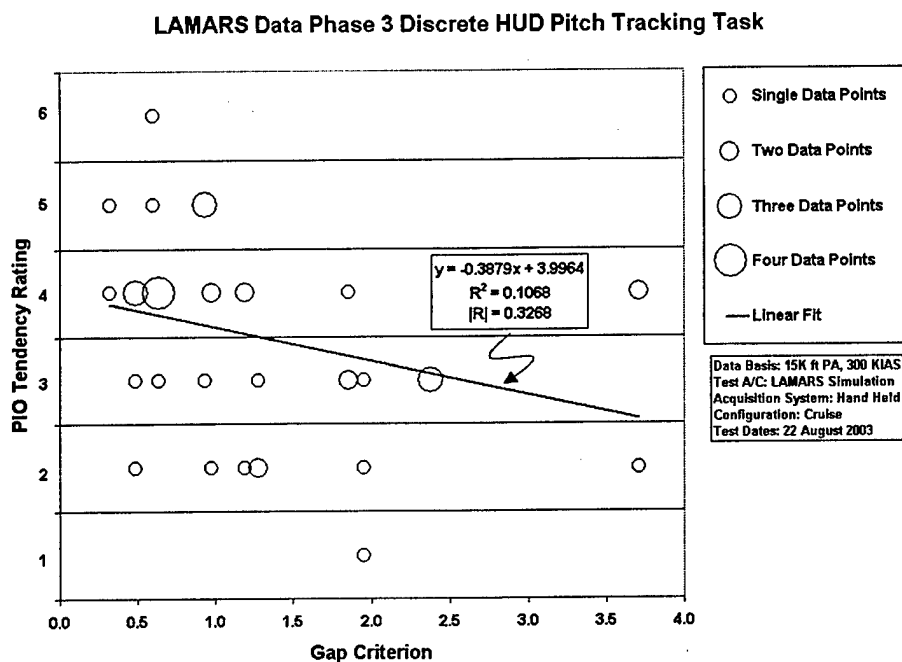


Figure G2A: MAX GAP Phase 3 HUD Discrete Tracking Task LAMARS Data (2D)

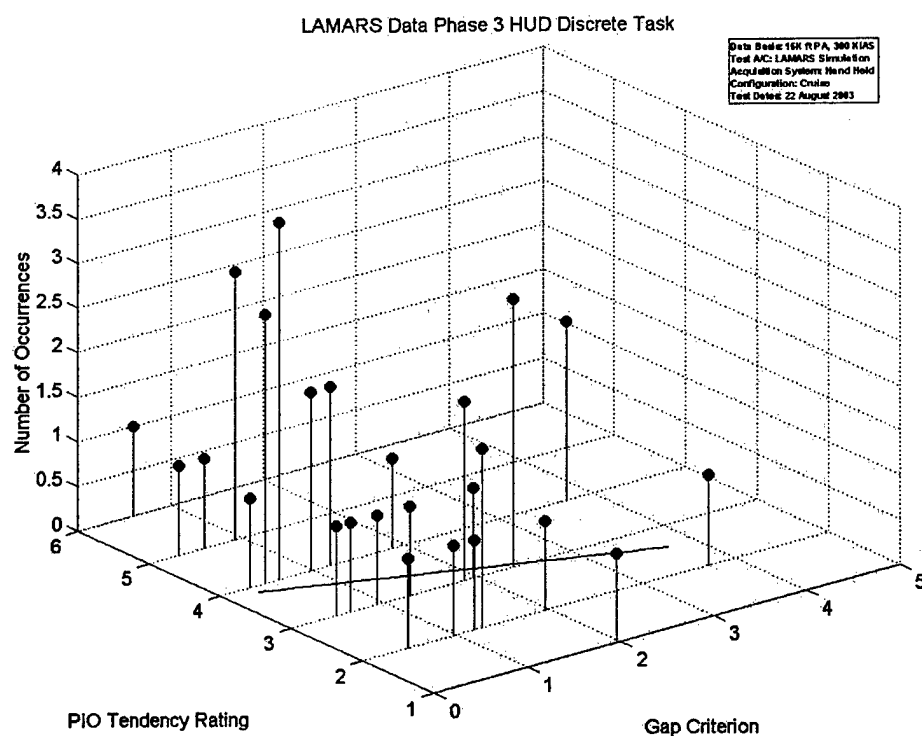


Figure G2B: MAX GAP Phase 3 HUD Discrete Tracking Task LAMARS Data (3D)

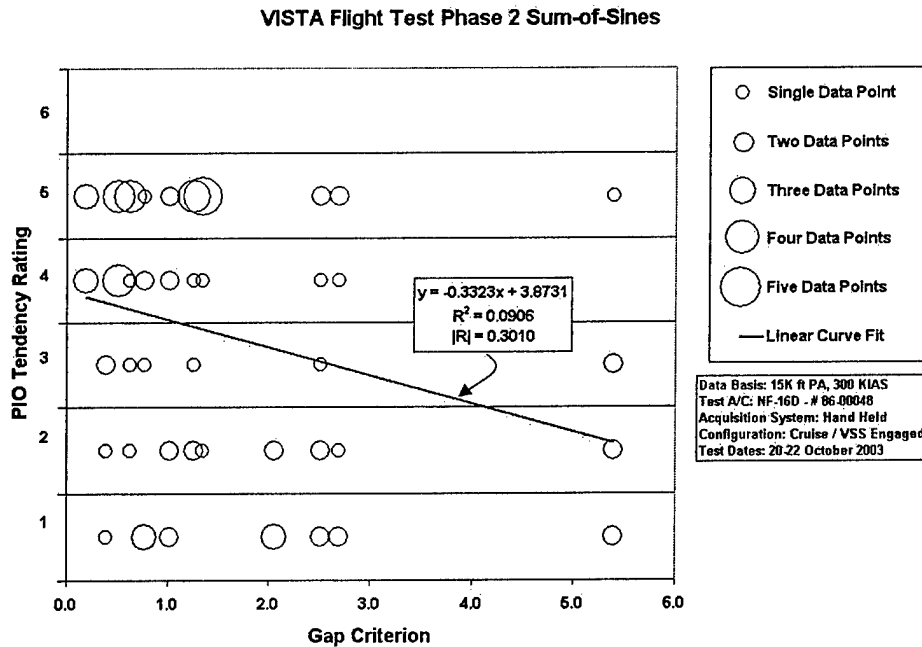


Figure G3A: MAX GAP Phase 3 Target Tracking Task LAMARS Data (2D)

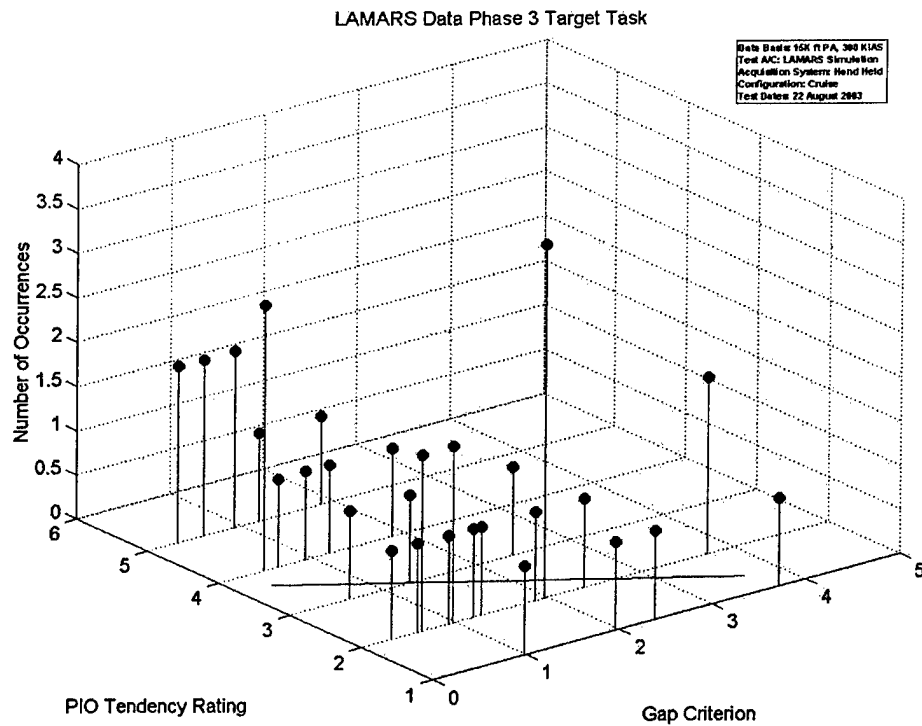


Figure G3B: MAX GAP Phase 3 HUD Target Tracking Task LAMARS Data (3D)

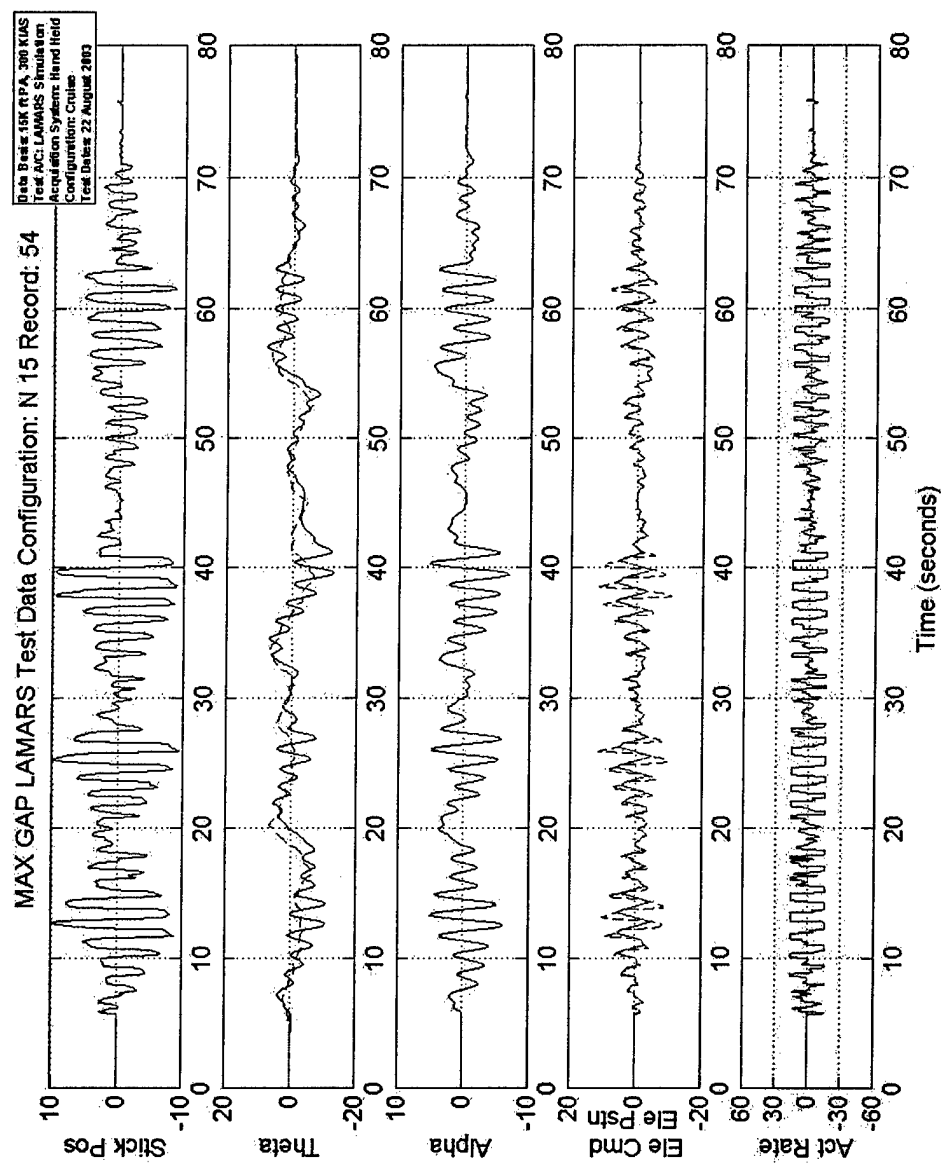


Figure G4: Phase 2 Sum-of-Sines, PIOR: 5

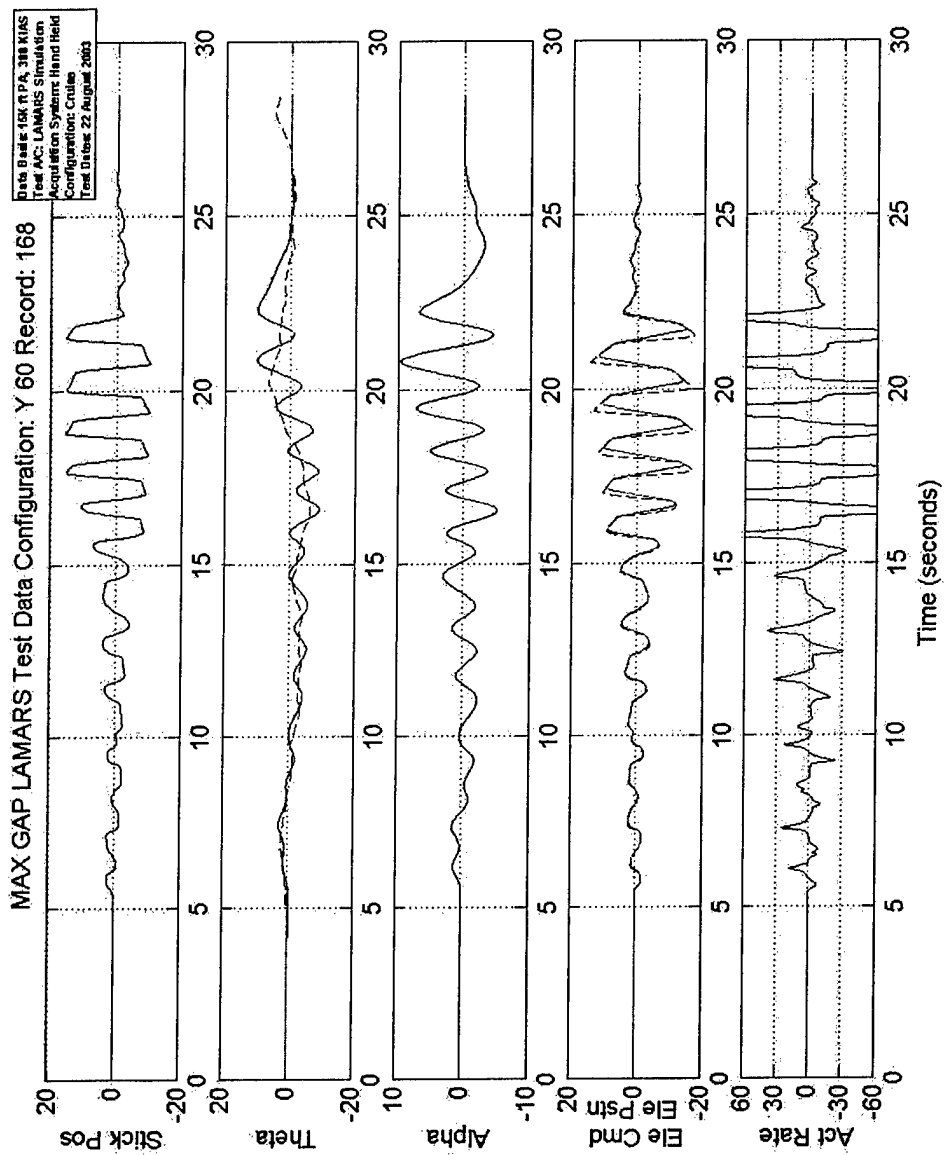


Figure G5: Phase 2 Sum-of-Sines, PIOR: 1

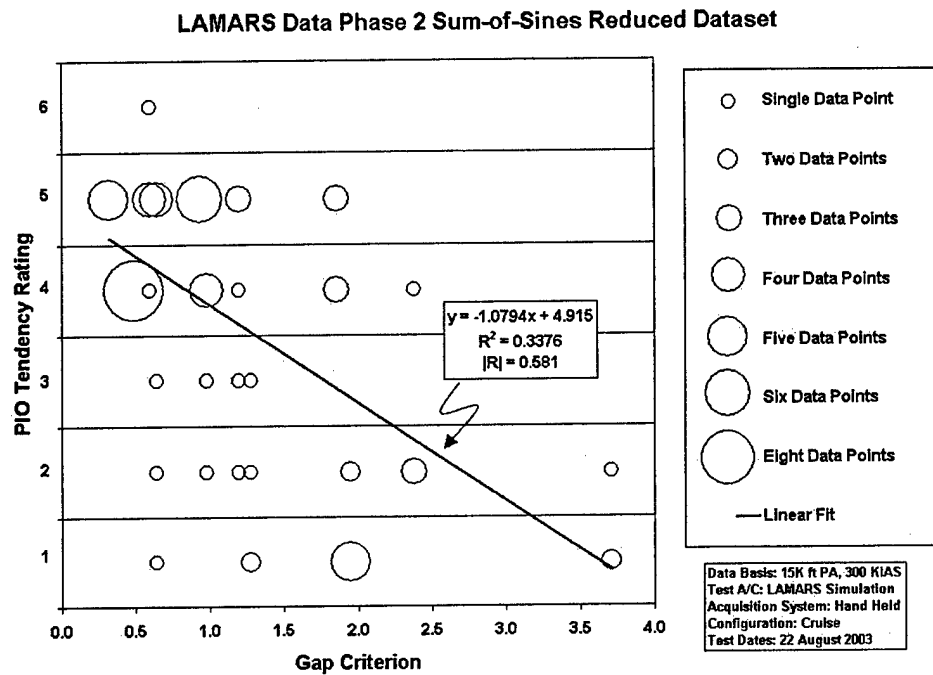


Figure G6A: MAX GAP Phase 2 Sum-of-Sines Tracking Task LAMARS Data Reduced (2D)

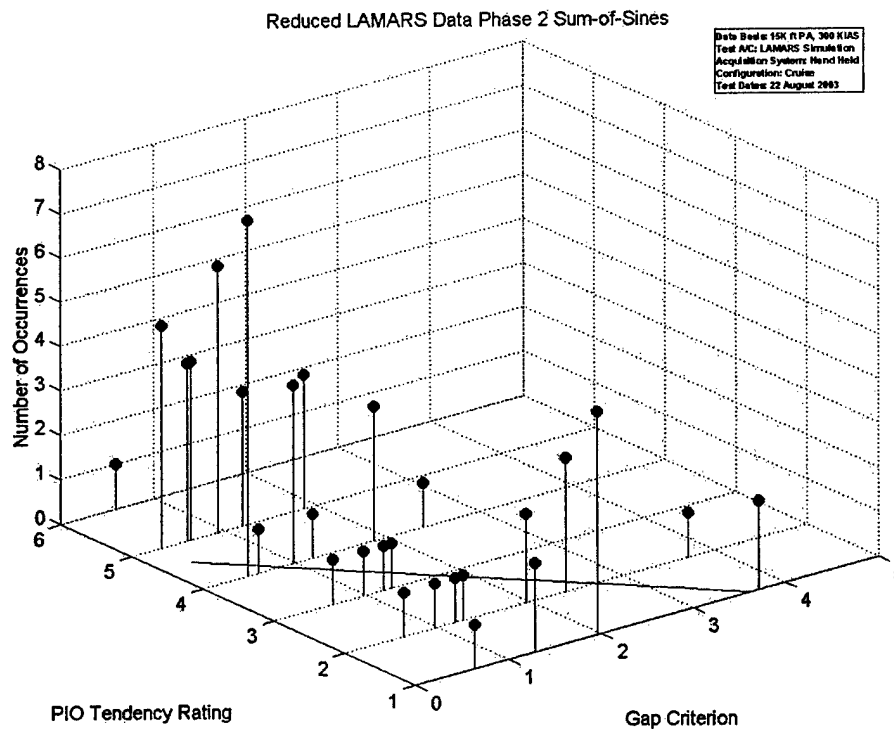


Figure G6B: MAX GAP Phase 2 Sum-of-Sines Tracking Task LAMARS Data Reduced (3D)

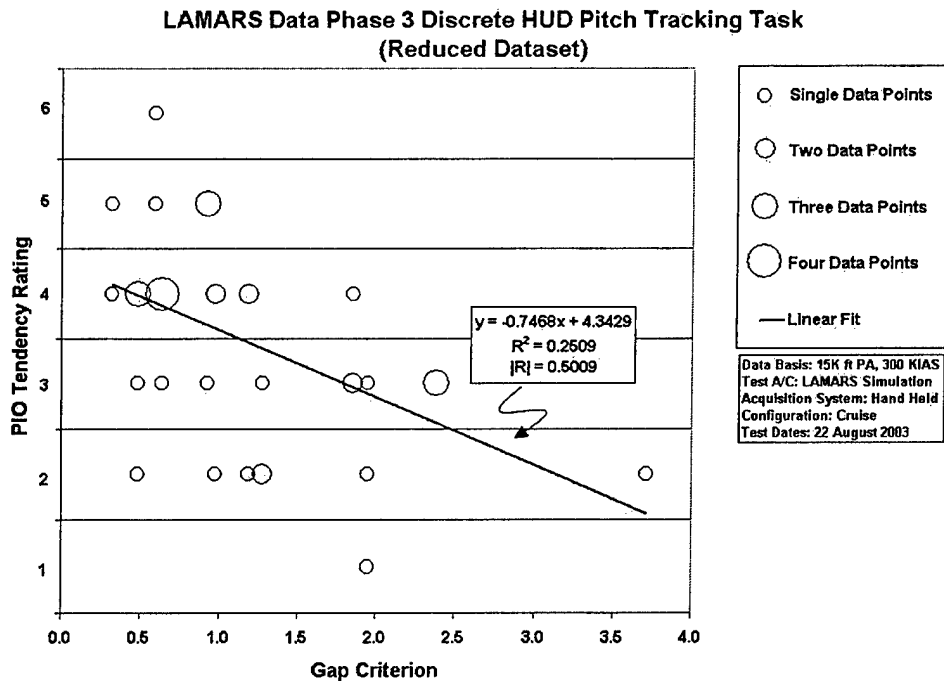


Figure G7A: MAX GAP Phase 3 Discrete Tracking Task LAMARS Data Reduced (2D)

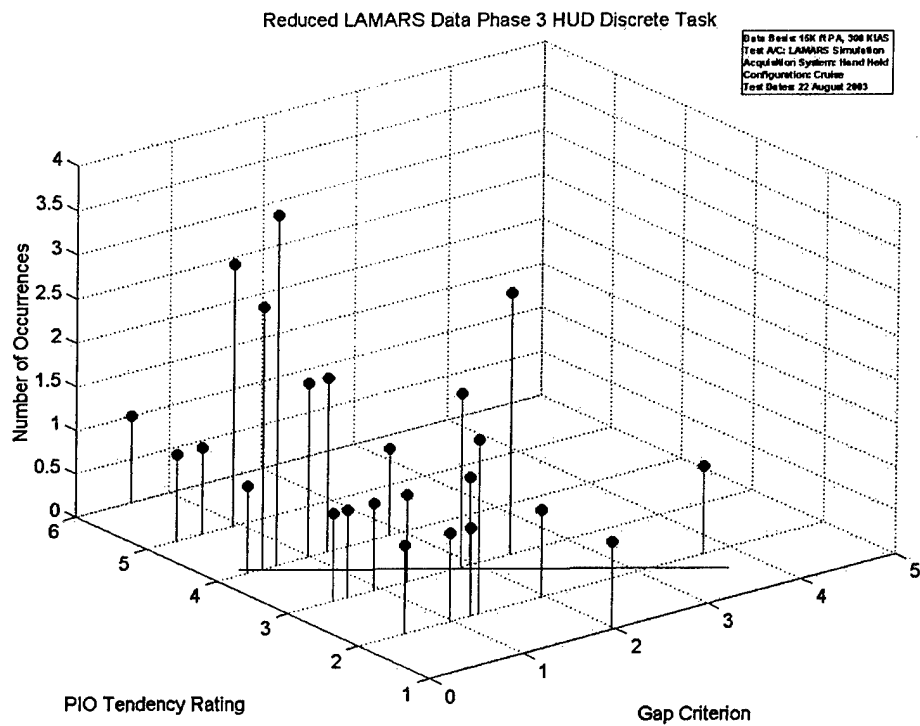


Figure G7B: MAX GAP Phase 3 Discrete Tracking Task LAMARS Data Reduced (3D)

APPENDIX H: VISTA DATA FIGURES

The MAX GAP flight test data figures are in this appendix. There are three types of charts shown. One is a 2D "bubble chart" of the PIO tendency rating versus the *Gap Criterion*. This "bubble chart" uses circles of different diameters to depict data density in terms of the number of times a similar PIO tendency rating is assigned to a single *Gap Criterion* value. Also, a linear curve fit with the corresponding equation, R^2 value, and correlation factor are shown on the 2D "bubble chart." The second type of figure is a 3D stem plot with the same data as the 2D "bubble chart" from a different perspective. The horizontal plane of the 3D chart contains the PIO tendency rating and the *Gap Criterion*. The vertical axis shows the number of occurrences for a single PIO tendency rating for a discrete *Gap Criterion*. An increasing height of the vertical bars corresponds to a greater number of occurrences. The same linear model from the 2D "bubble chart" is shown on the floor of the 3D view. This provides insight into how the data density drives to the model to match the *Gap Criterion* theory, which states that low *Gap* values should lead to the high PIO tendency ratings and vice versa. The third chart shown contains time histories of the following: VISTA longitudinal center stick position; variation of pitch angle and HUD task pitch angle; pilot g; left and right stab position; and commanded along with actual actuator rate.

VISTA Flight Test Phase 2 Sum-of-Sines

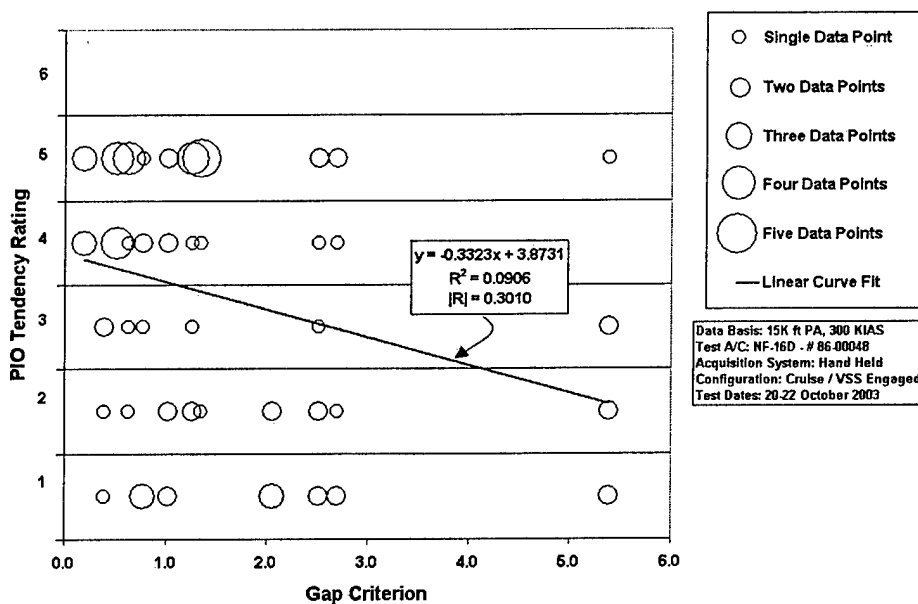


Figure H1A: MAX GAP Phase 2 Sum-of-Sines Task Flight Data (2D)

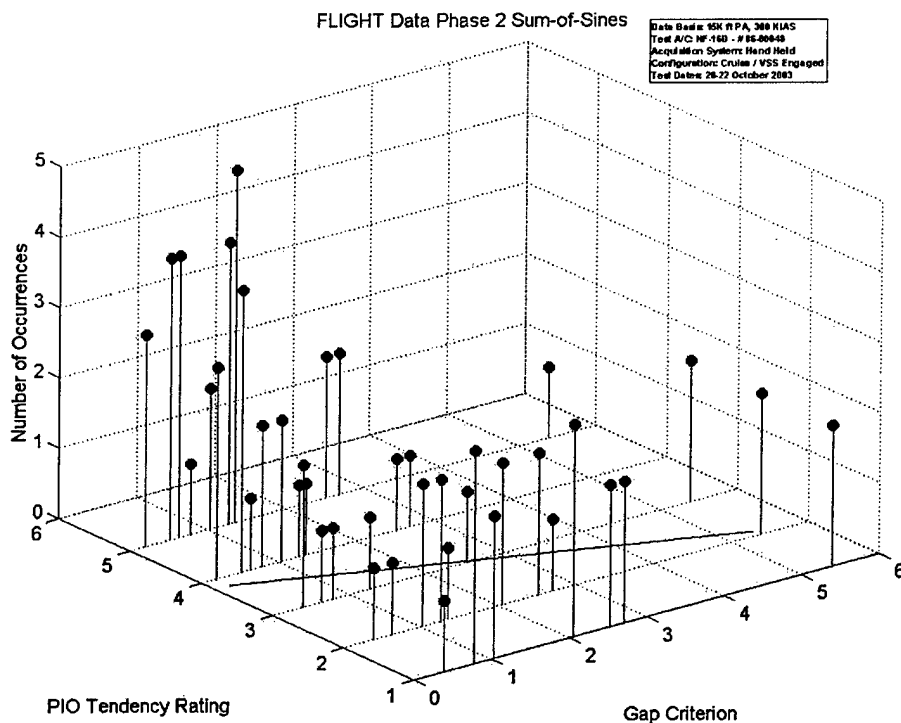


Figure H1B: MAX GAP Phase 2 Sum-of-Sines Task Flight Data (3D)

VISTA Flight Test Phase 3 Discrete Pitch Tracking Task

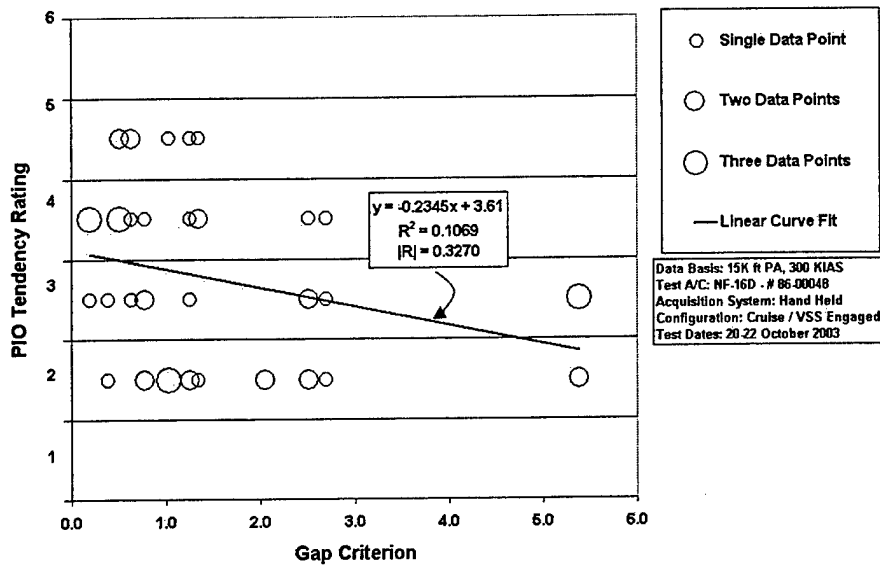


Figure H2A: MAX GAP Phase 3 Discrete HUD Tracking Task Flight Data (2D)

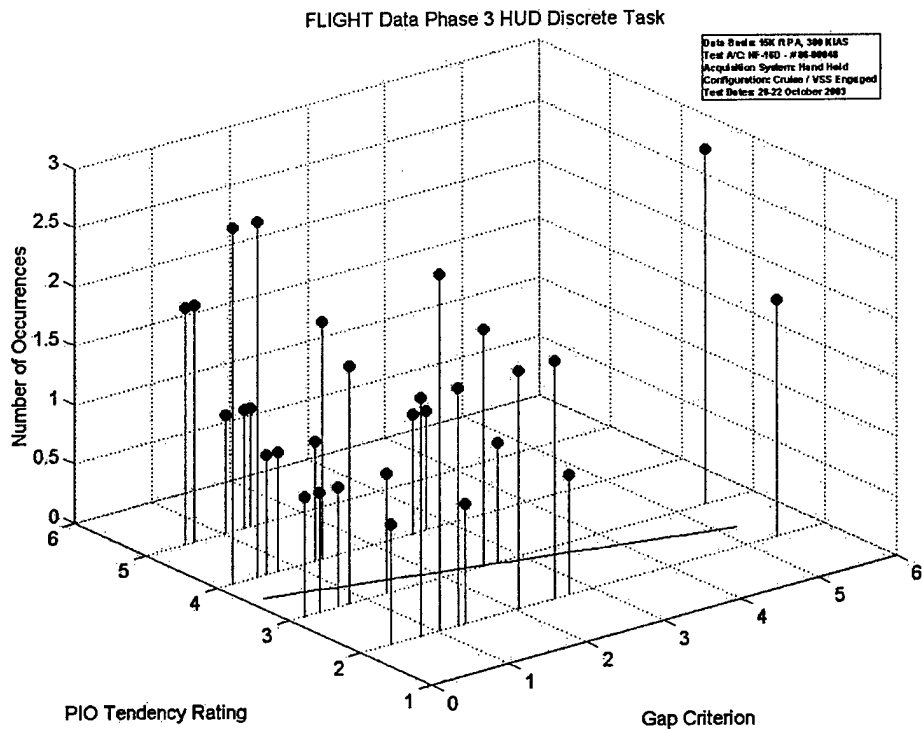


Figure H2B: MAX GAP Phase 3 Discrete HUD Tracking Task Flight Data (3D)

VISTA Flight Test Phase 3 Target Tracking Task

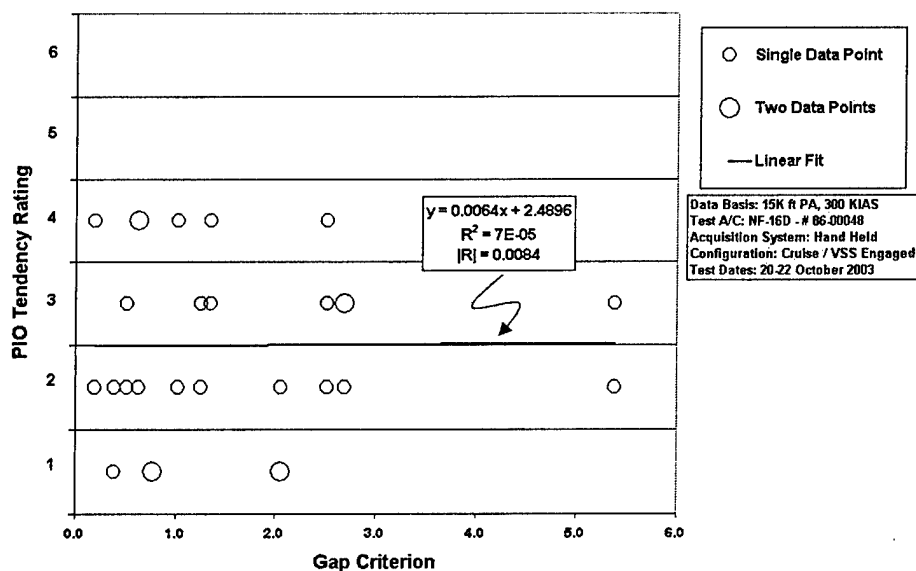


Figure H3A: MAX GAP Phase 3 Target Task Flight Data (2D)

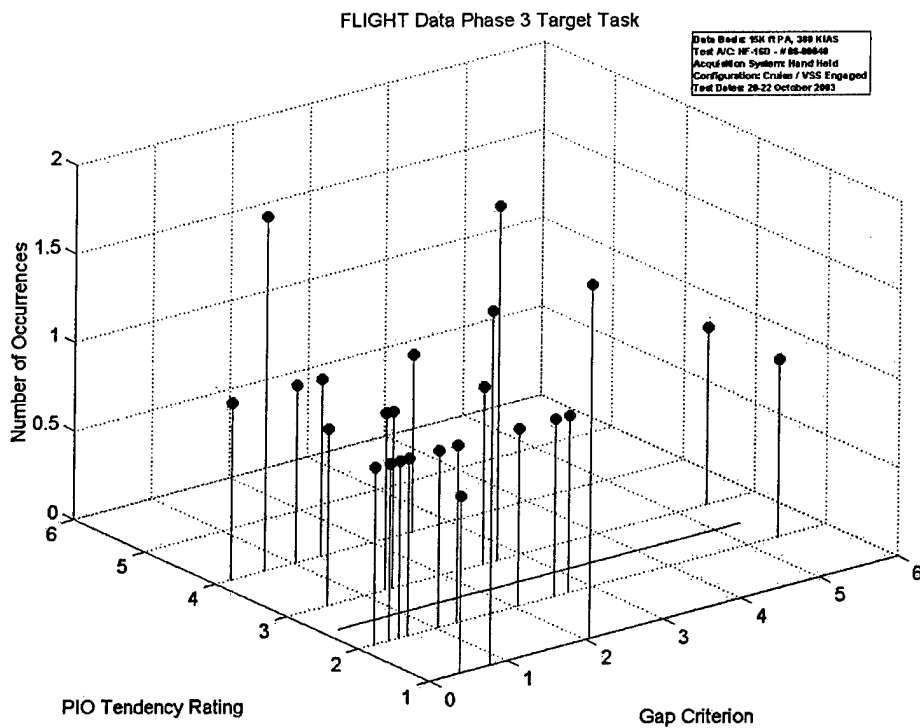


Figure H3B: MAX GAP Phase 3 Target Task Flight Data (3D)

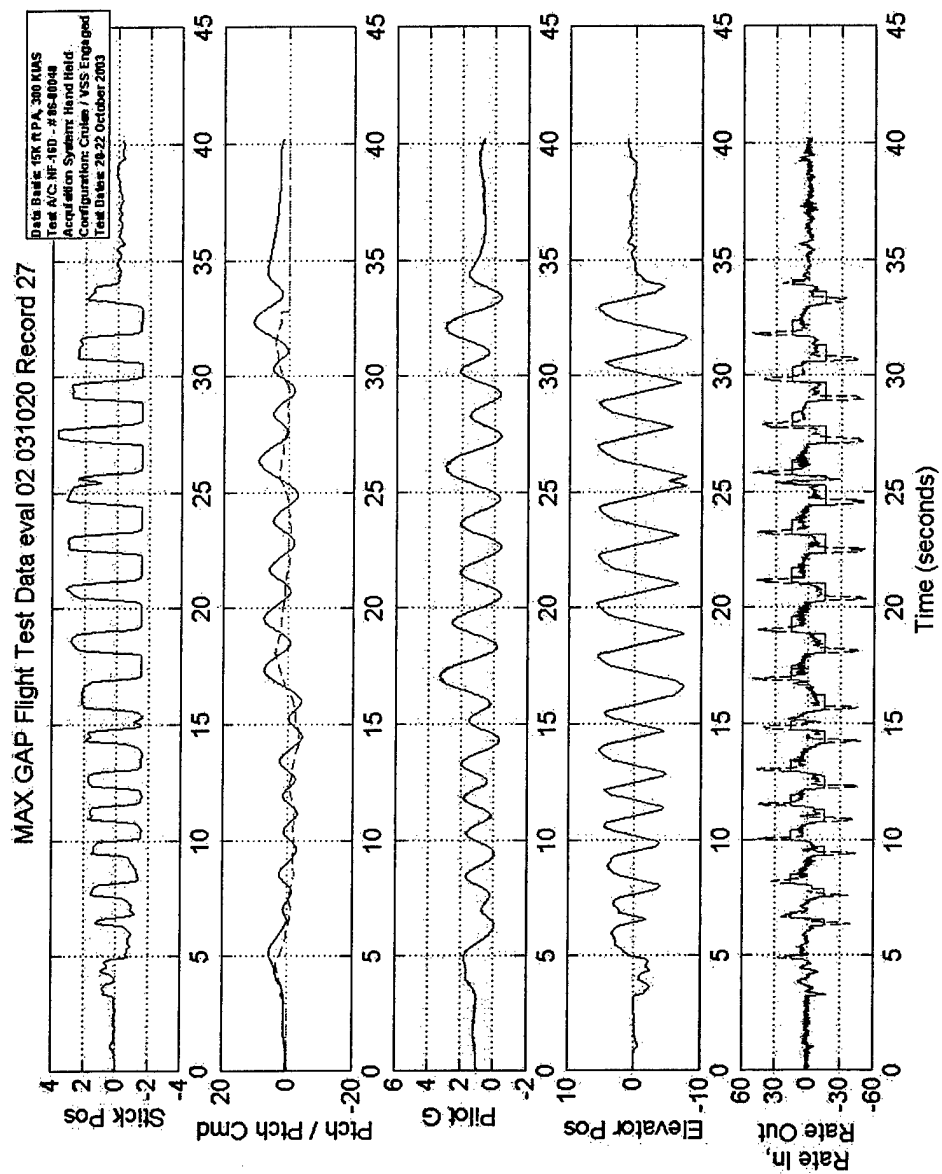


Figure H4: Phase 2 Sum-of-Sines, PIOR: 5

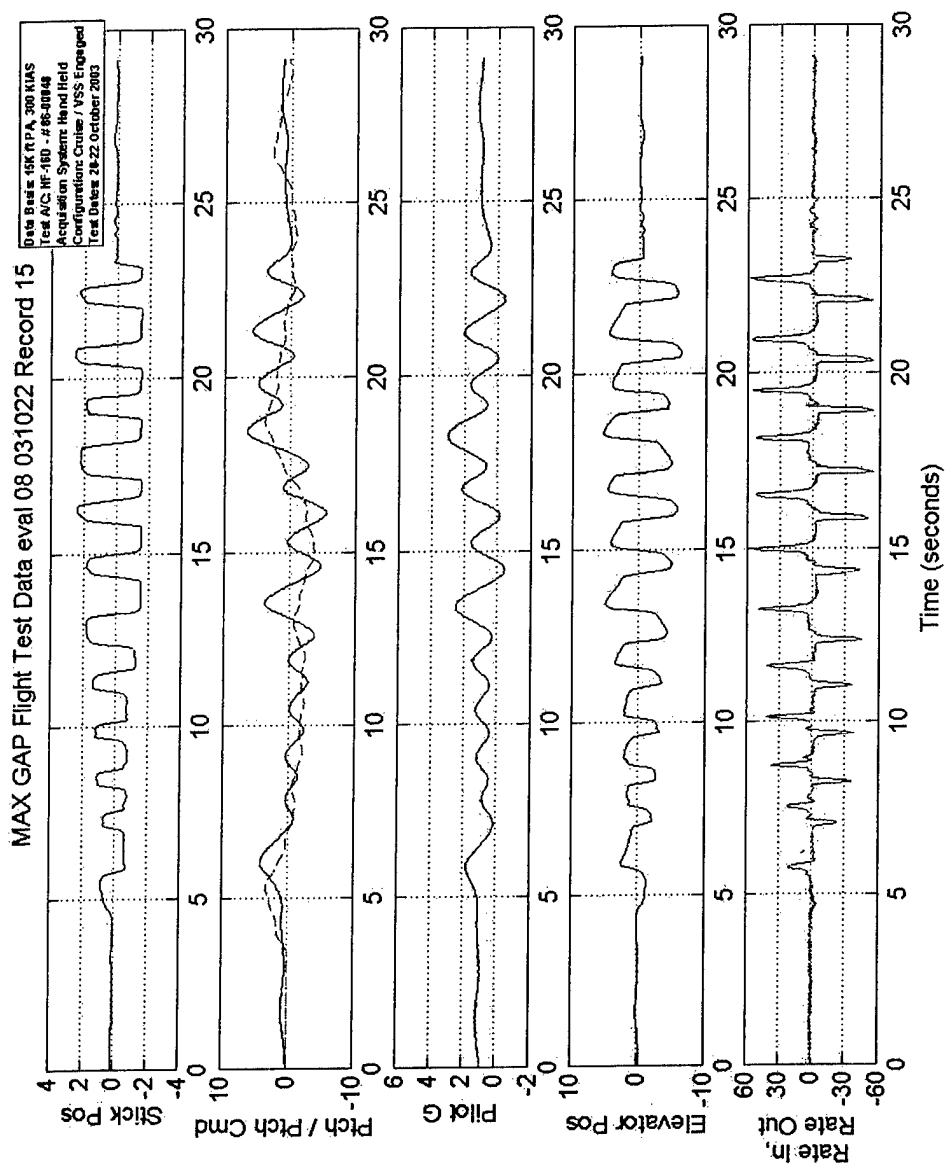


Figure H5: Phase 2 Sum-of-Sines, PIOR: 1

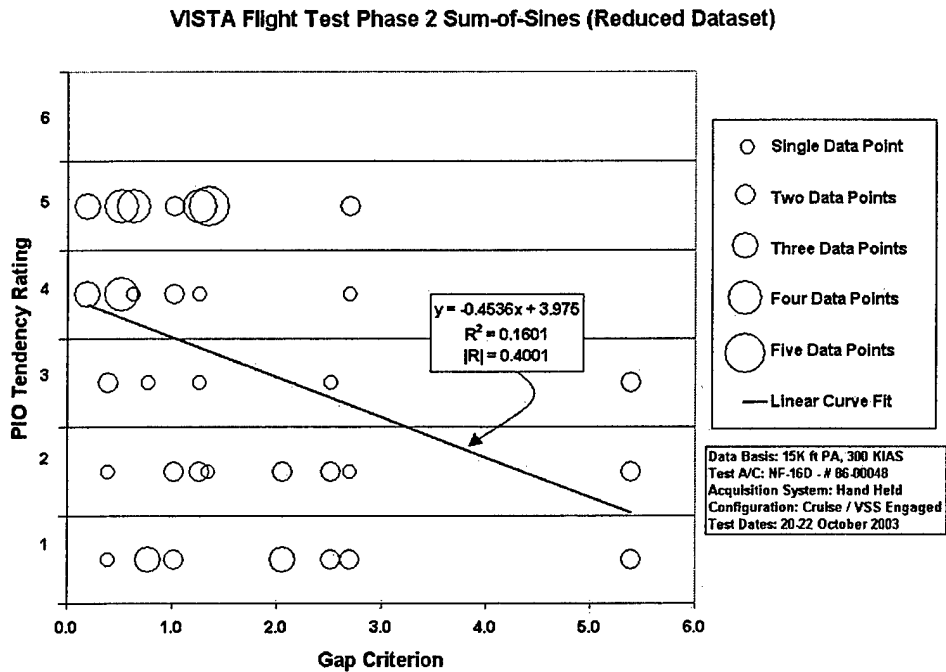


Figure H6A: MAX GAP Phase 2 Sum-of-Sines Task Flight Data Reduced (2D)

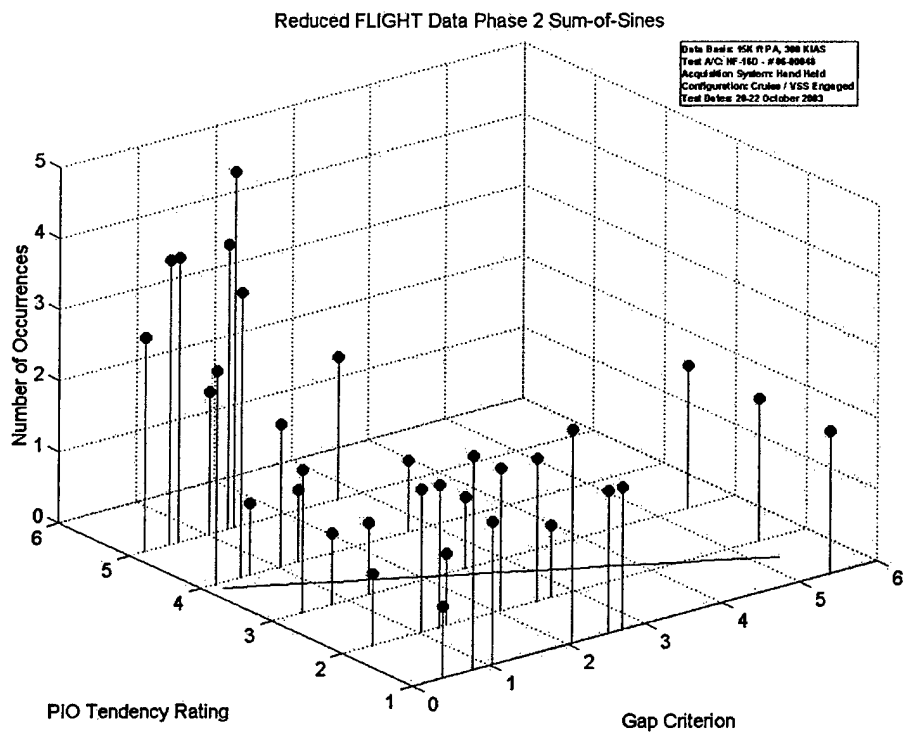


Figure H6B: MAX GAP Phase 2 Sum-of-Sines Task Flight Data Reduced (3D)

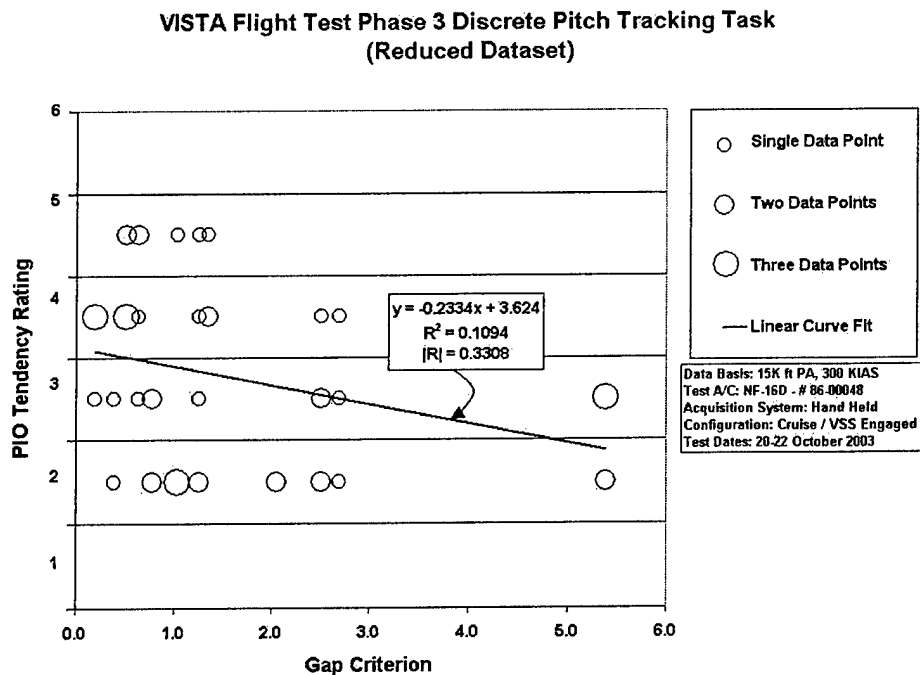


Figure H7A: MAX GAP Phase 3 Discrete HUD Tracking Task Flight Data Reduced (2D)

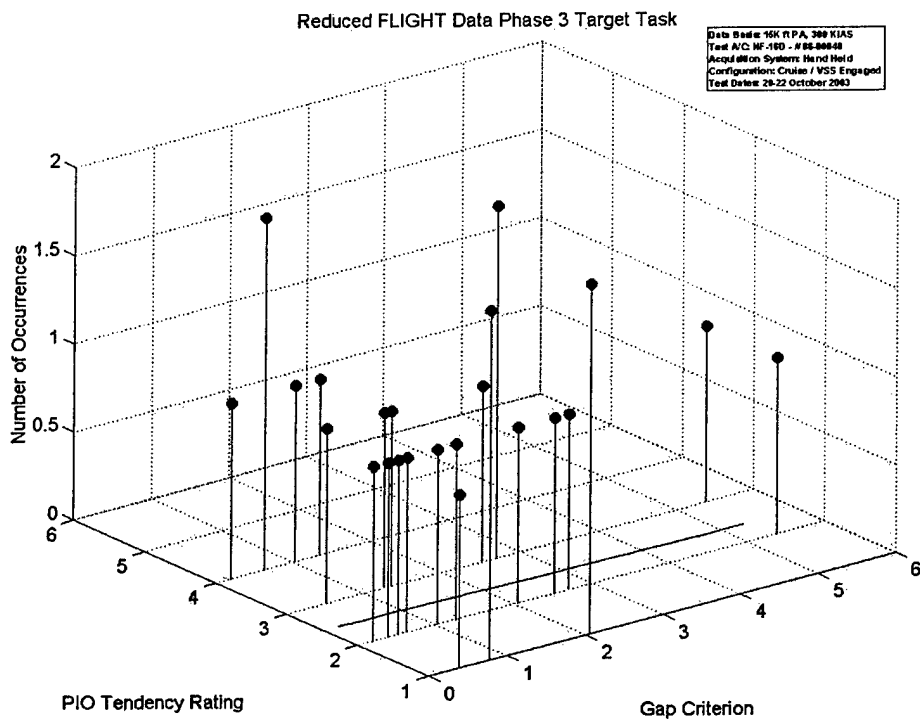


Figure H7B: MAX GAP Phase 3 Discrete HUD Tracking Task Flight Data Reduced (3D)

VISTA Flight Test Phase 3 Target Tracking Task (Reduced Dataset)

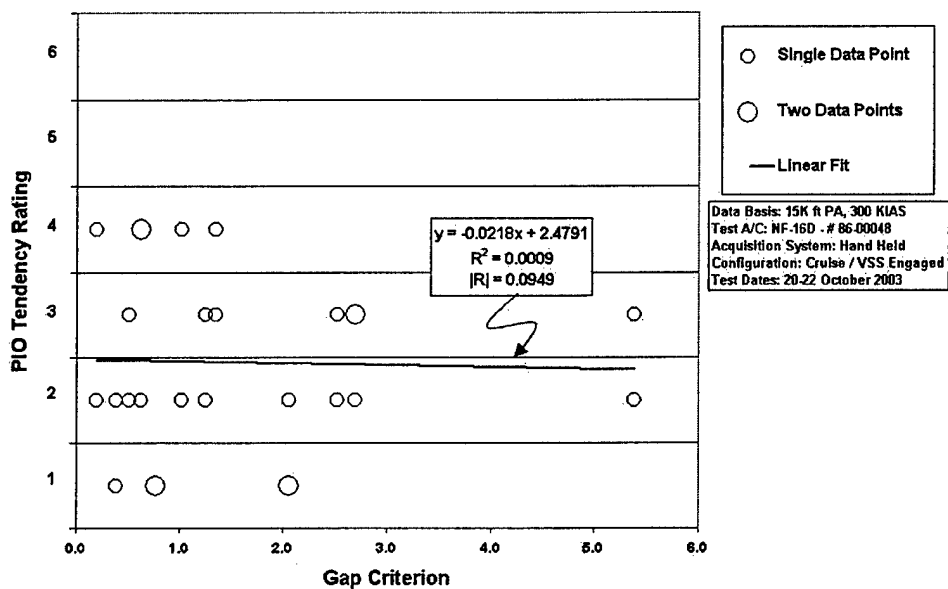


Figure H8A: MAX GAP Phase 3 Target Task Flight Data Reduced (2D)

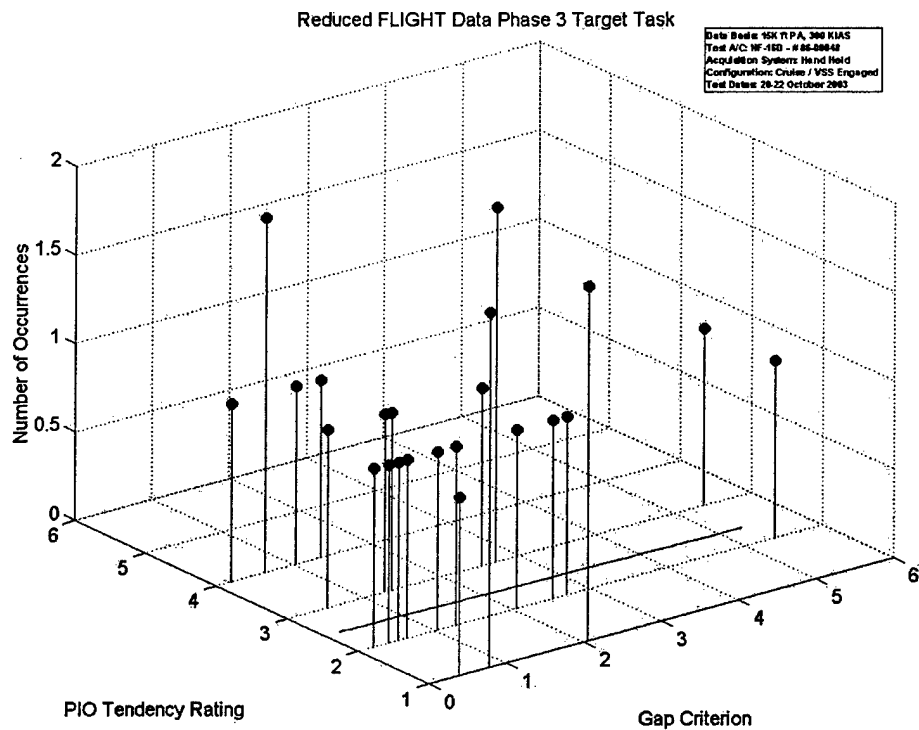


Figure H8B: MAX GAP Phase 3 Target Task Flight Data Reduced (3D)

THIS PAGE INTENTIONALLY LEFT BLANK

APPENDIX I: LAMARS SIMULATOR HISTOGRAMS

The MAX GAP LAMARS test histograms are contained in this appendix. Pilots 1, 2 and 3 were the same individual in each case.

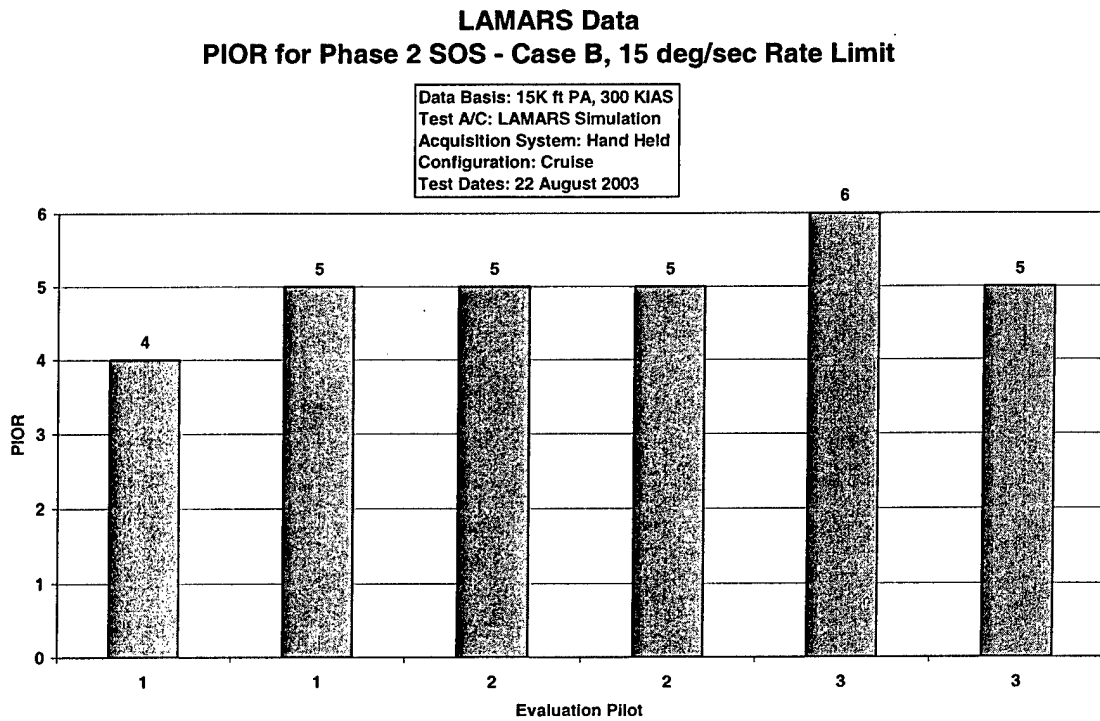


Figure I1 LAMARS Data, Case B, 15 deg/sec

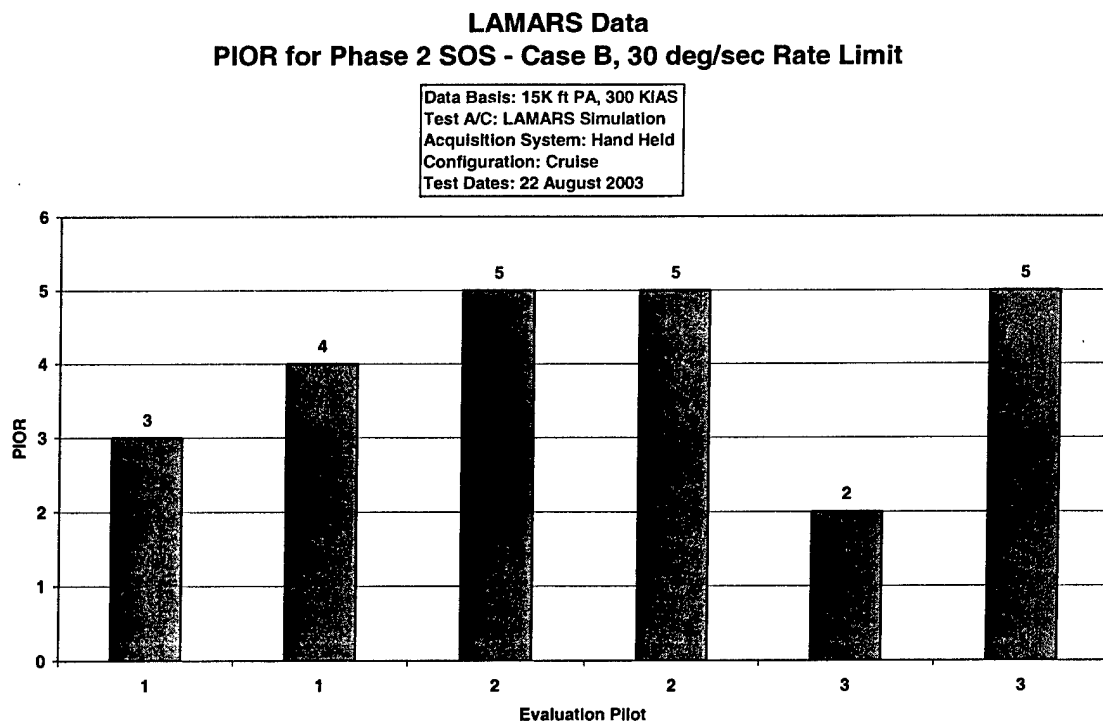


Figure I2 LAMARS Data, Case B, 30 deg/sec

LAMARS Data
PIOR for Phase 2 SOS - Case B, 60 deg/sec Rate Limit

Data Basis: 15K ft PA, 300 KIAS
Test A/C: LAMARS Simulation
Acquisition System: Hand Held
Configuration: Cruise
Test Dates: 22 August 2003

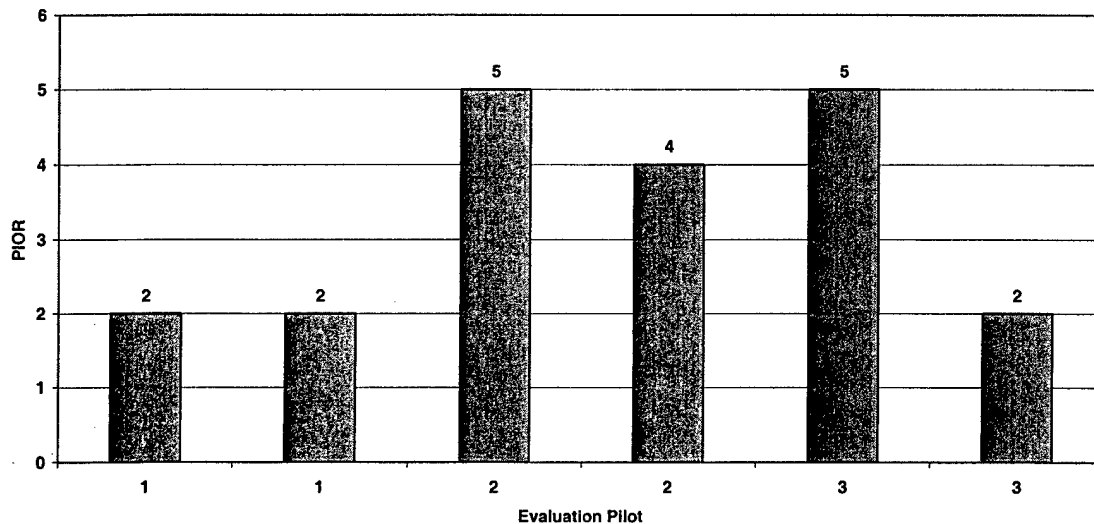


Figure I3 LAMARS Data, Case B, 60 deg/sec

LAMARS Data
PIOR for Phase 2 SOS - Case N, 15 deg/sec Rate Limit

Data Basis: 15K ft PA, 300 KIAS
Test A/C: LAMARS Simulation
Acquisition System: Hand Held
Configuration: Cruise
Test Dates: 22 August 2003

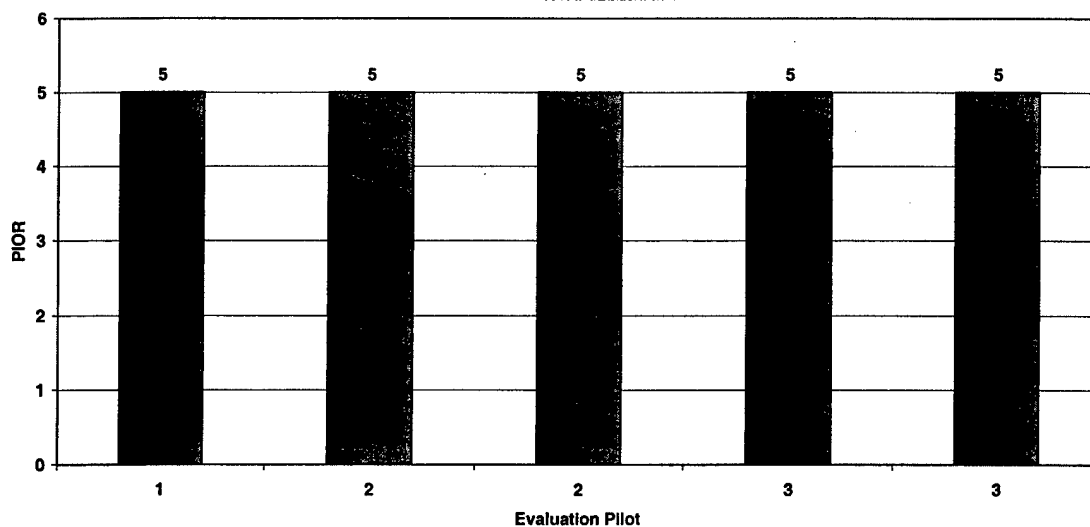


Figure I4 LAMARS Data, Case N, 15 deg/sec

LAMARS Data
PIOR for Phase 2 SOS - Case N, 30 deg/sec Rate Limit

Data Basis: 15K ft PA, 300 KIAS
Test A/C: LAMARS Simulation
Acquisition System: Hand Held
Configuration: Cruise
Test Dates: 22 August 2003

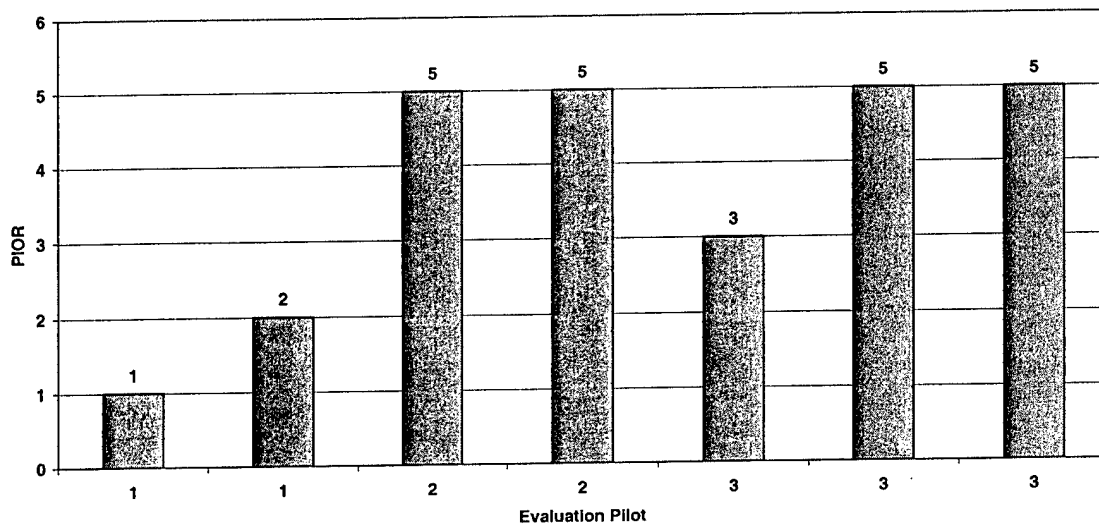


Figure I5 LAMARS Data, Case N, 30 deg/sec

LAMARS Data
PIOR for Phase 2 SOS - Case N, 60 deg/sec Rate Limit

Data Basis: 15K ft PA, 300 KIAS
Test A/C: LAMARS Simulation
Acquisition System: Hand Held
Configuration: Cruise
Test Dates: 22 August 2003

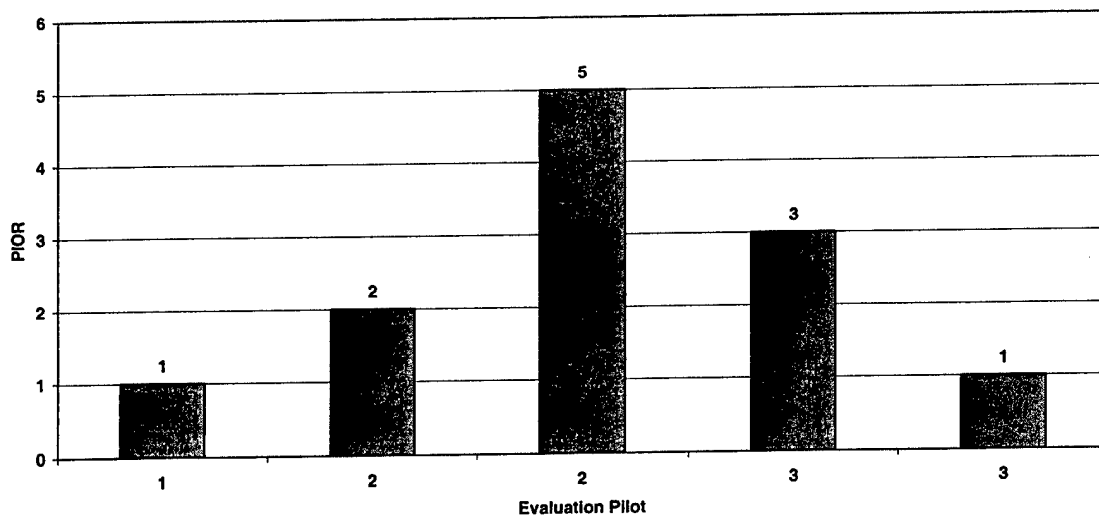


Figure I6 LAMARS Data, Case N, 60 deg/sec

LAMARS Data
PIOR for Phase 2 SOS - Case W, 15 deg/sec Rate Limit

Data Basis: 15K ft PA, 300 KIAS
Test A/C: LAMARS Simulation
Acquisition System: Hand Held
Configuration: Cruise
Test Dates: 22 August 2003

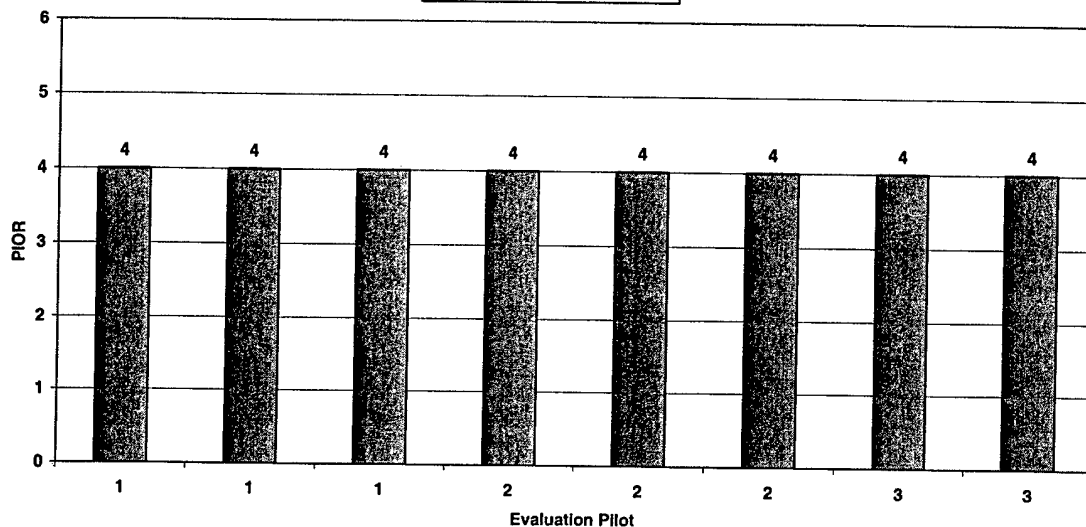


Figure I7 LAMARS Data, Case W, 15 deg/sec

LAMARS Data
PIOR for Phase 2 SOS - Case W, 30 deg/sec Rate Limit

Data Basis: 15K ft PA, 300 KIAS
Test A/C: LAMARS Simulation
Acquisition System: Hand Held
Configuration: Cruise
Test Dates: 22 August 2003

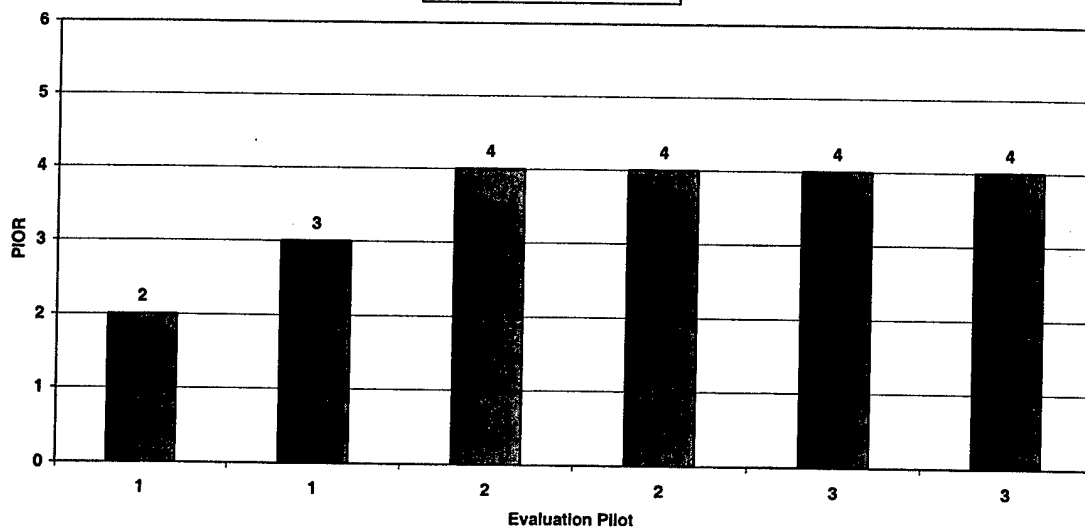


Figure I8 LAMARS Data, Case W, 30 deg/sec

LAMARS Data
PIOR for Phase 2 SOS - Case W, 60 deg/sec Rate Limit

Data Basis: 15K ft PA, 300 KIAS
Test A/C: LAMARS Simulation
Acquisition System: Hand Held
Configuration: Cruise
Test Dates: 22 August 2003

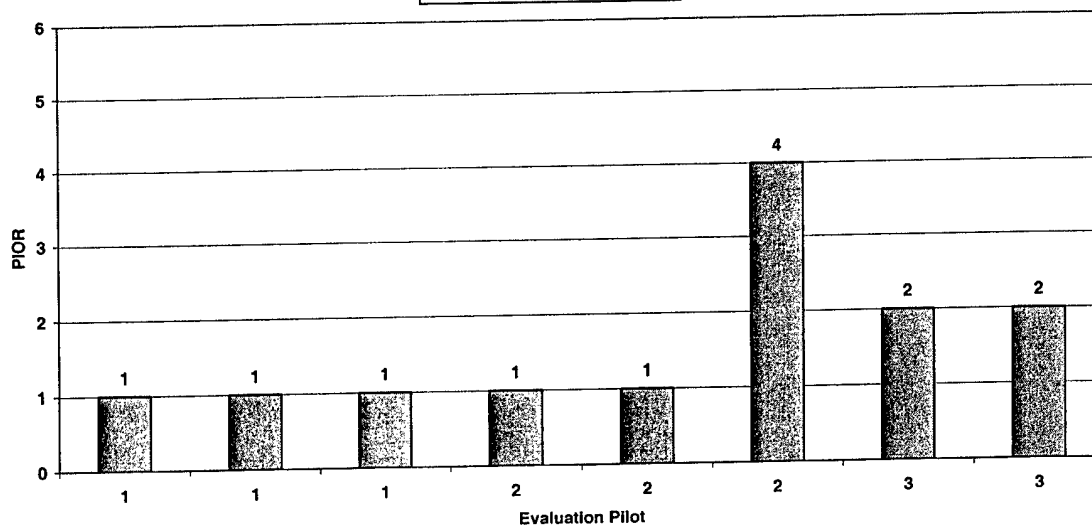


Figure I9 LAMARS Data, Case W, 60 deg/sec

LAMARS Data
PIOR for Phase 2 SOS - Case Y, 15 deg/sec Rate Limit

Data Basis: 15K ft PA, 300 KIAS
Test A/C: LAMARS Simulation
Acquisition System: Hand Held
Configuration: Cruise
Test Dates: 22 August 2003

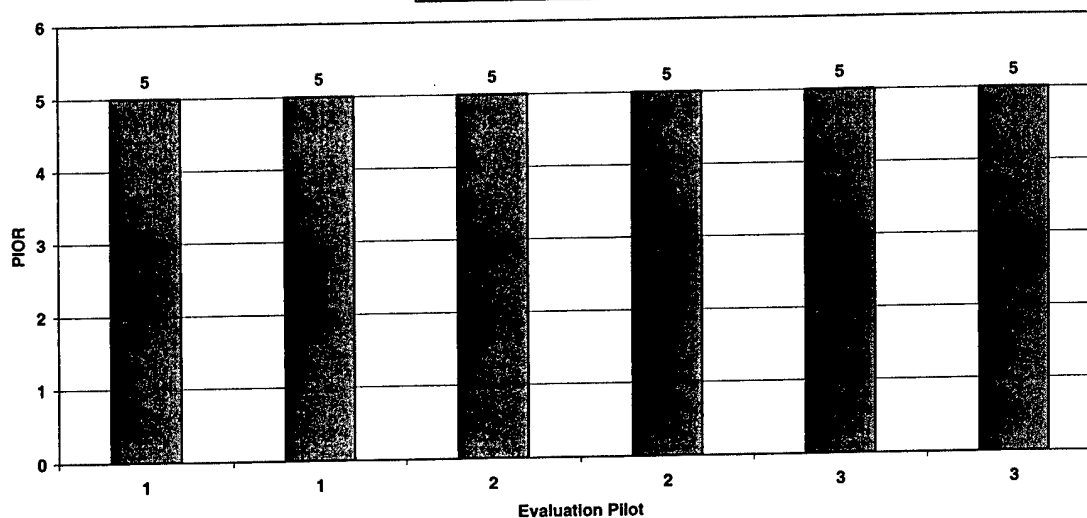


Figure I10 LAMARS Data, Case Y, 15 deg/sec

LAMARS Data
PIOR for Phase 2 SOS - Case Y, 30 deg/sec Rate Limit

Data Basis: 15K ft PA, 300 KIAS
Test A/C: LAMARS Simulation
Acquisition System: Hand Held
Configuration: Cruise
Test Dates: 22 August 2003

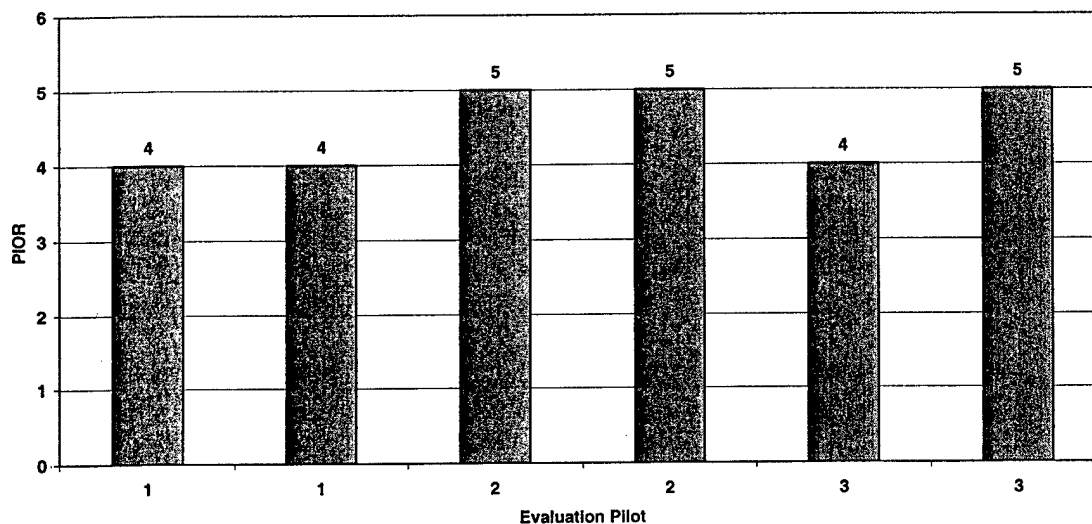


Figure I11 LAMARS Data, Case Y, 30 deg/sec

LAMARS Data
PIOR for Phase 2 SOS - Case Y, 60 deg/sec Rate Limit

Data Basis: 15K ft PA, 300 KIAS
Test A/C: LAMARS Simulation
Acquisition System: Hand Held
Configuration: Cruise
Test Dates: 22 August 2003

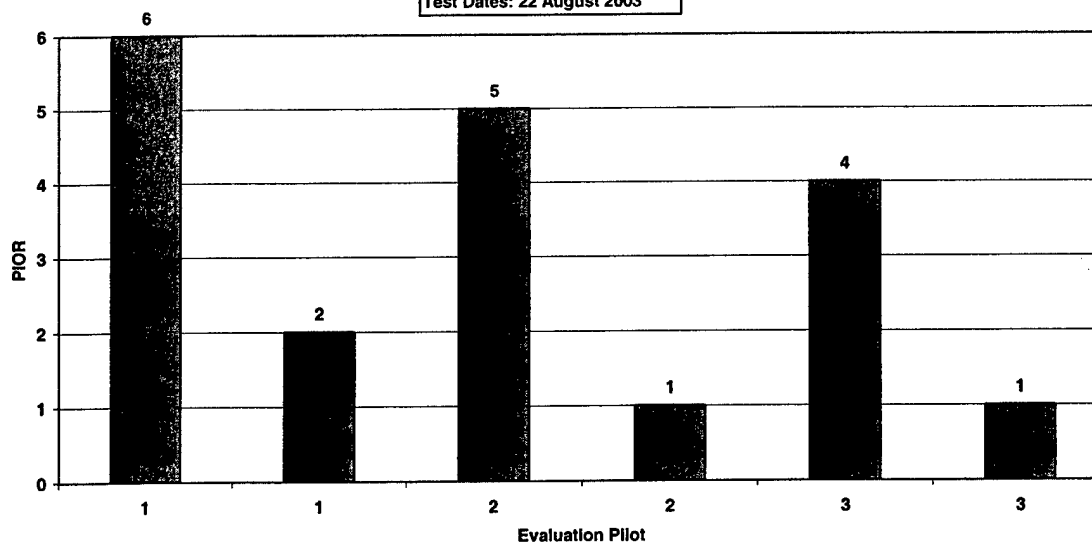


Figure I12 LAMARS Data, Case Y, 60 deg/sec

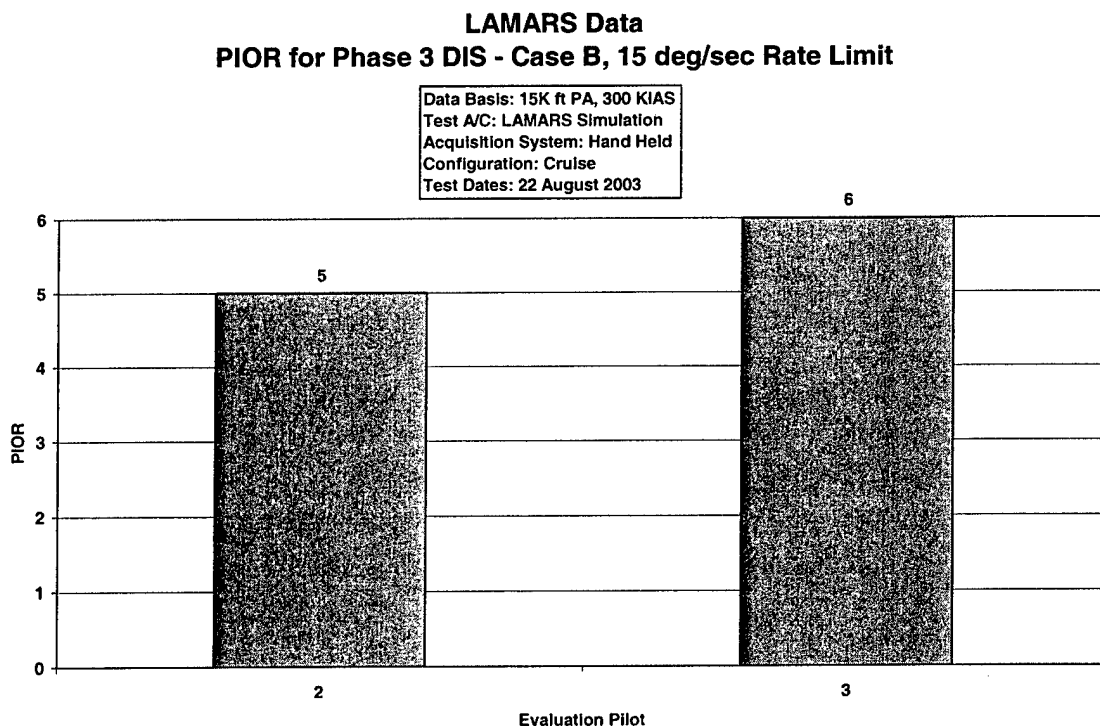


Figure I13 LAMARS Data, Case B, 15 deg/sec

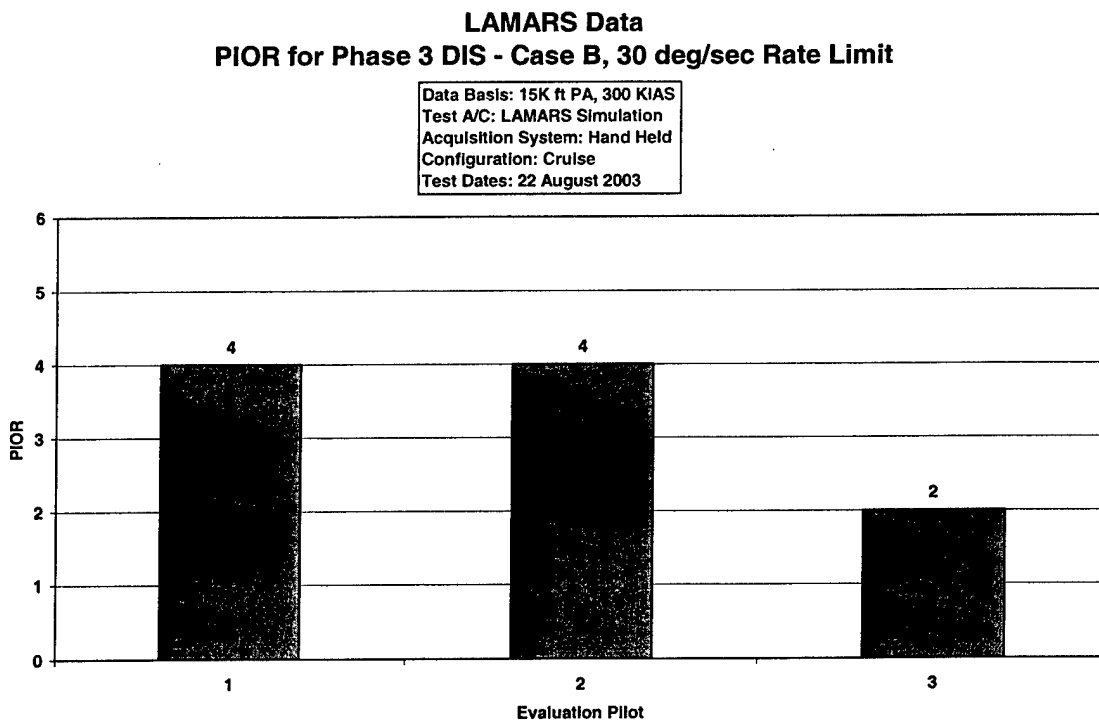


Figure I14 LAMARS Data, Case B, 30 deg/sec

LAMARS Data
PIOR for Phase 3 DIS - Case B, 60 deg/sec Rate Limit

Data Basis: 15K ft PA, 300 KIAS
Test A/C: LAMARS Simulation
Acquisition System: Hand Held
Configuration: Cruise
Test Dates: 22 August 2003

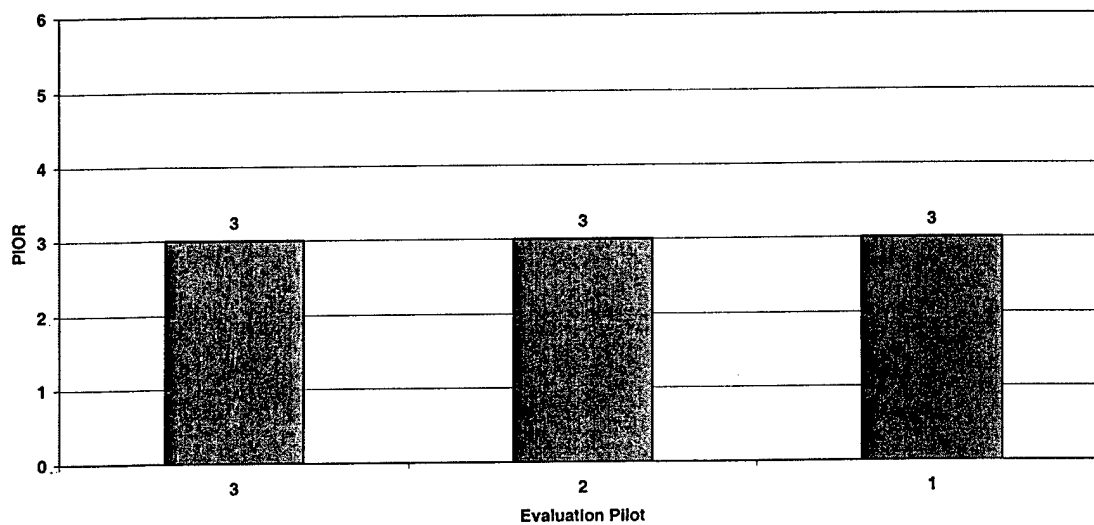


Figure I15 LAMARS Data, Case B, 60 deg/sec

LAMARS Data
PIOR for Phase 3 DIS - Case N, 15 deg/sec Rate Limit

Data Basis: 15K ft PA, 300 KIAS
Test A/C: LAMARS Simulation
Acquisition System: Hand Held
Configuration: Cruise
Test Dates: 22 August 2003

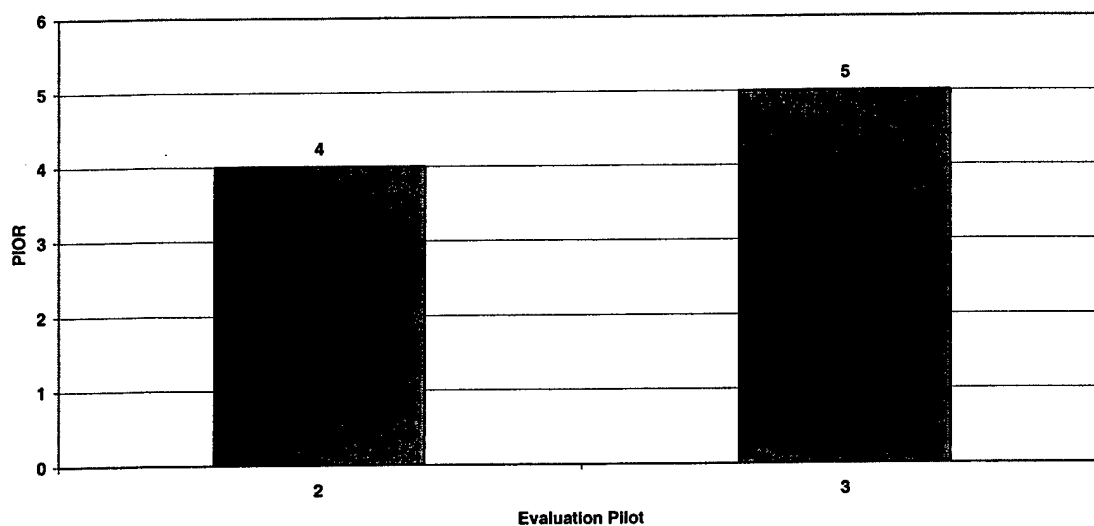


Figure I16 LAMARS Data, Case N, 15 deg/sec

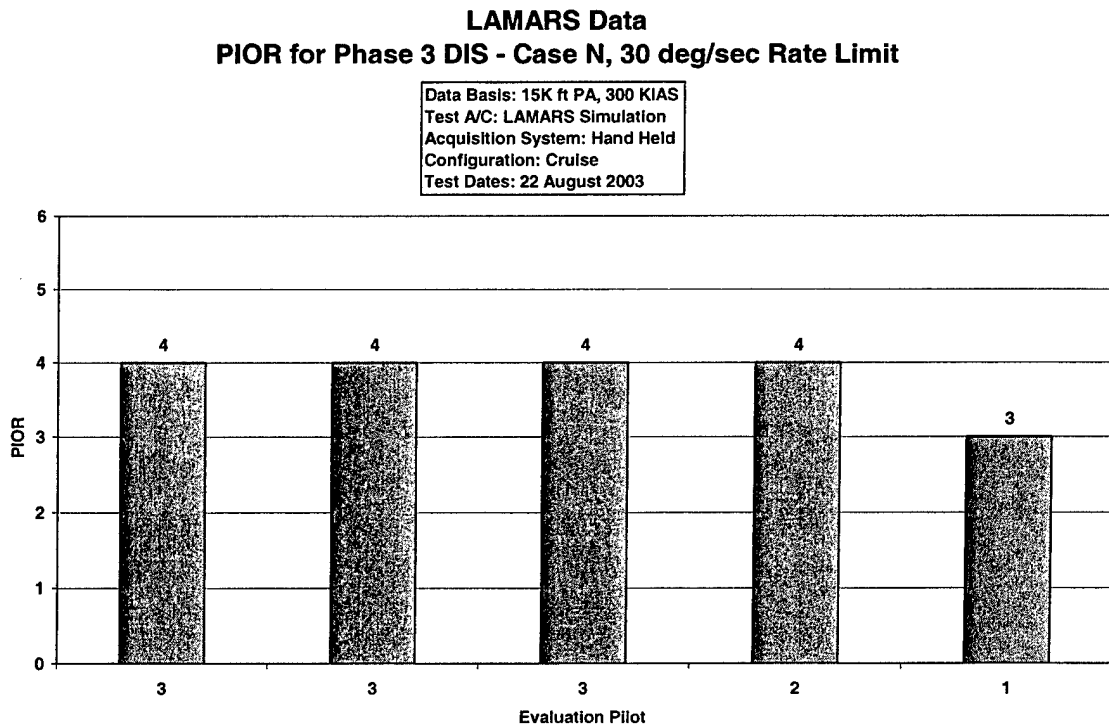


Figure I17 LAMARS Data, Case N, 30 deg/sec

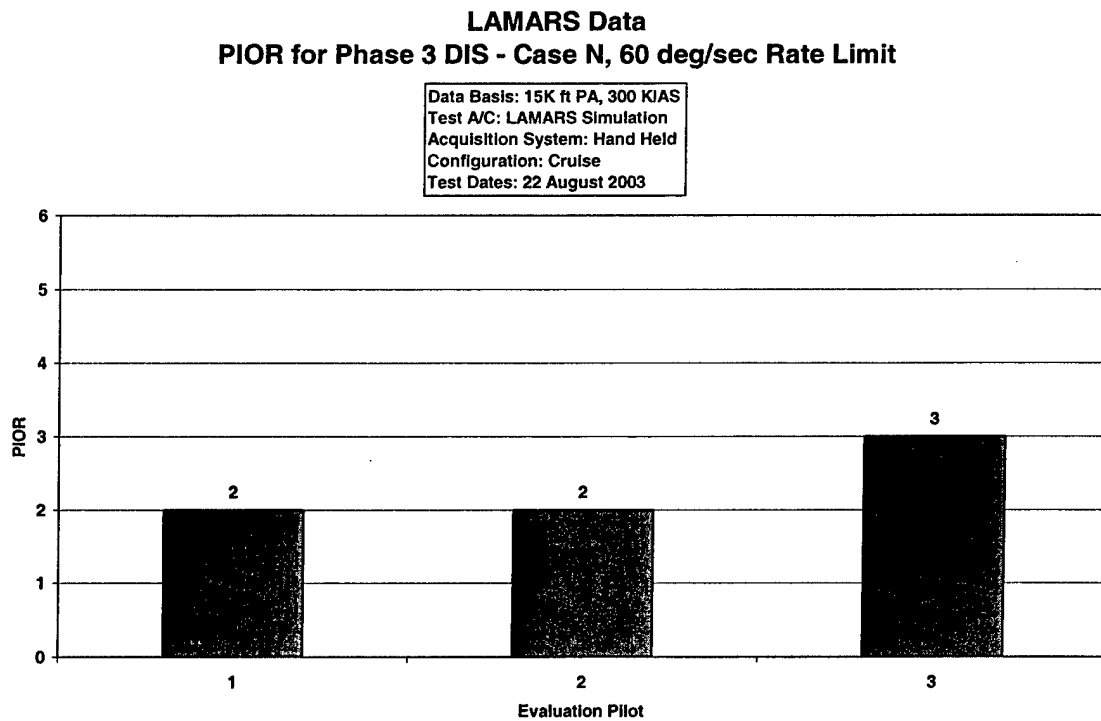


Figure I18 LAMARS Data, Case N, 60 deg/sec

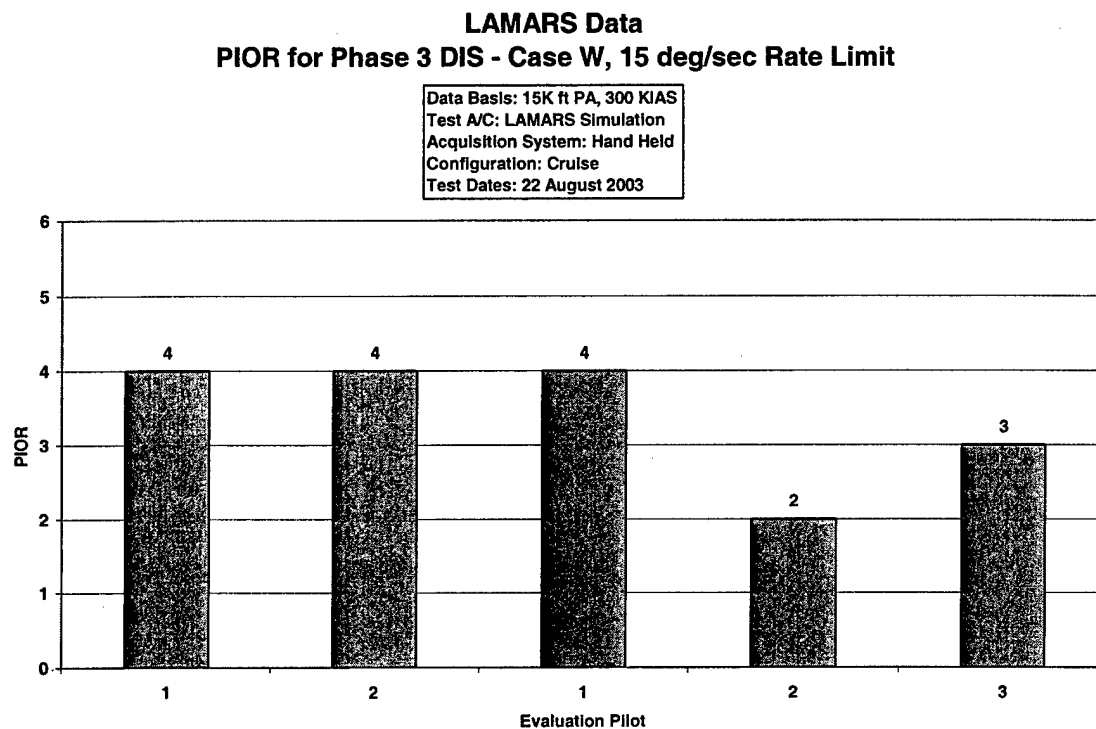


Figure I19 LAMARS Data, Case W, 15 deg/sec

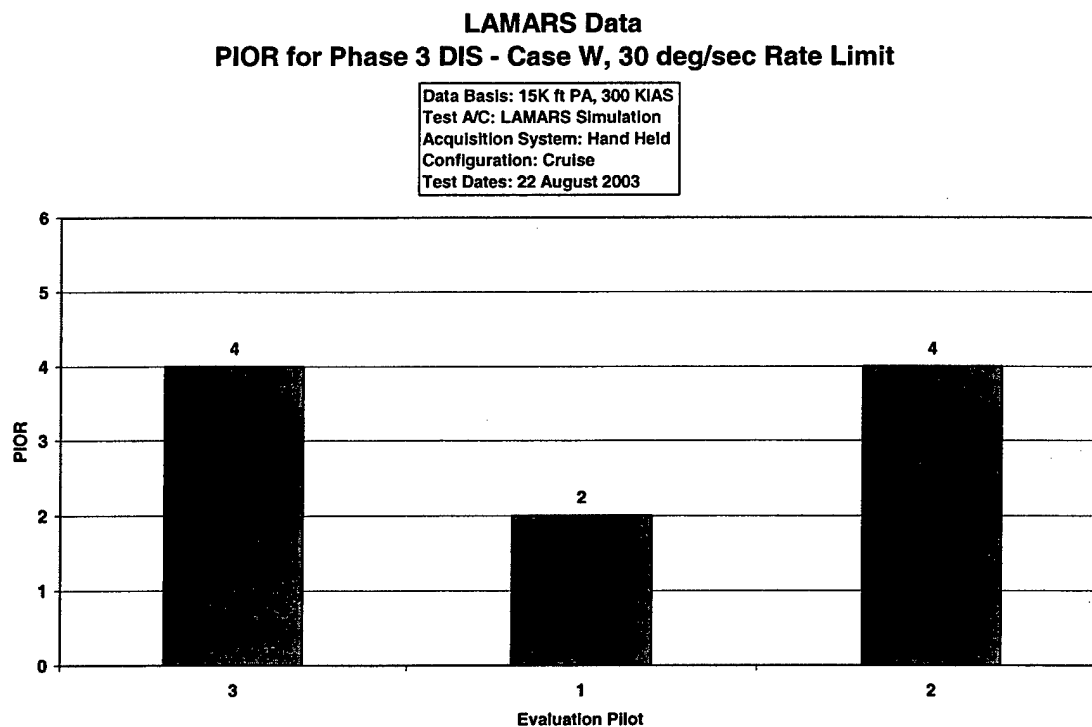


Figure I20 LAMARS Data, Case W, 30 deg/sec

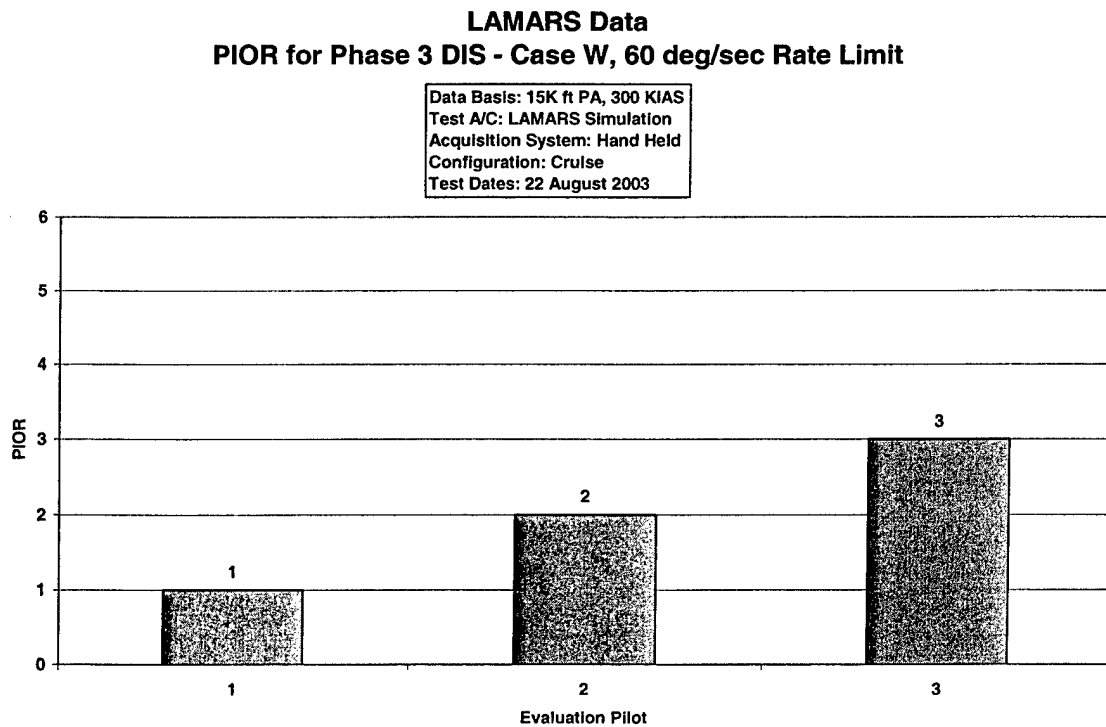


Figure I21 LAMARS Data, Case W, 60 deg/sec

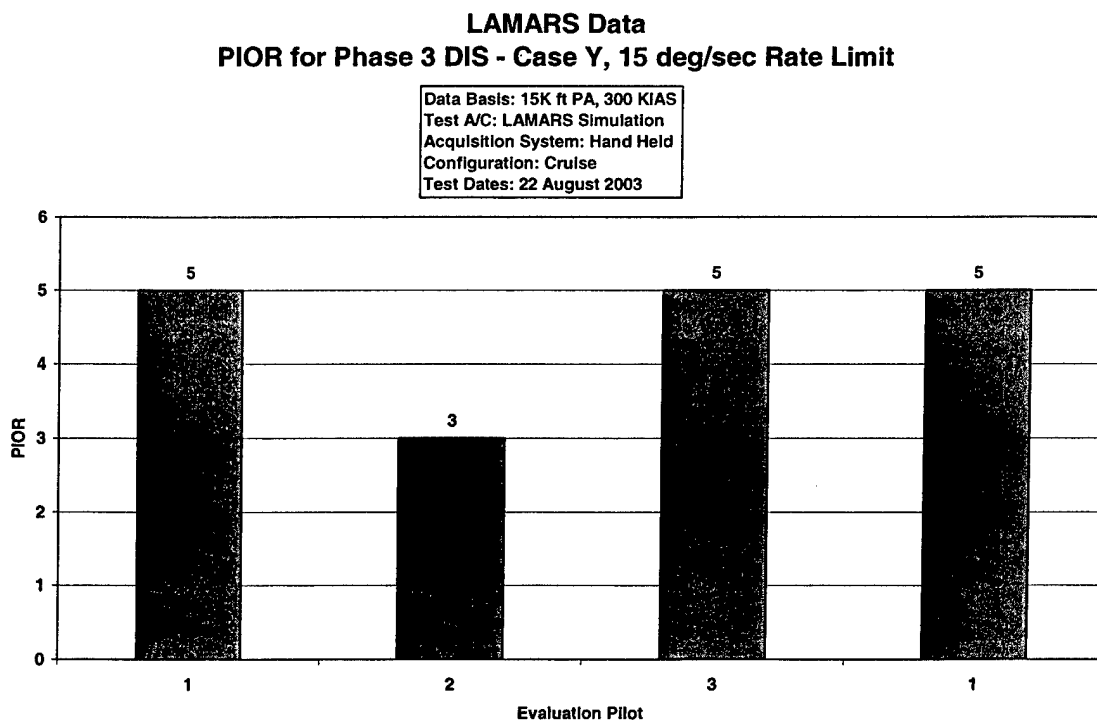


Figure I22 LAMARS Data, Case Y, 15 deg/sec

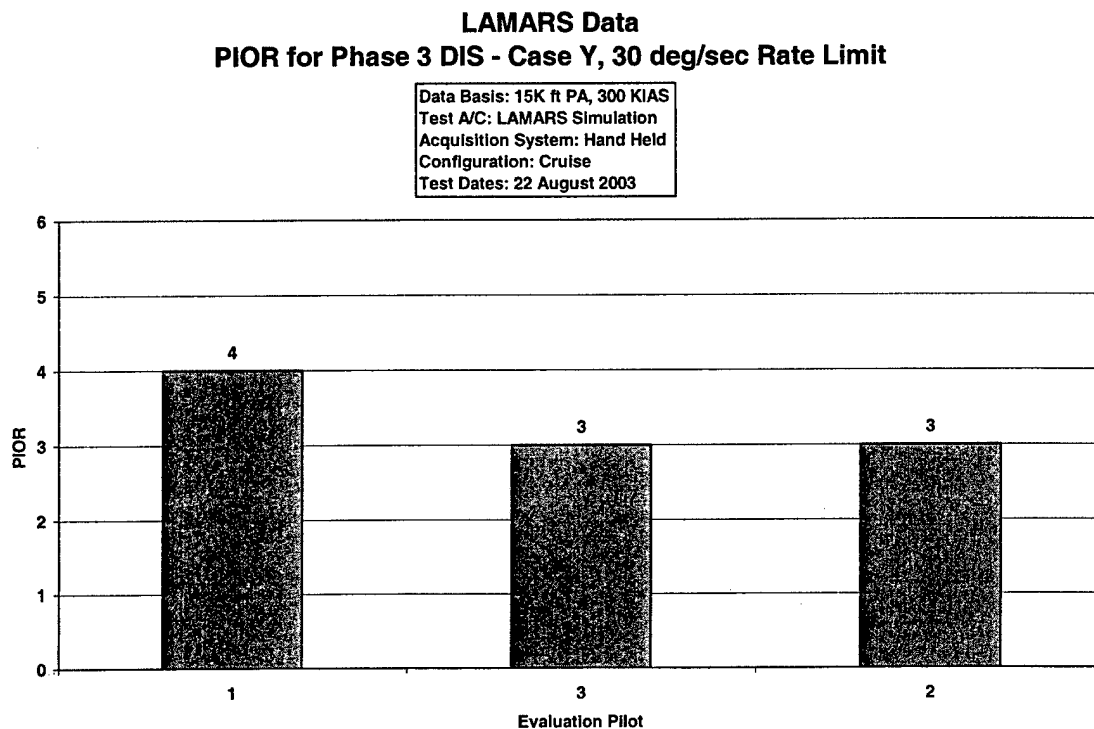


Figure I23 LAMARS Data, Case Y, 30 deg/sec

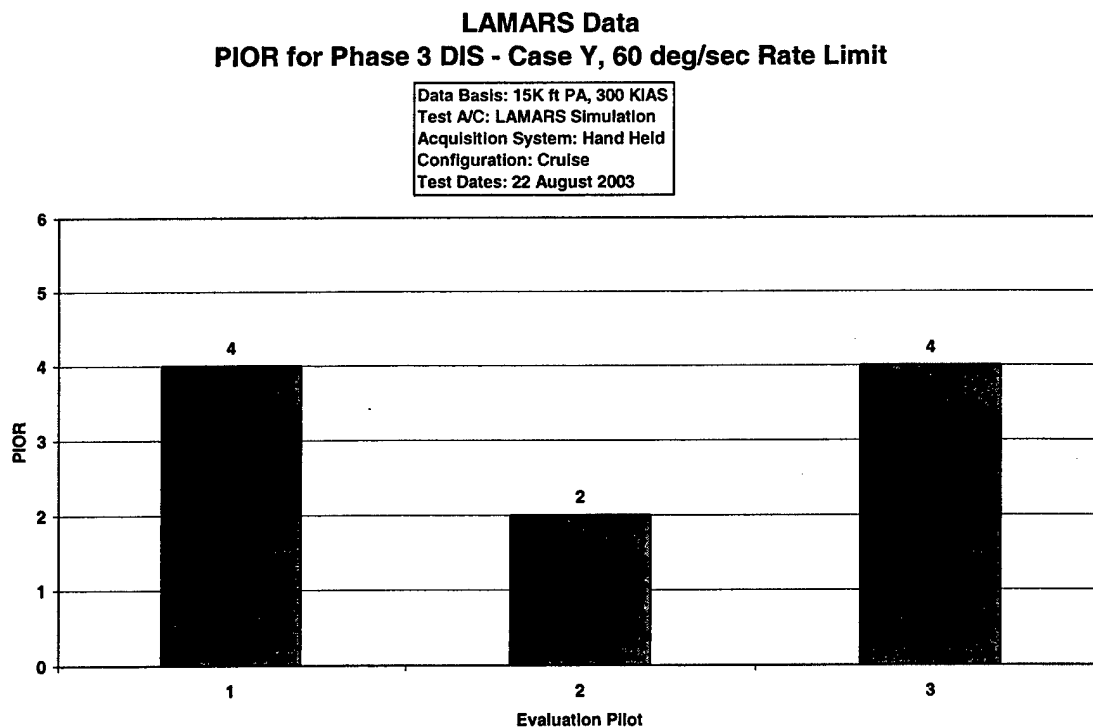


Figure I24 LAMARS Data, Case Y, 60 deg/sec

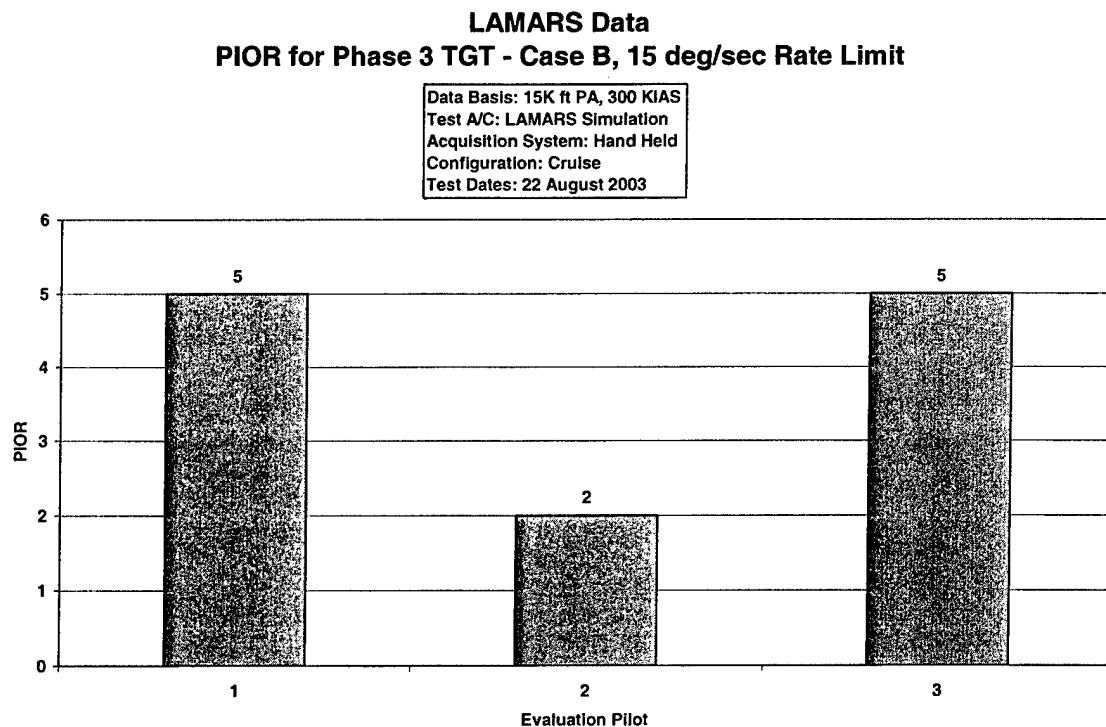


Figure I25 LAMARS Data, Case B, 15 deg/sec

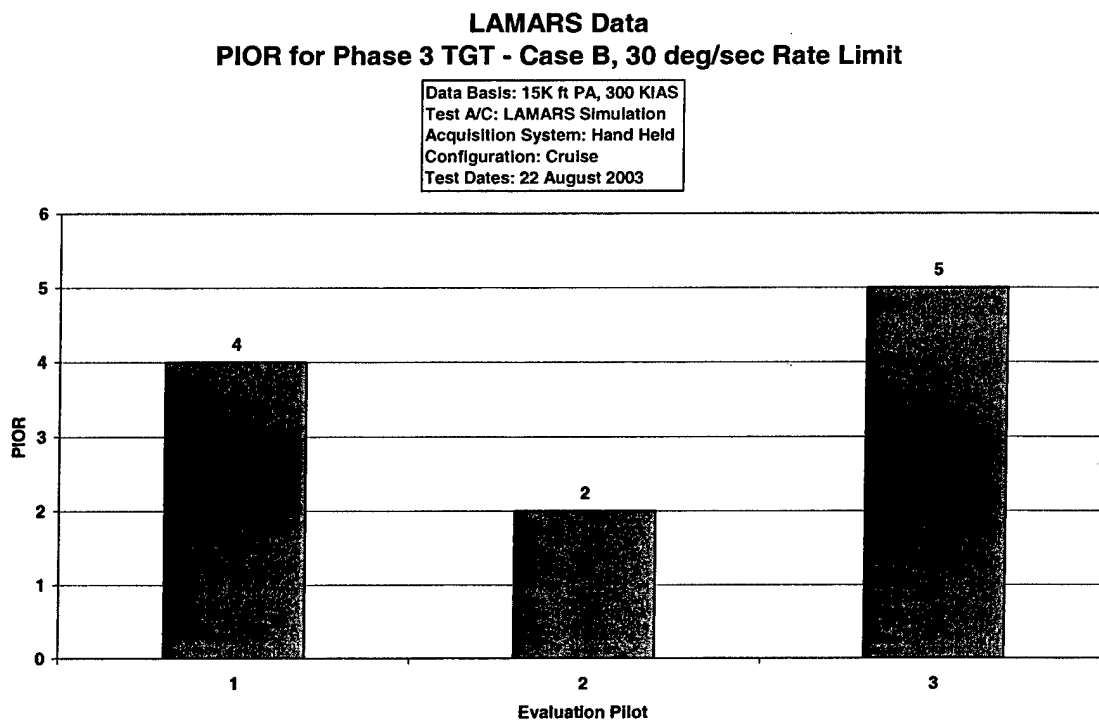


Figure I26 LAMARS Data, Case B, 30 deg/sec

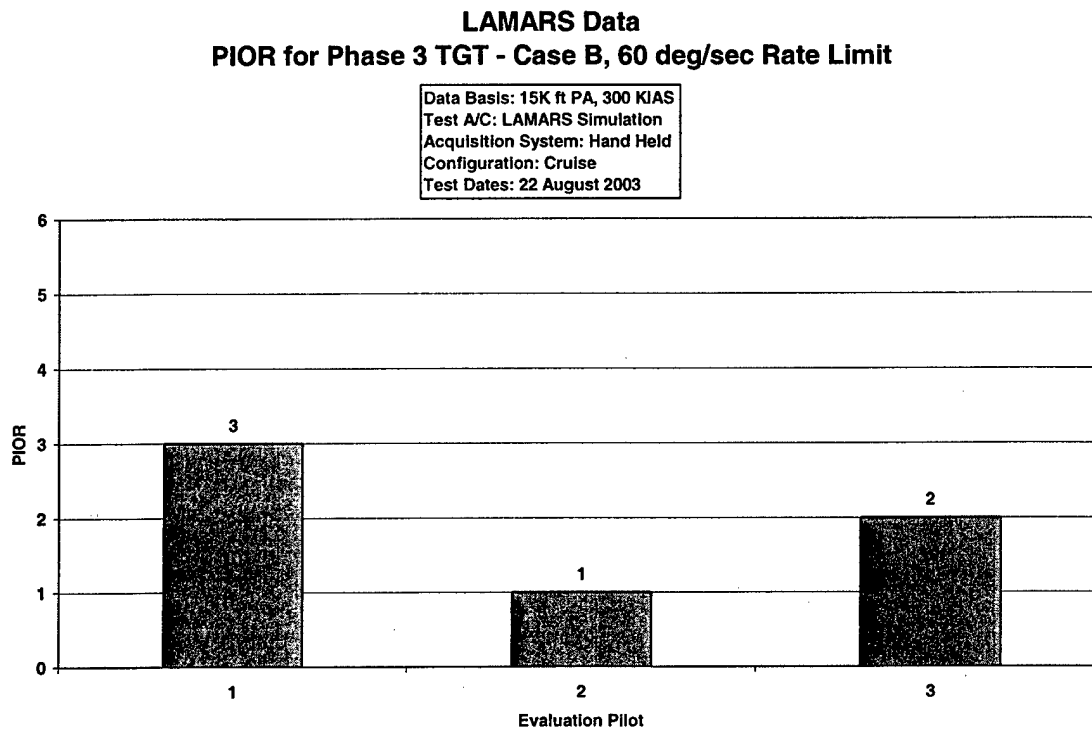


Figure I27 LAMARS Data, Case B, 60 deg/sec

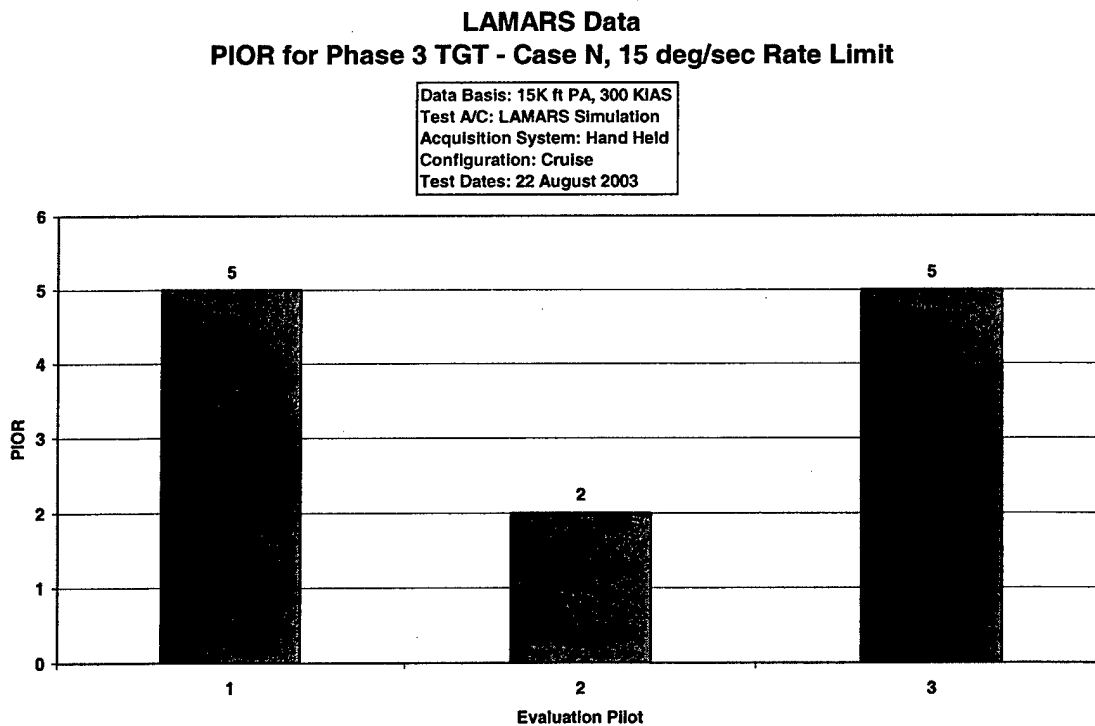


Figure I28 LAMARS Data, Case N, 15 deg/sec

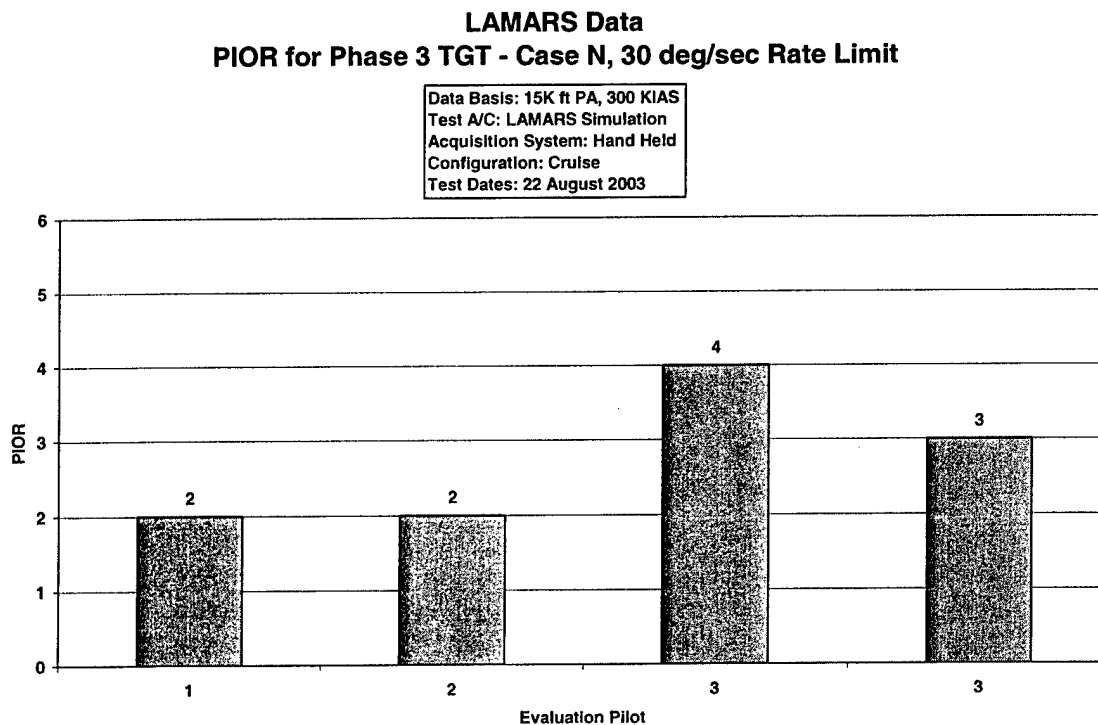


Figure I29 LAMARS Data, Case N, 30 deg/sec

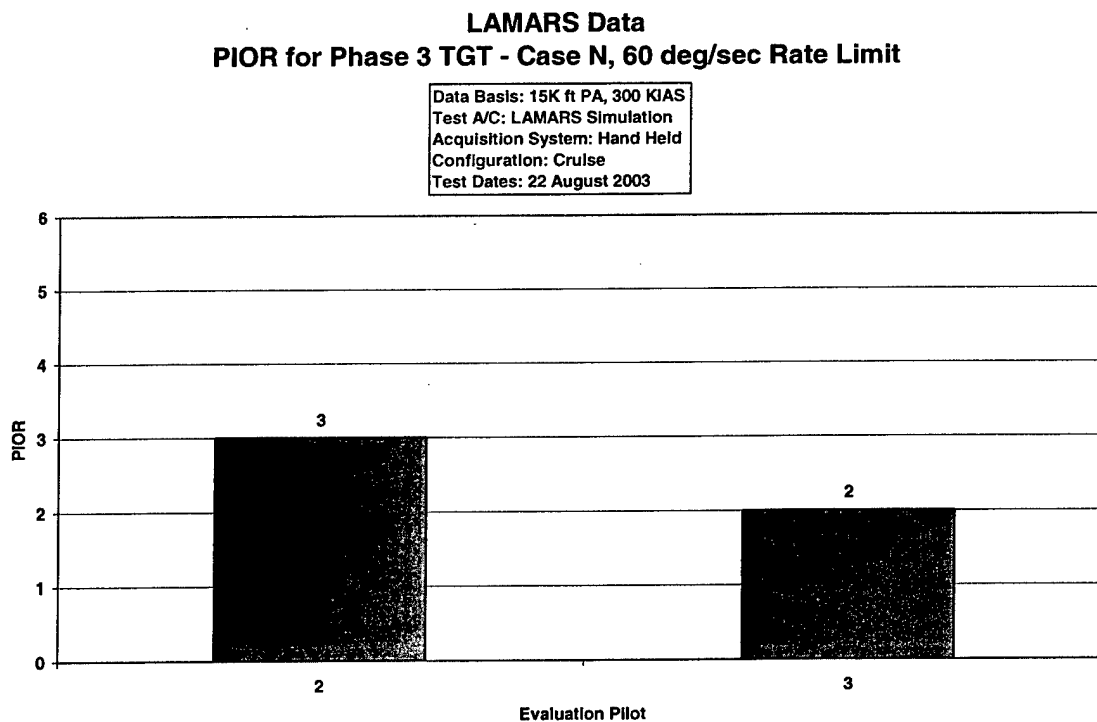


Figure I30 LAMARS Data, Case N, 60 deg/sec

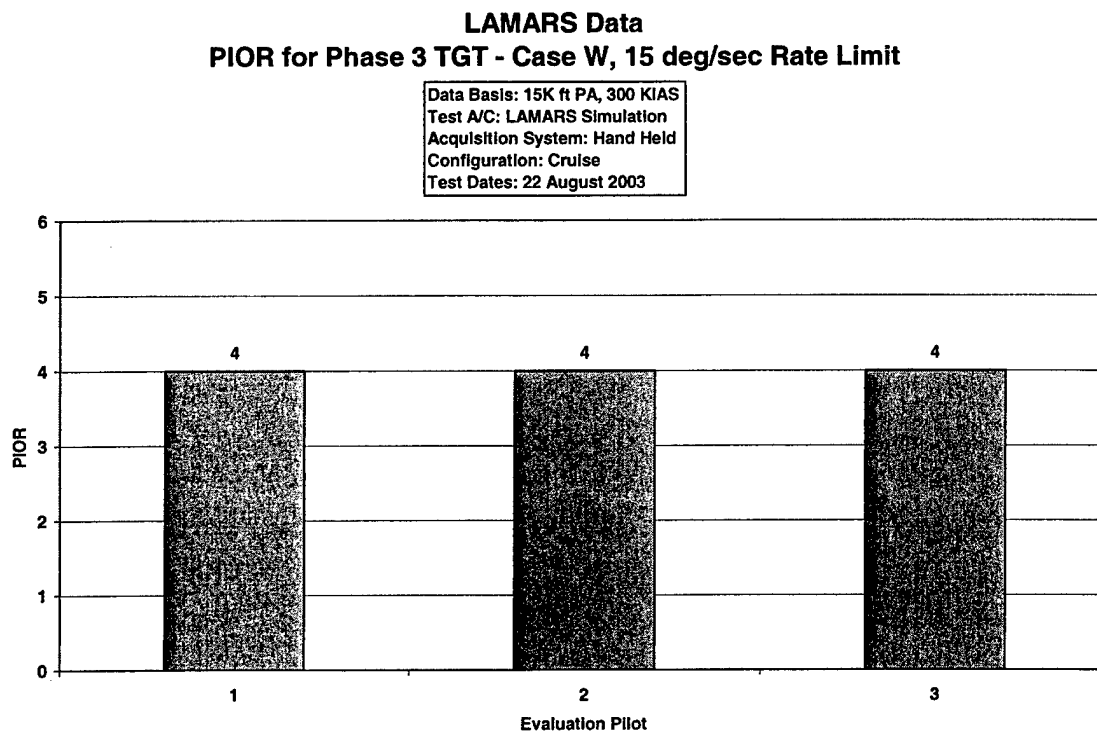


Figure I31 LAMARS Data, Case W, 15 deg/sec

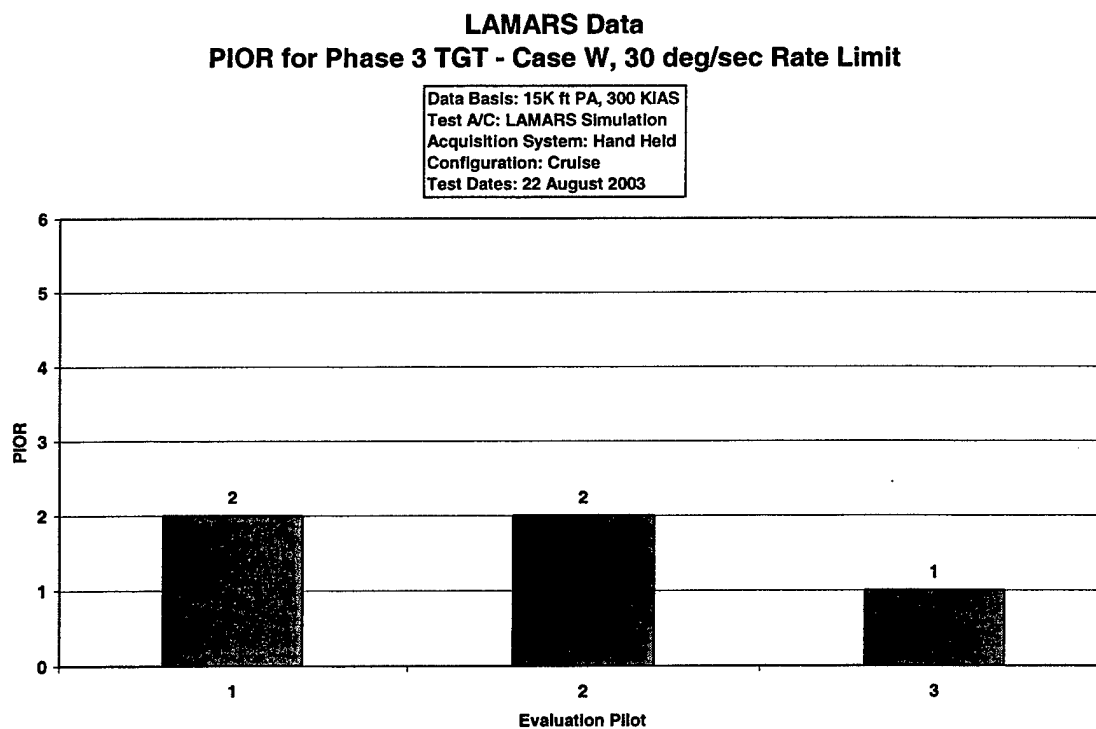


Figure I32 LAMARS Data, Case W, 30 deg/sec

LAMARS Data
PIOR for Phase 3 TGT - Case W, 60 deg/sec Rate Limit

Data Basis: 15K ft PA, 300 KIAS
Test A/C: LAMARS Simulation
Acquisition System: Hand Held
Configuration: Cruise
Test Dates: 22 August 2003

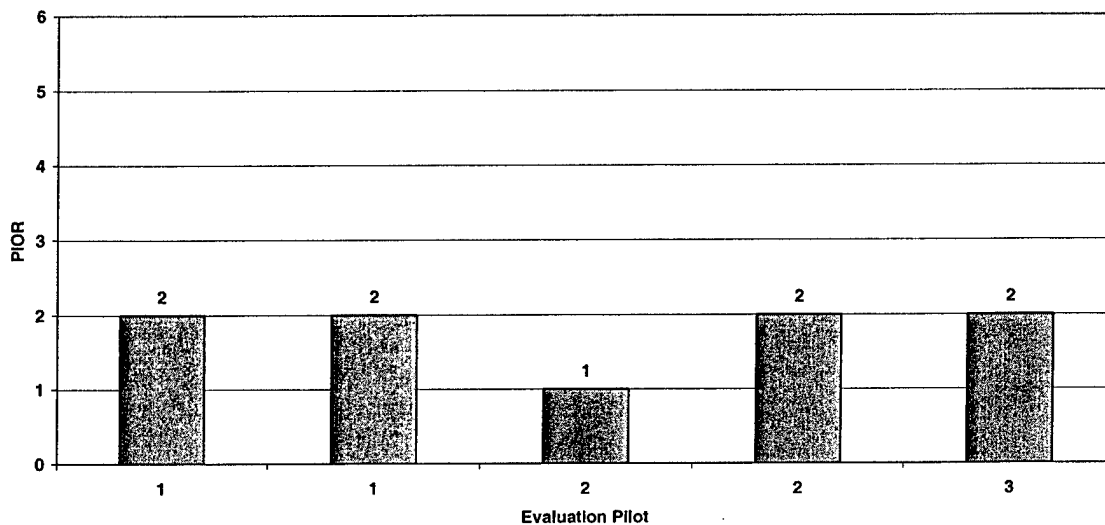


Figure I33 LAMARS Data, Case W, 60 deg/sec

LAMARS Data
PIOR for Phase 3 TGT - Case Y, 15 deg/sec Rate Limit

Data Basis: 15K ft PA, 300 KIAS
Test A/C: LAMARS Simulation
Acquisition System: Hand Held
Configuration: Cruise
Test Dates: 22 August 2003

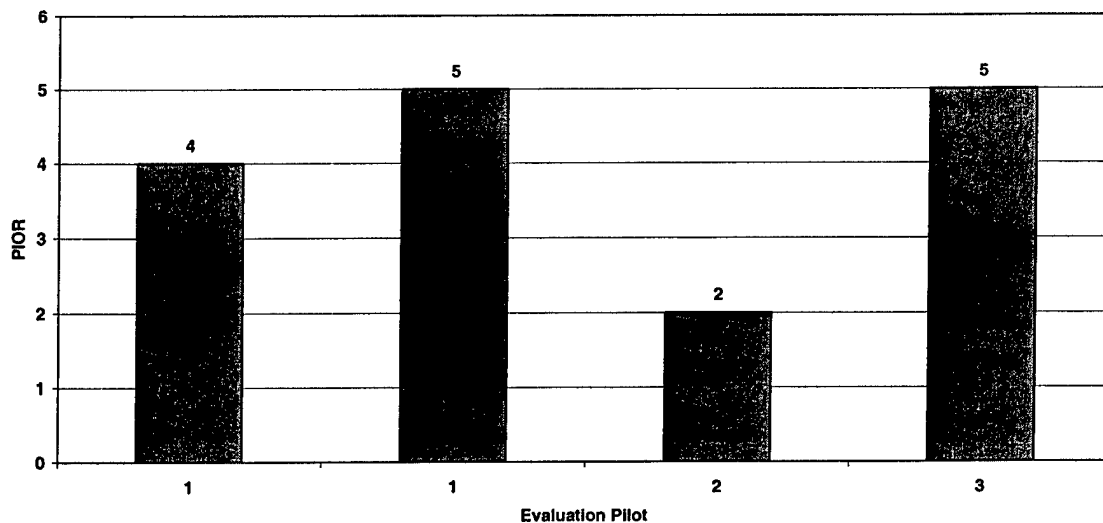


Figure I34 LAMARS Data, Case Y, 15 deg/sec

LAMARS Data
PIOR for Phase 3 TGT - Case Y, 30 deg/sec Rate Limit

Data Basis: 15K ft PA, 300 KIAS
Test A/C: LAMARS Simulation
Acquisition System: Hand Held
Configuration: Cruise
Test Dates: 22 August 2003

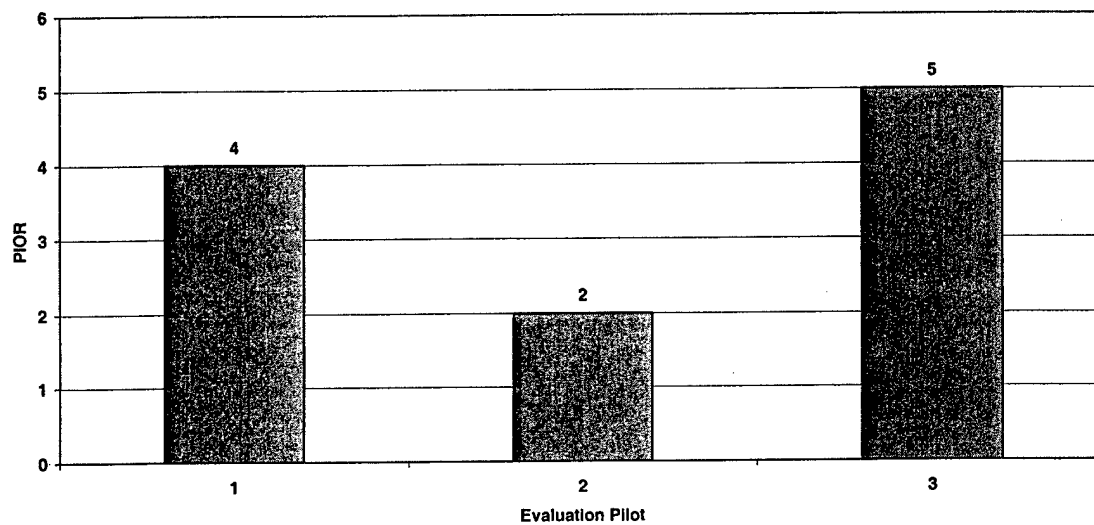


Figure I35 LAMARS Data, Case Y, 30 deg/sec

LAMARS Data
PIOR for Phase 3 TGT - Case Y, 60 deg/sec Rate Limit

Data Basis: 15K ft PA, 300 KIAS
Test A/C: LAMARS Simulation
Acquisition System: Hand Held
Configuration: Cruise
Test Dates: 22 August 2003

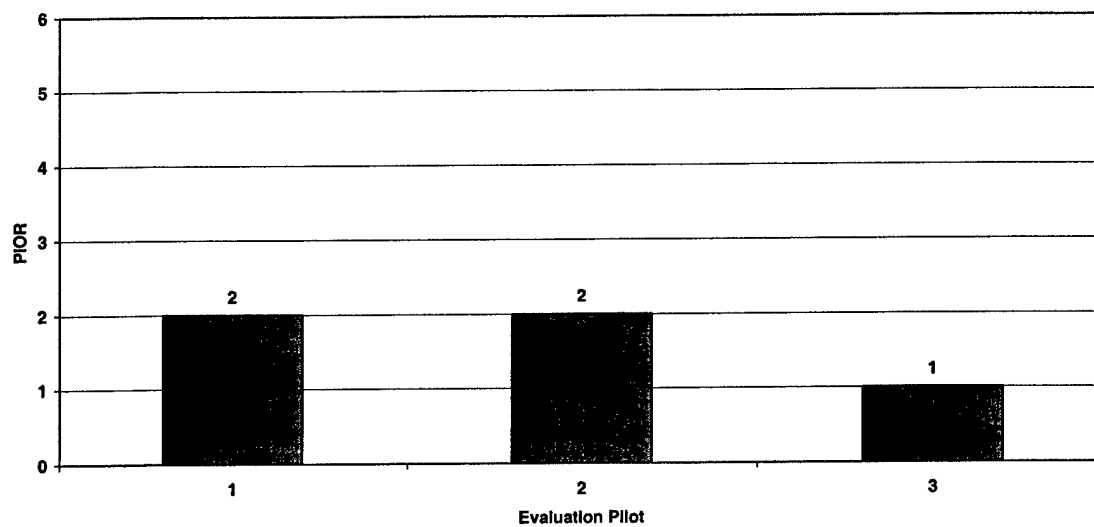


Figure I36 LAMARS Data, Case Y, 60 deg/sec

THIS PAGE INTENTIONALLY LEFT BLANK

APPENDIX J: VISTA FLIGHT HISTOGRAMS

The MAX GAP VISTA flight test histograms are in this appendix. Pilots 1, 2 and 3 were the same individual in each case

MAX GAP Flight Test Data
Phase 2 SOS - Case B - 15 deg/sec

Data Basis: 15K ft PA, 300 KIAS
Test A/C: NF-16D - # 86-00048
Acquisition System: Hand Held
Configuration: Cruise / VSS Engaged
Test Dates: 20-22 October 2003

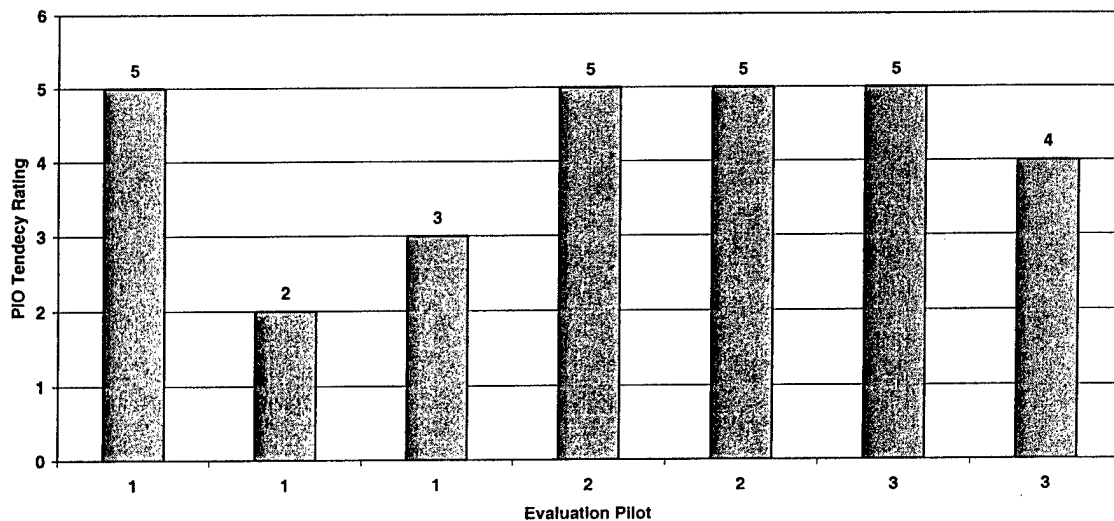


Figure J1 Flight Test Data, Case B, 15 deg/sec

MAX GAP Flight Test Data
Phase 2 SOS - Case B - 30 deg/sec

Data Basis: 15K ft PA, 300 KIAS
Test A/C: NF-16D - # 86-00048
Acquisition System: Hand Held
Configuration: Cruise / VSS Engaged
Test Dates: 20-22 October 2003

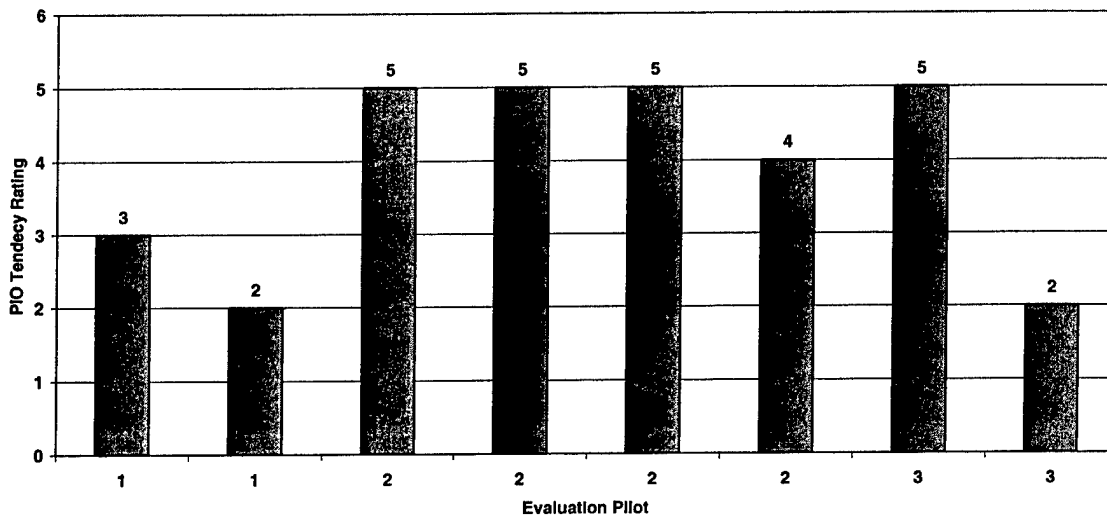


Figure J2 Flight Test Data, Case B, 30 deg/sec

**MAX GAP Flight Test Data
Phase 2 SOS - Case B - 60 deg/sec**

Data Basis: 15K ft PA, 300 KIAS
Test A/C: NF-16D - # 86-00048
Acquisition System: Hand Held
Configuration: Cruise / VSS Engaged
Test Dates: 20-22 October 2003

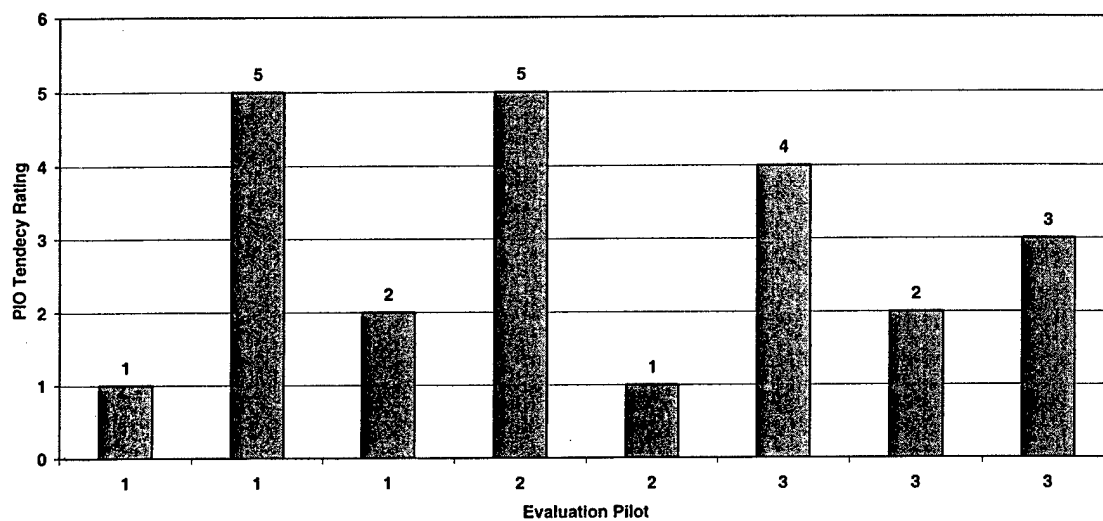


Figure J3 Flight Test Data, Case B, 60 deg/sec

**MAX GAP Flight Test Data
Phase 2 SOS - Case N - 15 deg/sec**

Data Basis: 15K ft PA, 300 KIAS
Test A/C: NF-16D - # 86-00048
Acquisition System: Hand Held
Configuration: Cruise / VSS Engaged
Test Dates: 20-22 October 2003

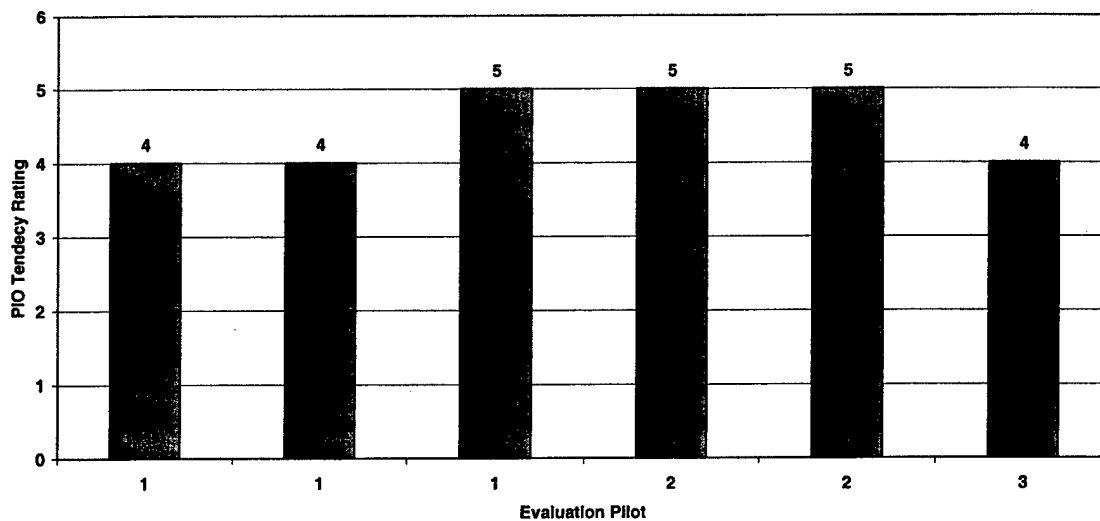


Figure J4 Flight Test Data, Case N, 15 deg/sec

MAX GAP Flight Test Data
Phase 2 SOS - Case N - 30 deg/sec

Data Basis: 15K ft PA, 300 KIAS
Test A/C: NF-16D - # 86-00048
Acquisition System: Hand Held
Configuration: Cruise / VSS Engaged
Test Dates: 20-22 October 2003

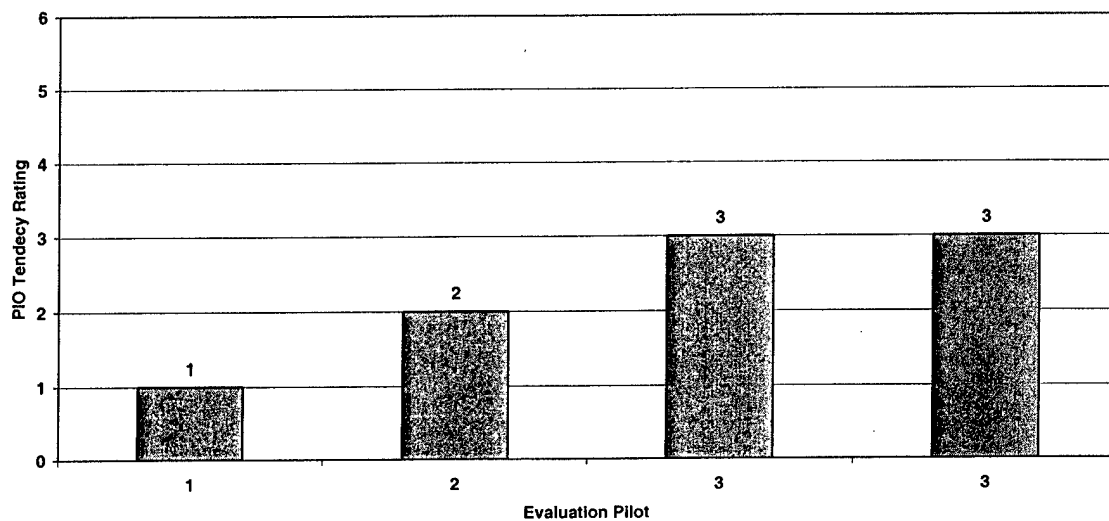


Figure J5 Flight Test Data, Case N, 30 deg/sec

MAX GAP Flight Test Data
Phase 2 SOS - Case N - 60 deg/sec

Data Basis: 15K ft PA, 300 KIAS
Test A/C: NF-16D - # 86-00048
Acquisition System: Hand Held
Configuration: Cruise / VSS Engaged
Test Dates: 20-22 October 2003

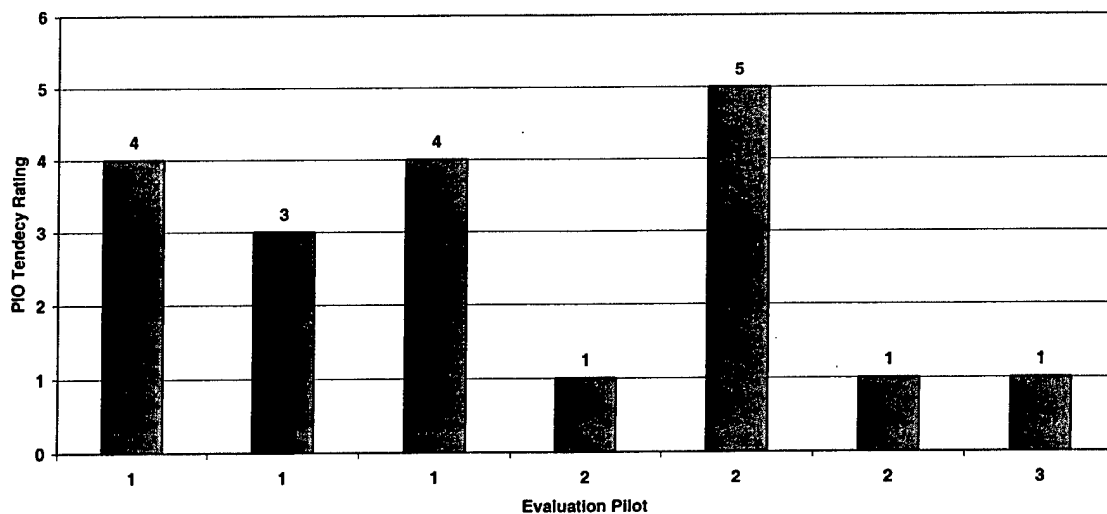


Figure J6 Flight Test Data, Case N, 60 deg/sec

MAX GAP Flight Test Data
Phase 2 SOS - Case W - 15 deg/sec

Data Basis: 15K ft PA, 300 KIAS
Test A/C: NF-16D - # 86-00048
Acquisition System: Hand Held
Configuration: Cruise / VSS Engaged
Test Dates: 20-22 October 2003

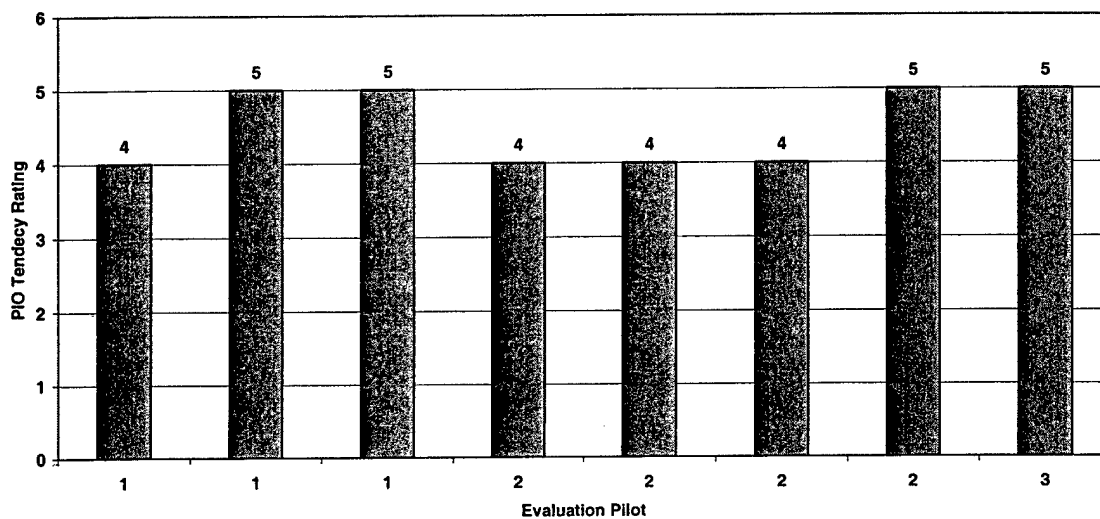


Figure J7 Flight Test Data, Case W, 15 deg/sec

MAX GAP Flight Test Data
Phase 2 SOS - Case W - 30 deg/sec

Data Basis: 15K ft PA, 300 KIAS
Test A/C: NF-16D - # 86-00048
Acquisition System: Hand Held
Configuration: Cruise / VSS Engaged
Test Dates: 20-22 October 2003

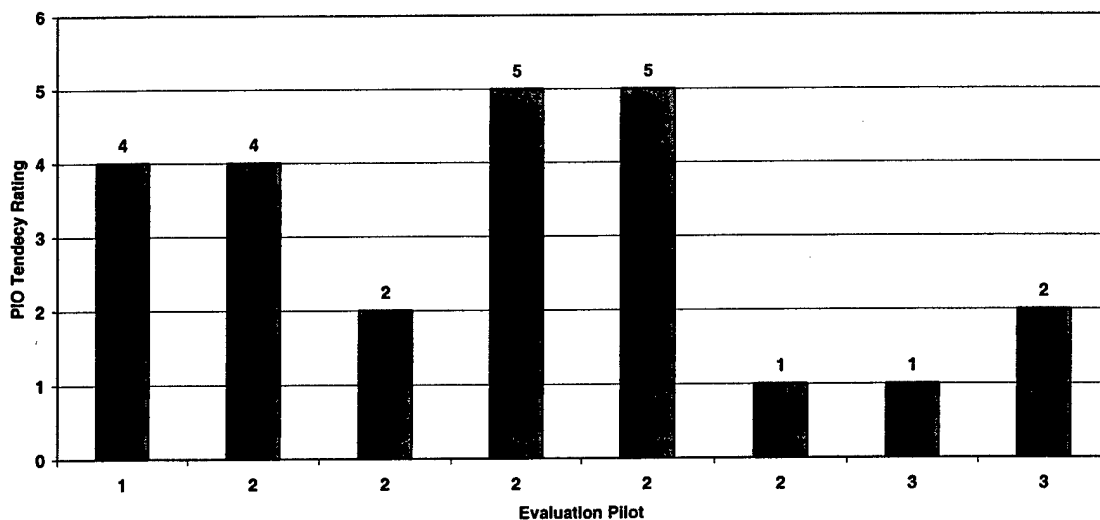


Figure J8 Flight Test Data, Case W, 30 deg/sec

MAX GAP Flight Test Data
Phase 2 SOS - Case W - 60 deg/sec

Data Basis: 15K ft PA, 300 KIAS
Test A/C: NF-16D - # 86-00048
Acquisition System: Hand Held
Configuration: Cruise / VSS Engaged
Test Dates: 20-22 October 2003

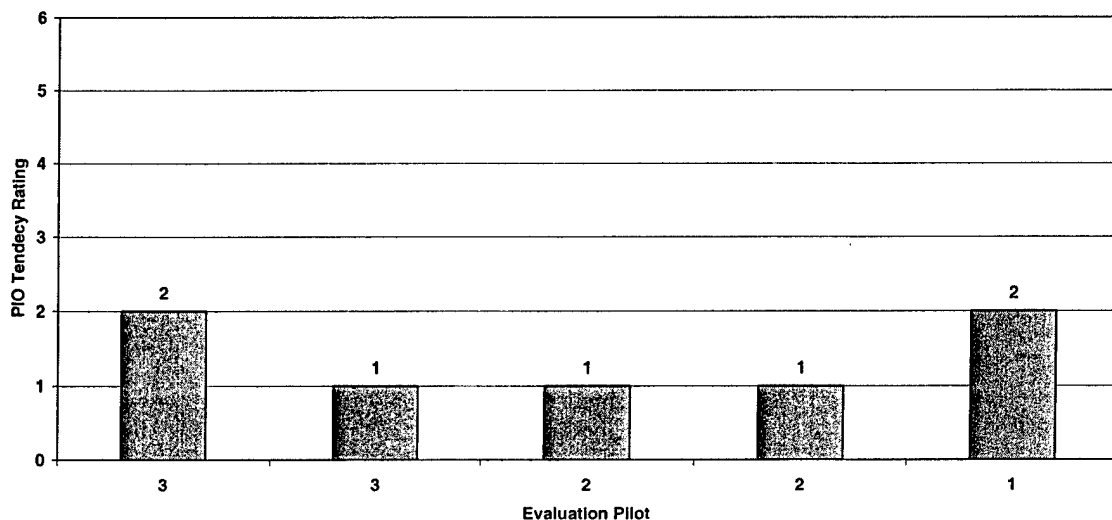


Figure J9 Flight Test Data, Case W, 60 deg/sec

MAX GAP Flight Test Data
Phase 2 SOS - Case Y - 15 deg/sec

Data Basis: 15K ft PA, 300 KIAS
Test A/C: NF-16D - # 86-00048
Acquisition System: Hand Held
Configuration: Cruise / VSS Engaged
Test Dates: 20-22 October 2003

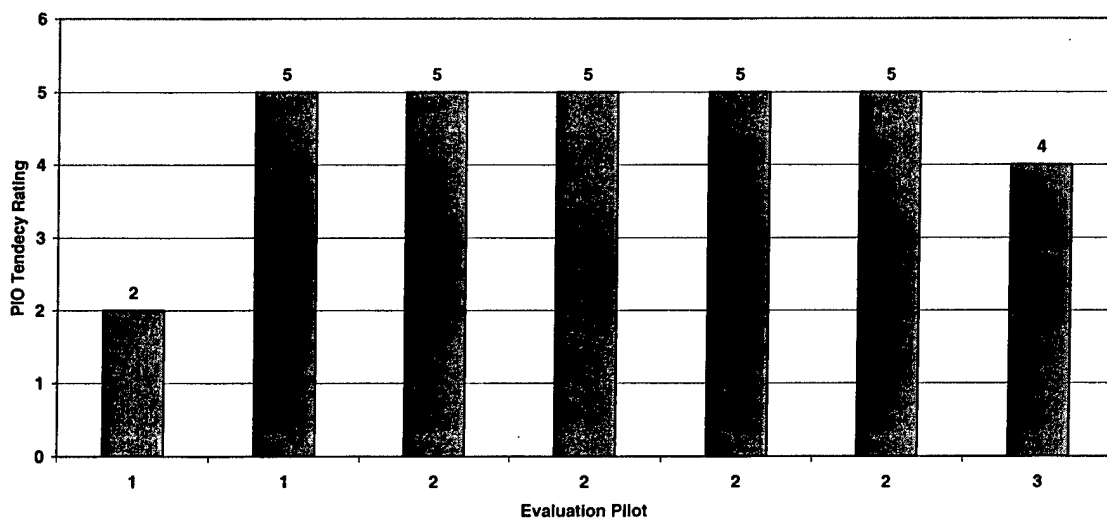


Figure J10 Flight Test Data, Case Y, 15 deg/sec

MAX GAP Flight Test Data
Phase 2 SOS - Case Y - 30 deg/sec

Data Basis: 15K ft PA, 300 KIAS
Test A/C: NF-16D - # 86-00048
Acquisition System: Hand Held
Configuration: Cruise / VSS Engaged
Test Dates: 20-22 October 2003

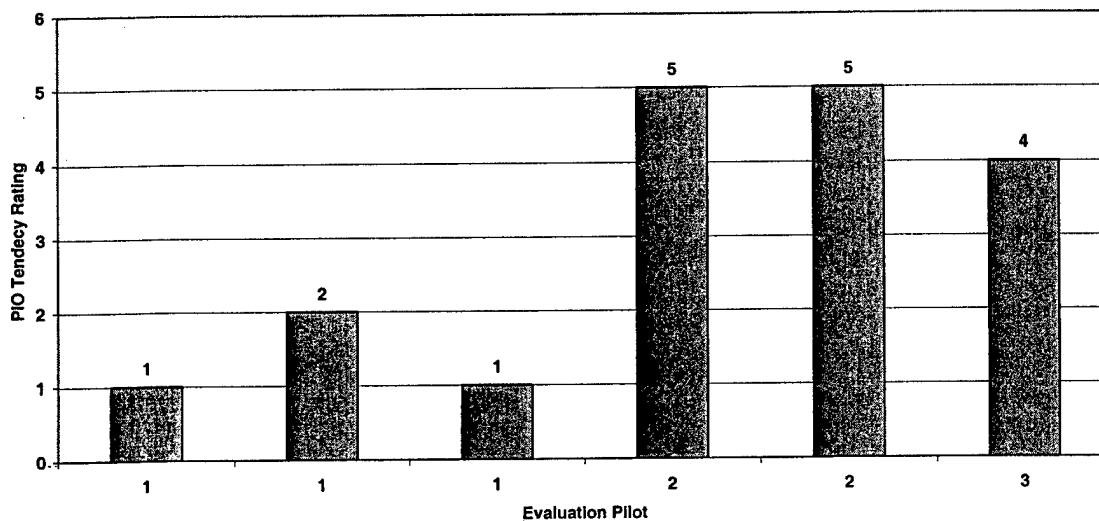


Figure J11 Flight Test Data, Case Y, 30 deg/sec

MAX GAP Flight Test Data
Phase 2 SOS - Case Y - 60 deg/sec

Data Basis: 15K ft PA, 300 KIAS
Test A/C: NF-16D - # 86-00048
Acquisition System: Hand Held
Configuration: Cruise / VSS Engaged
Test Dates: 20-22 October 2003

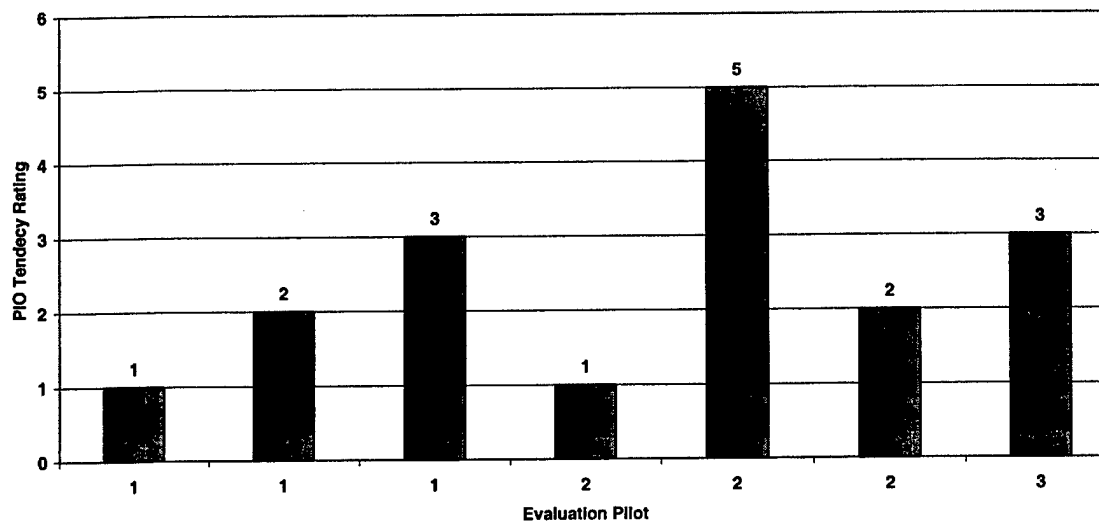


Figure J12 Flight Test Data, Case Y, 60 deg/sec

MAX GAP Flight Test Data
Phase 3 DIS - Case B - 15 deg/sec

Data Basis: 15K ft PA, 300 KIAS
Test A/C: NF-16D - # 86-00048
Acquisition System: Hand Held
Configuration: Cruise / VSS Engaged
Test Dates: 20-22 October 2003

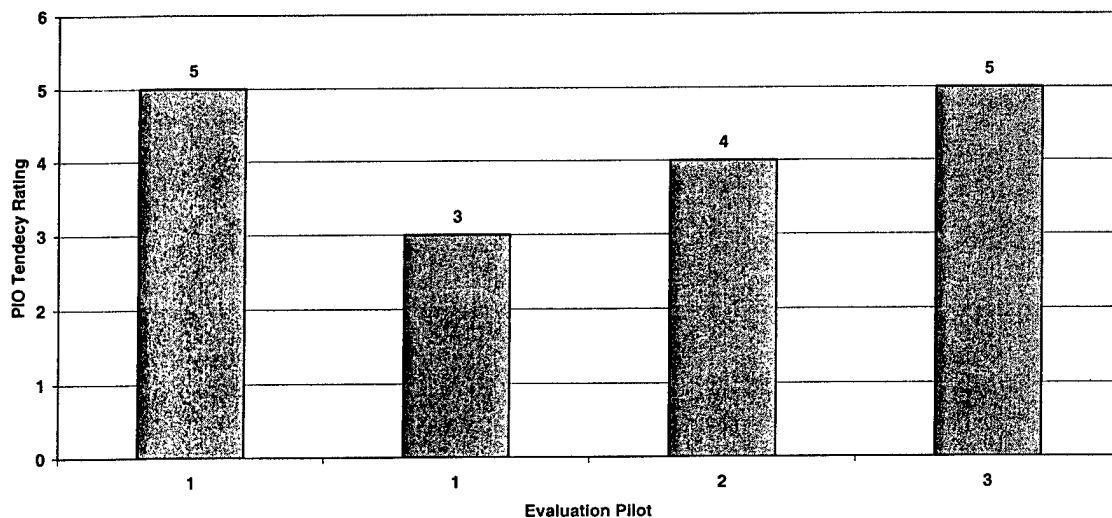


Figure J13 Flight Test Data, Case B, 15 deg/sec

MAX GAP Flight Test Data
Phase 3 DIS - Case B - 30 deg/sec

Data Basis: 15K ft PA, 300 KIAS
Test A/C: NF-16D - # 86-00048
Acquisition System: Hand Held
Configuration: Cruise / VSS Engaged
Test Dates: 20-22 October 2003

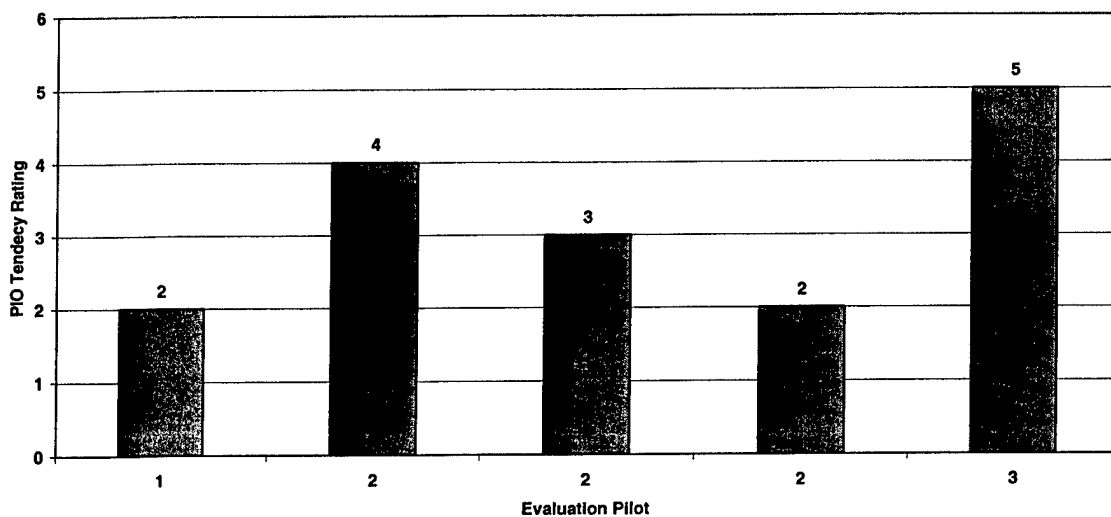


Figure J14 Flight Test Data, Case B, 30 deg/sec

MAX GAP Flight Test Data
Phase 3 DIS - Case B - 60 deg/sec

Data Basis: 15K ft PA, 300 KIAS
Test A/C: NF-16D - # 86-00048
Acquisition System: Hand Held
Configuration: Cruise / VSS Engaged
Test Dates: 20-22 October 2003

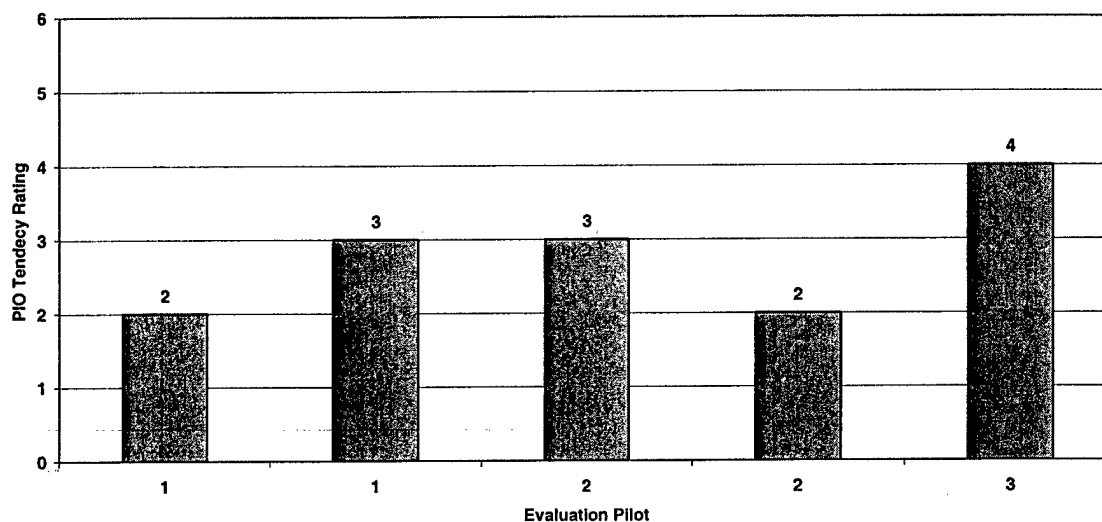


Figure J15 Flight Test Data, Case B, 30 deg/sec

MAX GAP Flight Test Data
Phase 3 DIS - Case N - 15 deg/sec

Data Basis: 15K ft PA, 300 KIAS
Test A/C: NF-16D - # 86-00048
Acquisition System: Hand Held
Configuration: Cruise / VSS Engaged
Test Dates: 20-22 October 2003

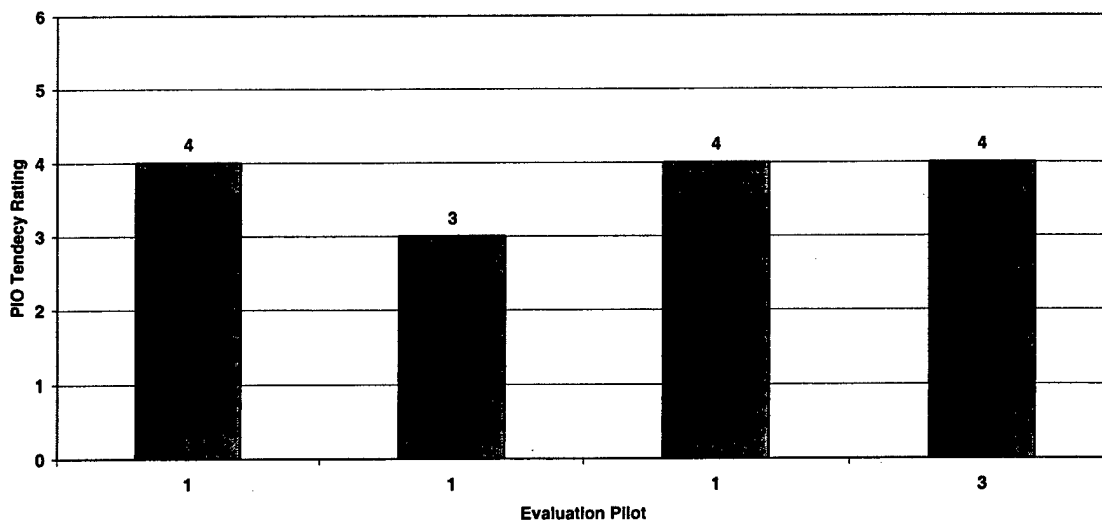


Figure J16 Flight Test Data, Case N, 15 deg/sec

MAX GAP Flight Test Data
Phase 3 DIS - Case N - 30 deg/sec

Data Basis: 15K ft PA, 300 KIAS
Test A/C: NF-16D - # 86-00048
Acquisition System: Hand Held
Configuration: Cruise / VSS Engaged
Test Dates: 20-22 October 2003

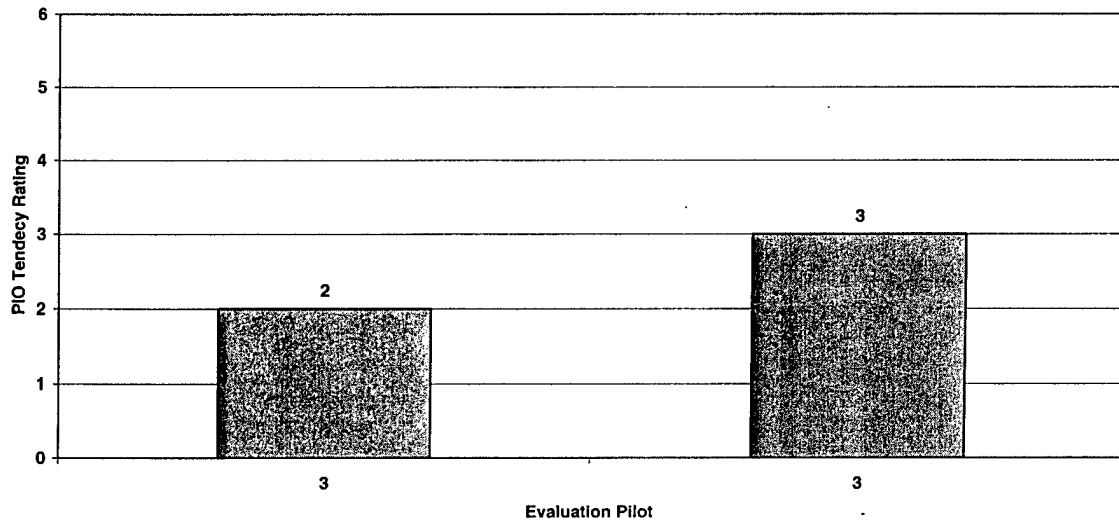


Figure J17 Flight Test Data, Case N, 30 deg/sec

MAX GAP Flight Test Data
Phase 3 DIS - Case N - 60 deg/sec

Data Basis: 15K ft PA, 300 KIAS
Test A/C: NF-16D - # 86-00048
Acquisition System: Hand Held
Configuration: Cruise / VSS Engaged
Test Dates: 20-22 October 2003

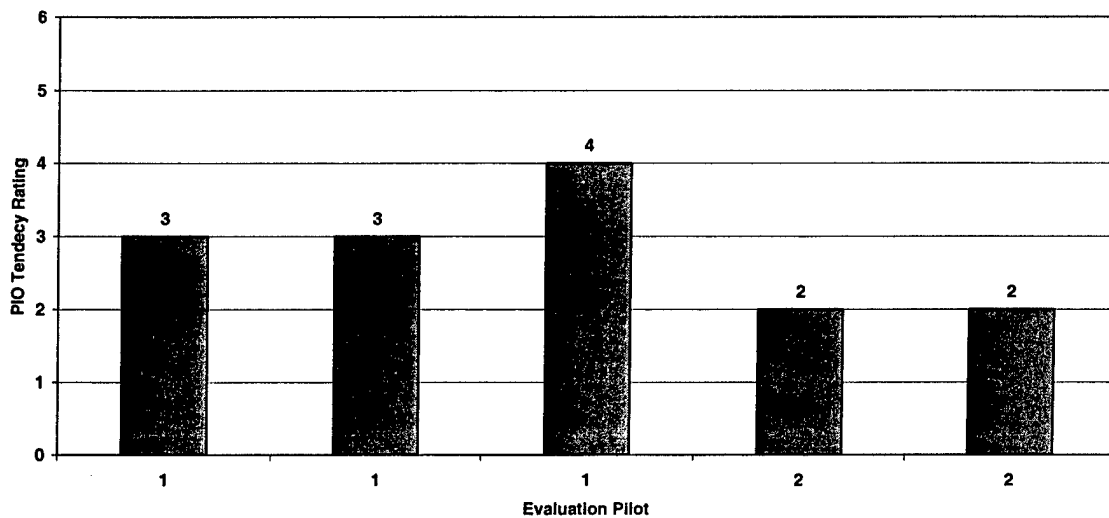


Figure J18 Flight test Data, Case N, 60 deg/sec

MAX GAP Flight Test Data
Phase 3 DIS - Case W - 15 deg/sec

Data Basis: 15K ft PA, 300 KIAS
Test A/C: NF-16D - # 86-00048
Acquisition System: Hand Held
Configuration: Cruise / VSS Engaged
Test Dates: 20-22 October 2003

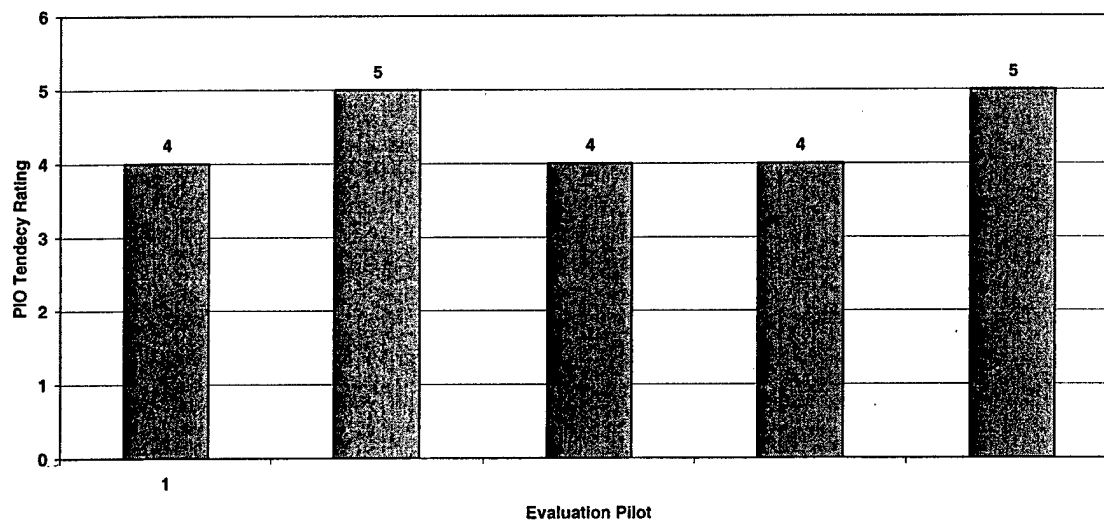


Figure J19 Flight Test Data, Case W, 15 deg/sec

MAX GAP Flight Test Data
Phase 3 DIS - Case W - 30 deg/sec

Data Basis: 15K ft PA, 300 KIAS
Test A/C: NF-16D - # 86-00048
Acquisition System: Hand Held
Configuration: Cruise / VSS Engaged
Test Dates: 20-22 October 2003

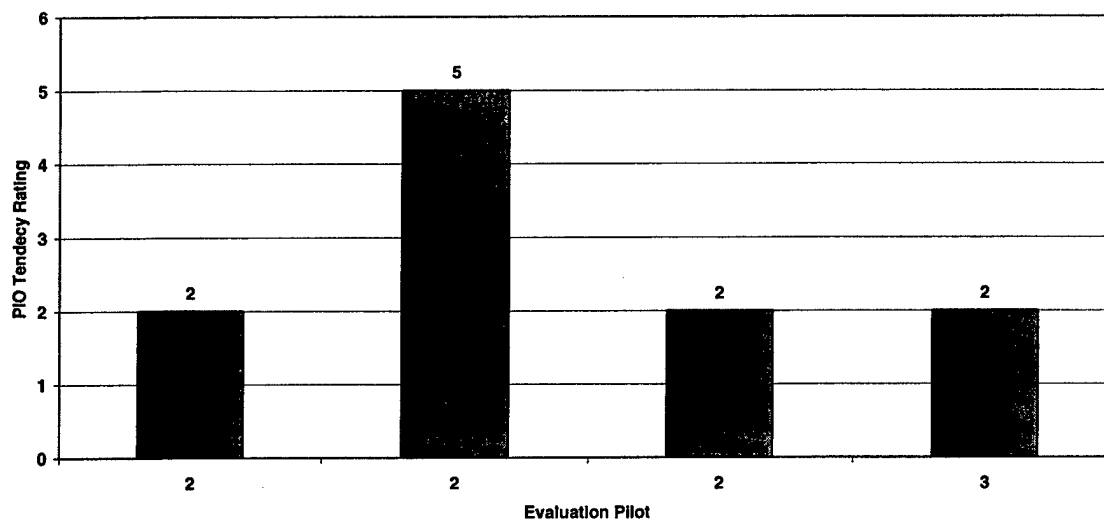


Figure J20 Flight Test Data, Case W, 30 deg/sec

MAX GAP Flight Test Data
Phase 3 DIS - Case W - 60 deg/sec

Data Basis: 15K ft PA, 300 KIAS
Test A/C: NF-16D - # 86-00048
Acquisition System: Hand Held
Configuration: Cruise / VSS Engaged
Test Dates: 20-22 October 2003

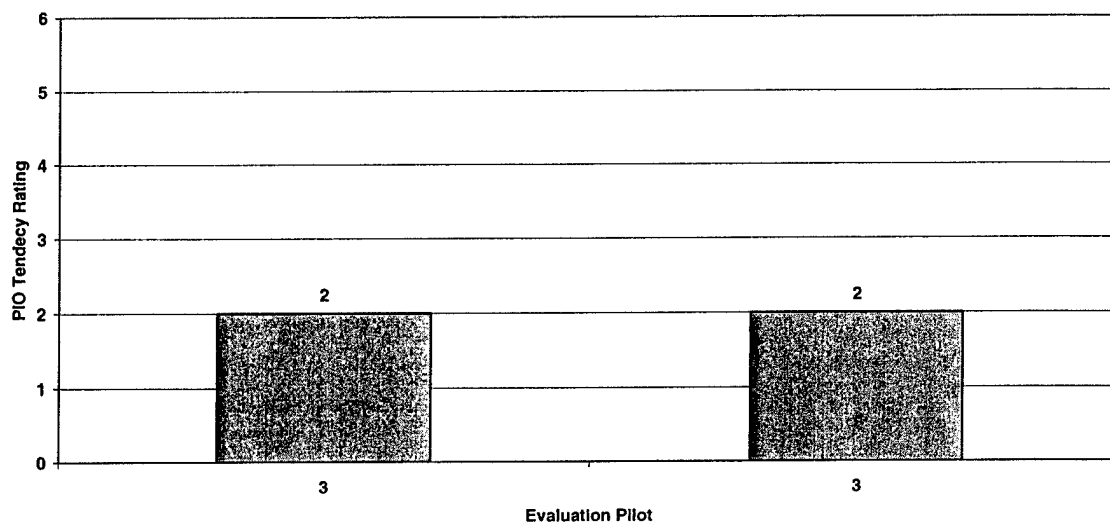


Figure J21 Flight Test Data, Case W, 60 deg/sec

MAX GAP Flight Test Data
Phase 3 DIS - Case Y - 15 deg/sec

Data Basis: 15K ft PA, 300 KIAS
Test A/C: NF-16D - # 86-00048
Acquisition System: Hand Held
Configuration: Cruise / VSS Engaged
Test Dates: 20-22 October 2003

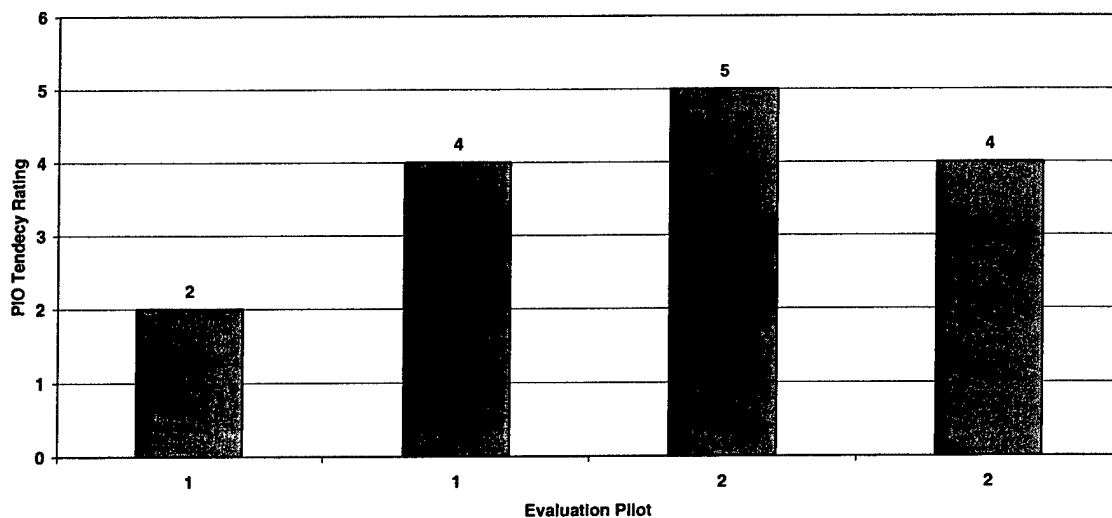


Figure J22 Flight Test Data, Case Y, 15 deg/sec

MAX GAP Flight Test Data
Phase 3 DIS - Case Y - 30 deg/sec

Data Basis: 15K ft PA, 300 KIAS
Test A/C: NF-16D - # 86-00048
Acquisition System: Hand Held
Configuration: Cruise / VSS Engaged
Test Dates: 20-22 October 2003

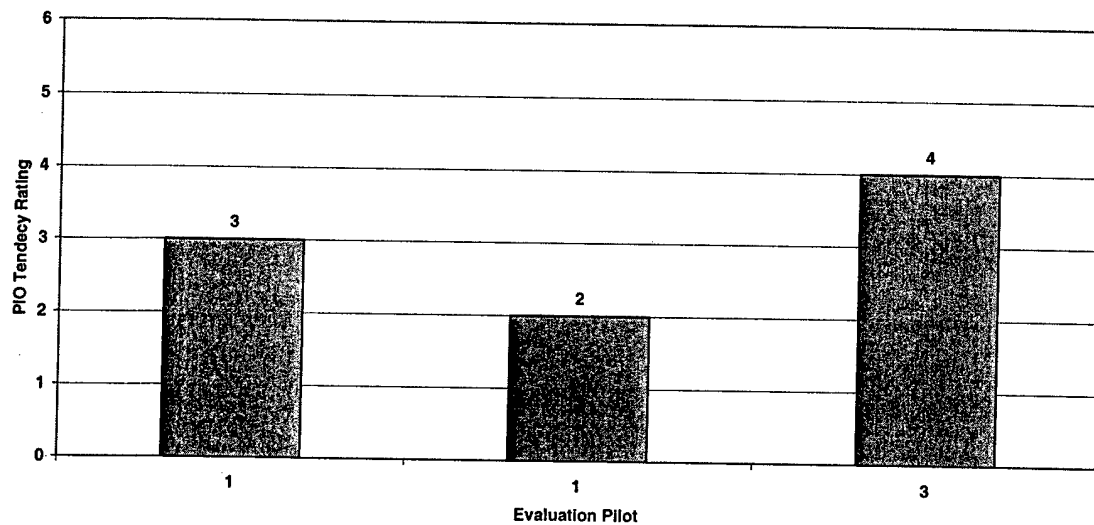


Figure J23 Flight Test Data, Case Y, 30 deg/sec

MAX GAP Flight Test Data
Phase 3 DIS - Case Y - 60 deg/sec

Data Basis: 15K ft PA, 300 KIAS
Test A/C: NF-16D - # 86-00048
Acquisition System: Hand Held
Configuration: Cruise / VSS Engaged
Test Dates: 20-22 October 2003

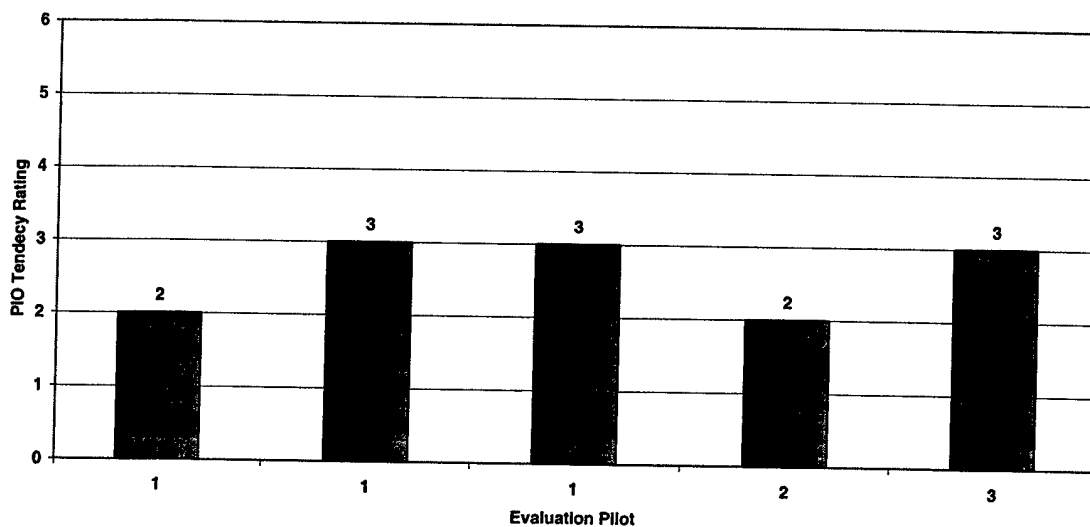


Figure J24 Flight Test Data, Case Y, 60 deg/sec

MAX GAP Flight Test Data
Phase 3 TGT - Case B - 15 deg/sec

Data Basis: 15K ft PA, 300 KIAS
Test A/C: NF-16D - # 86-00048
Acquisition System: Hand Held
Configuration: Cruise / VSS Engaged
Test Dates: 20-22 October 2003

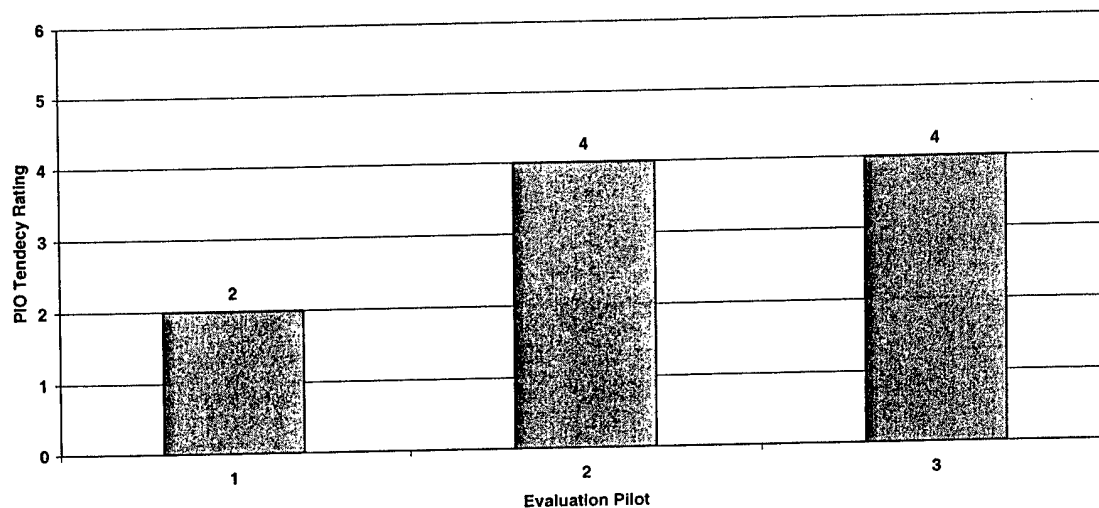


Figure J25 Flight Test Data, Case B, 15 deg/sec

MAX GAP Flight Test Data
Phase 3 TGT - Case B - 30 deg/sec

Data Basis: 15K ft PA, 300 KIAS
Test A/C: NF-16D - # 86-00048
Acquisition System: Hand Held
Configuration: Cruise / VSS Engaged
Test Dates: 20-22 October 2003

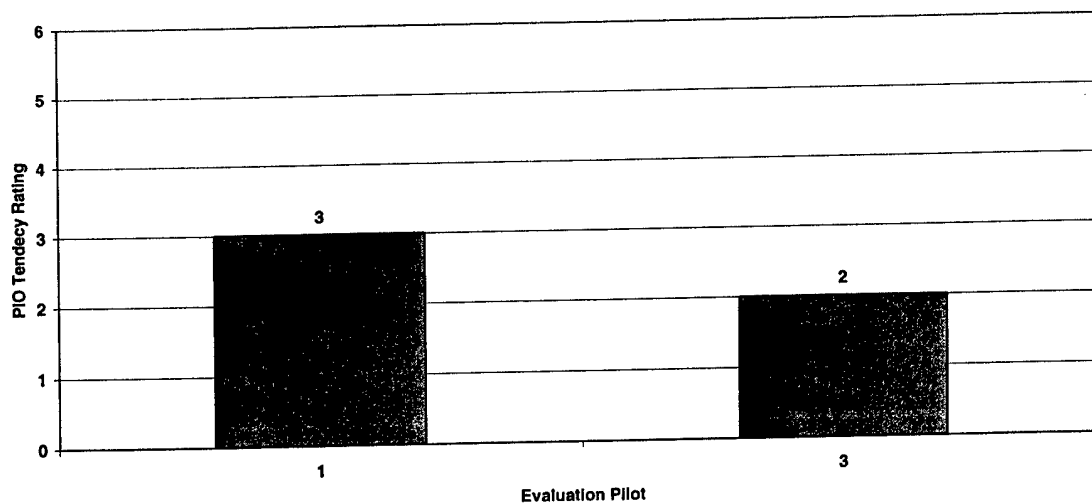


Figure J26 Flight Test Data, Case B, 30 deg/sec

MAX GAP Flight Test Data
Phase 3 TGT - Case B - 60 deg/sec

Data Basis: 15K ft PA, 300 KIAS
Test A/C: NF-16D - # 86-00048
Acquisition System: Hand Held
Configuration: Cruise / VSS Engaged
Test Dates: 20-22 October 2003

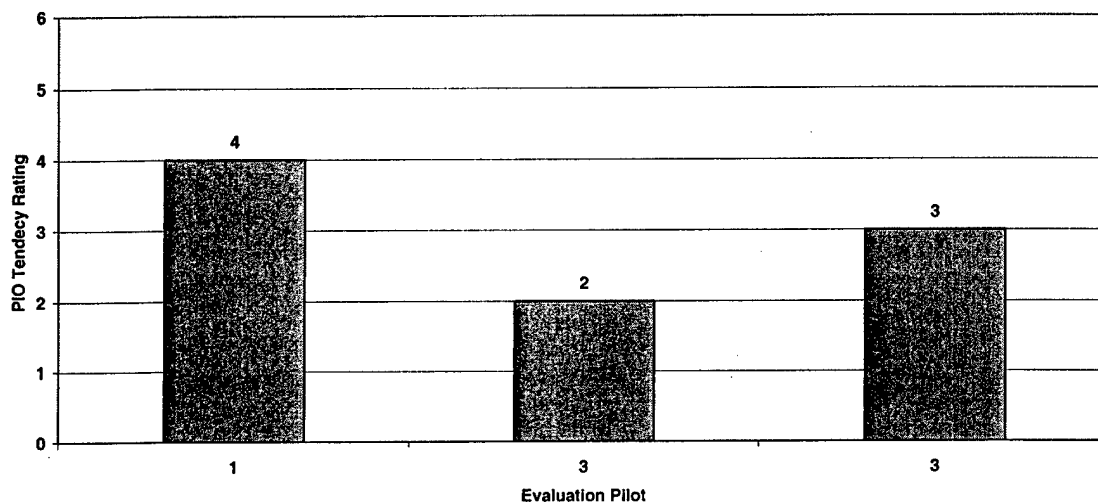


Figure J27 Flight Test Data, Case B, 60 deg/sec

MAX GAP Flight Test Data
Phase 3 TGT - Case N - 15 deg/sec

Data Basis: 15K ft PA, 300 KIAS
Test A/C: NF-16D - # 86-00048
Acquisition System: Hand Held
Configuration: Cruise / VSS Engaged
Test Dates: 20-22 October 2003

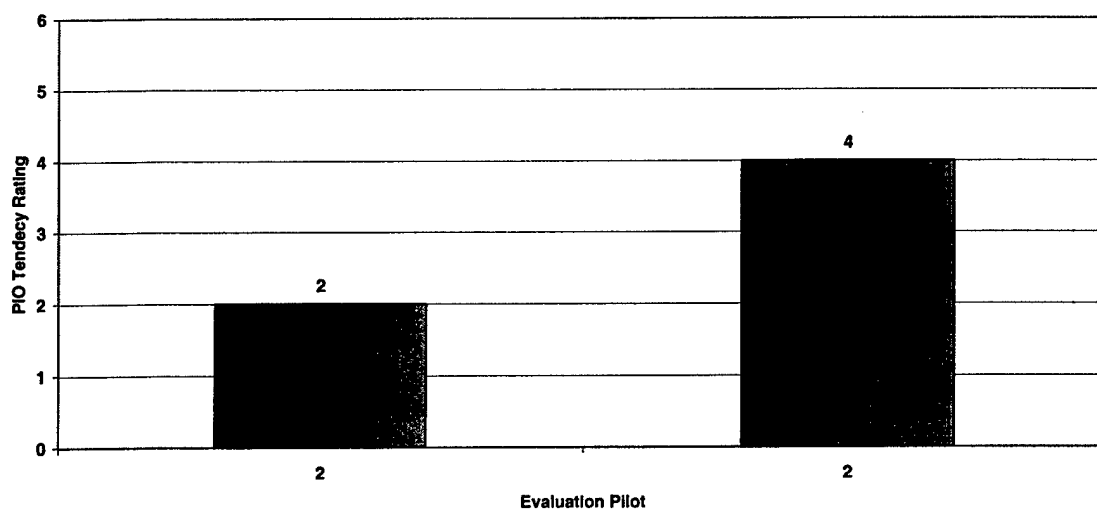


Figure J28 Flight Test Data, Case N, 15 deg/sec

MAX GAP Flight Test Data
Phase 3 TGT - Case N - 30 deg/sec

Data Basis: 15K ft PA, 300 KIAS
Test A/C: NF-16D - # 86-00048
Acquisition System: Hand Held
Configuration: Cruise / VSS Engaged
Test Dates: 20-22 October 2003

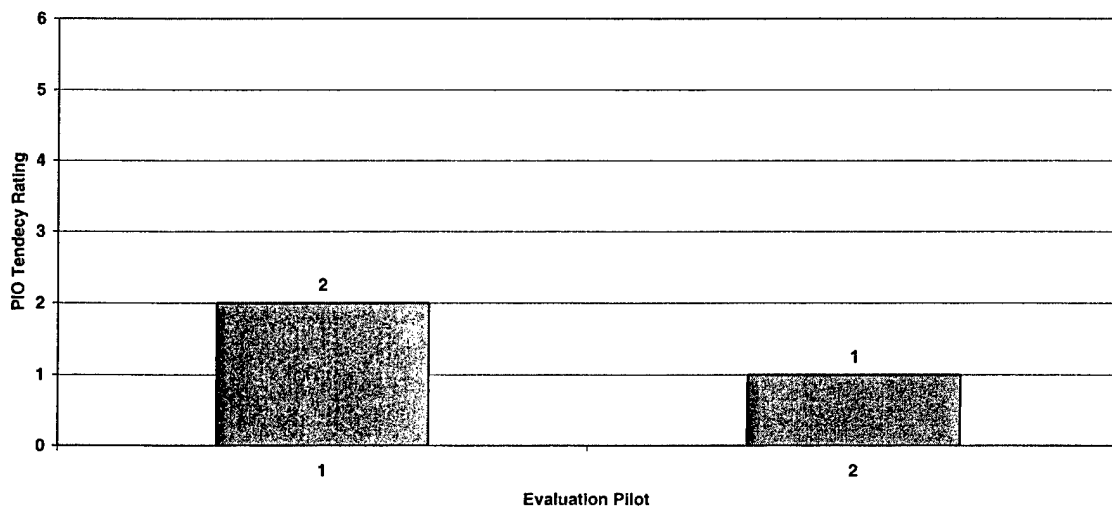


Figure J29 Flight Test Data, Case N, 30 deg/sec

MAX GAP Flight Test Data
Phase 3 TGT - Case N - 60 deg/sec

Data Basis: 15K ft PA, 300 KIAS
Test A/C: NF-16D - # 86-00048
Acquisition System: Hand Held
Configuration: Cruise / VSS Engaged
Test Dates: 20-22 October 2003

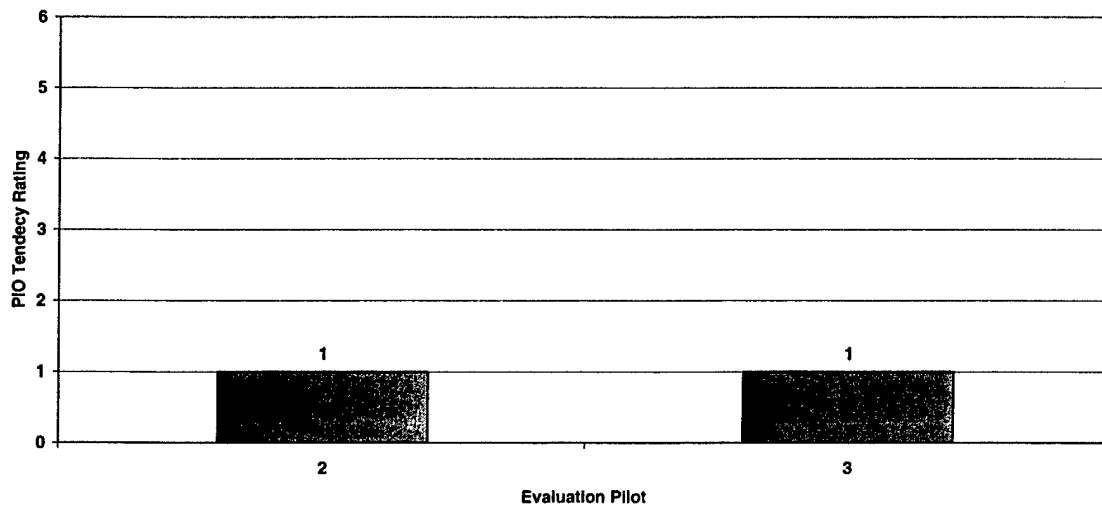


Figure J30 Flight Test Data, Case N, 60 deg/sec

MAX GAP Flight Test Data
Phase 3 TGT - Case W - 15 deg/sec

Data Basis: 15K ft PA, 300 KIAS
Test A/C: NF-16D - # 86-00048
Acquisition System: Hand Held
Configuration: Cruise / VSS Engaged
Test Dates: 20-22 October 2003

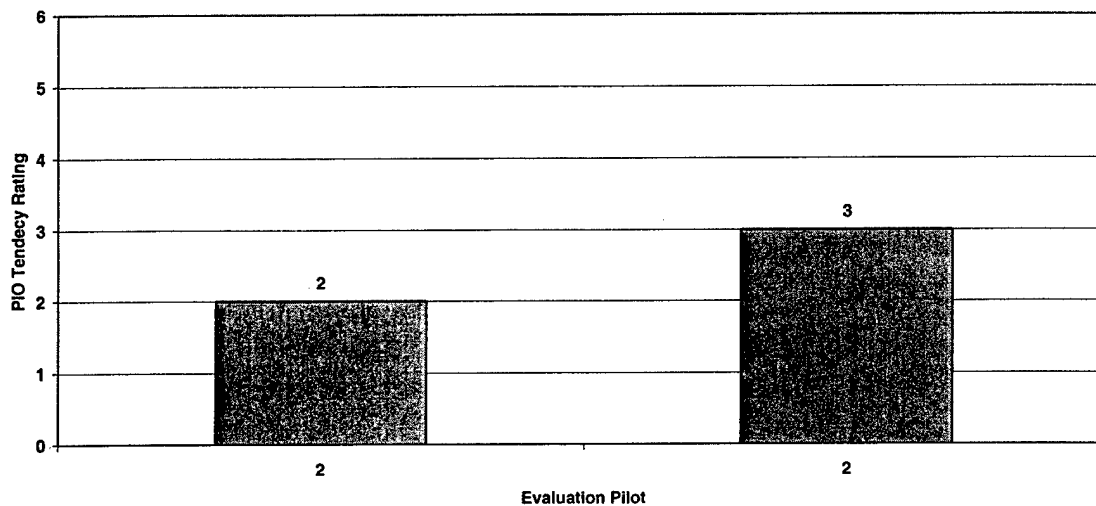


Figure J31 Flight Test Data, Case W, 15 deg/sec

MAX GAP Flight Test Data
Phase 3 TGT - Case W - 30 deg/sec

Data Basis: 15K ft PA, 300 KIAS
Test A/C: NF-16D - # 86-00048
Acquisition System: Hand Held
Configuration: Cruise / VSS Engaged
Test Dates: 20-22 October 2003

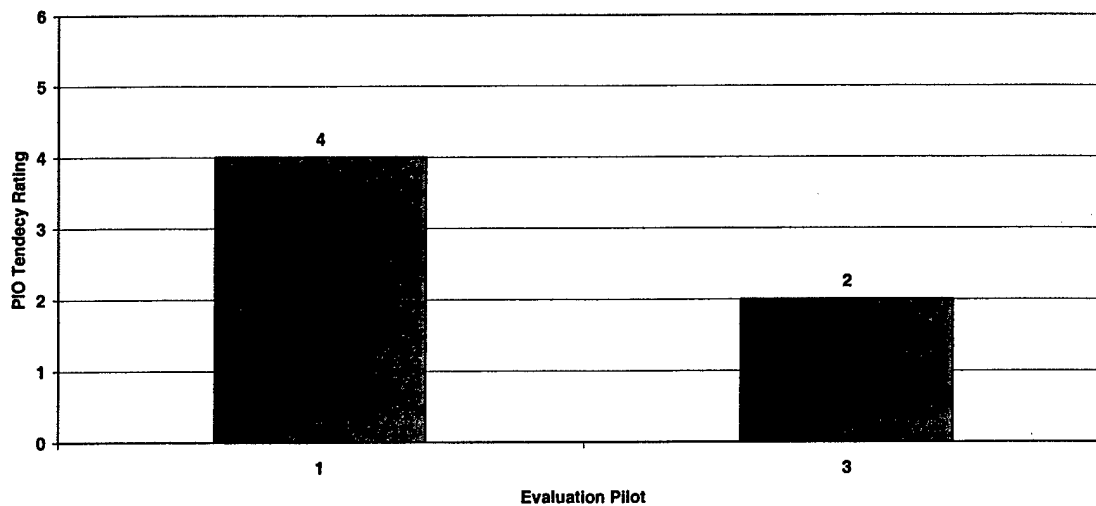


Figure J32 Flight Test Data, Case W, 30 deg/sec

MAX GAP Flight Test Data
Phase 3 TGT - Case W - 60 deg/sec

Data Basis: 15K ft PA, 300 KIAS
Test A/C: NF-16D - # 86-00048
Acquisition System: Hand Held
Configuration: Cruise / VSS Engaged
Test Dates: 20-22 October 2003

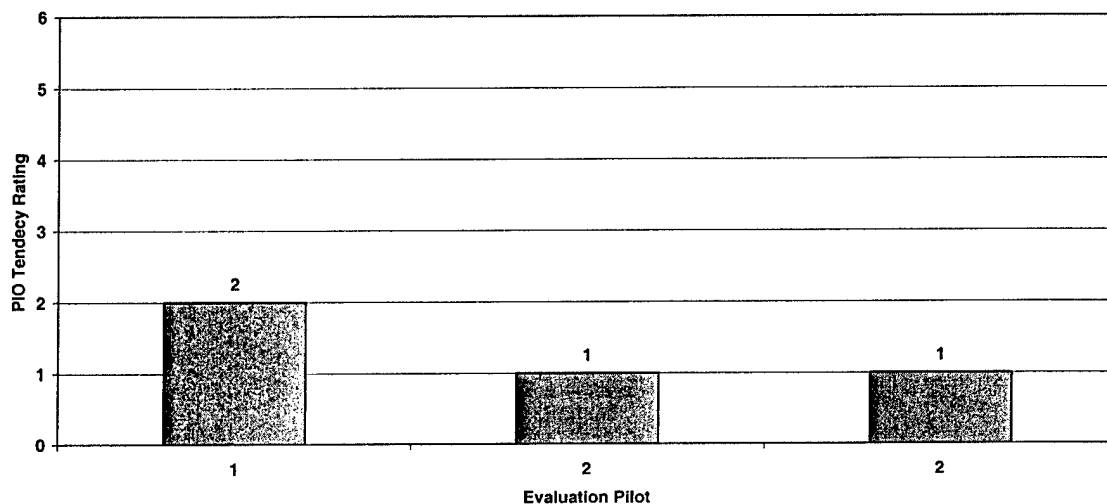


Figure J33 Flight Test Data, Case W, 60 deg/sec

MAX GAP Flight Test Data
Phase 3 TGT - Case Y - 15 deg/sec

Data Basis: 15K ft PA, 300 KIAS
Test A/C: NF-16D - # 86-00048
Acquisition System: Hand Held
Configuration: Cruise / VSS Engaged
Test Dates: 20-22 October 2003

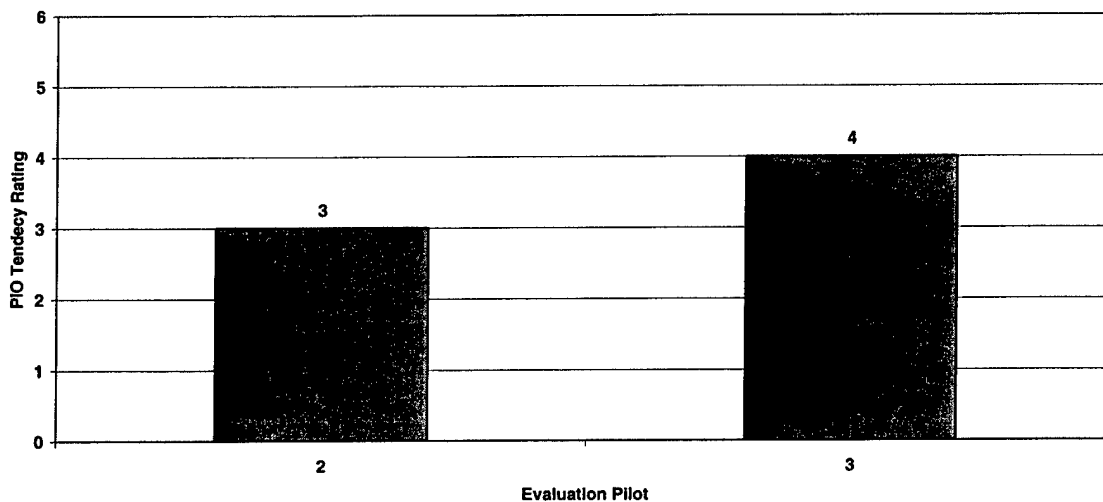


Figure J34 Flight Test Data, Case Y, 15 deg/sec

MAX GAP Flight Test Data
Phase 3 TGT - Case Y - 30 deg/sec

Data Basis: 15K ft PA, 300 KIAS
Test A/C: NF-16D - # 86-00048
Acquisition System: Hand Held
Configuration: Cruise / VSS Engaged
Test Dates: 20-22 October 2003

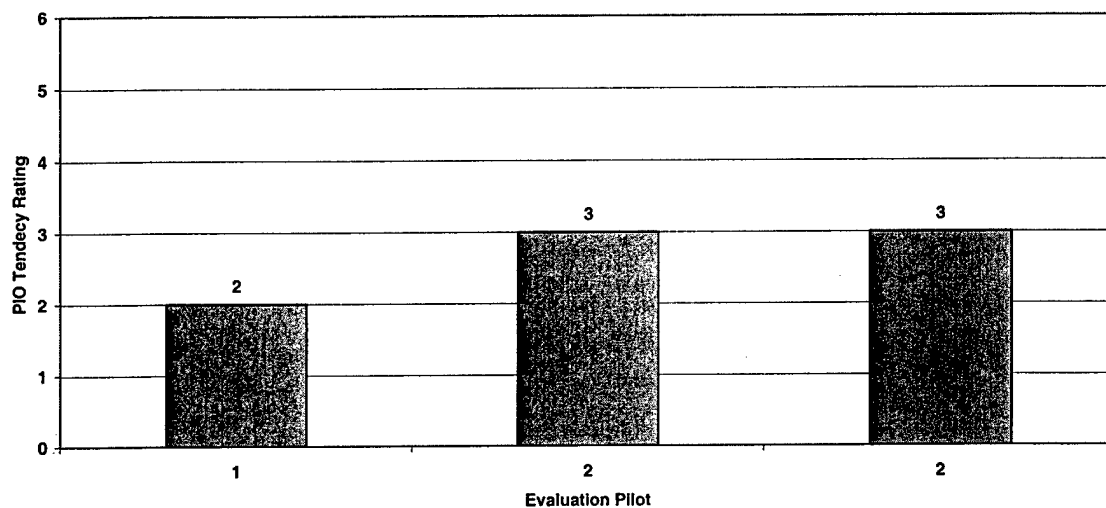


Figure J35 Flight Test Data, Case Y, 30 deg/sec

MAX GAP Flight Test Data
Phase 3 TGT - Case Y - 60 deg/sec

Data Basis: 15K ft PA, 300 KIAS
Test A/C: NF-16D - # 86-00048
Acquisition System: Hand Held
Configuration: Cruise / VSS Engaged
Test Dates: 20-22 October 2003

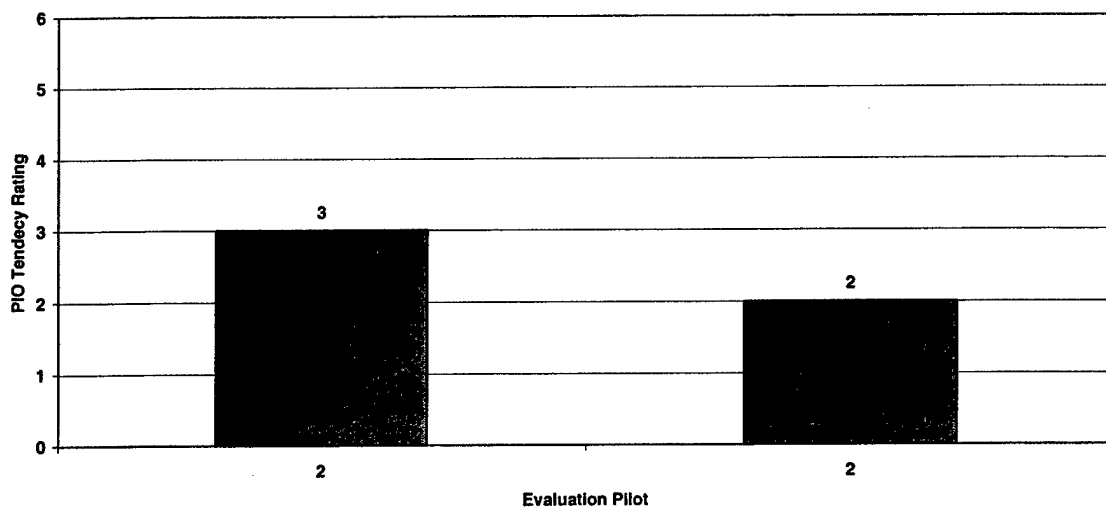


Figure J36 Flight Test Data, Case Y, 60 deg/sec

THIS PAGE INTENTIONALLY LEFT BLANK

APPENDIX K: LESSONS LEARNED

The MAX GAP lessons learned are contained in this appendix.

1. The selection of tracking tasks used to determine PIO tendency ratings proved to be critical to the quality of the assigned rating. The task must be repeatable and must be designed to isolate any undesired effects. The Phase 3 target tracking task should be redesigned to ensure repeatability and to induce high-gain pilot inputs during capture and tracking.
2. Variability of PIO tendency ratings occurred expectedly between test pilots. Variability of PIO tendency ratings assigned by the same test pilot for the same test case from the same tracking task should not occur. Every effort should be made to eliminate this effect to increase the validity of the assigned ratings. Calibration of test pilots should be conducted prior to each test phase to enhance ability to identify and rate PIO
3. Even after precisely defining and controlling the task and calibrating test pilots, data scatter occurred. A stringent method of determining data validity must be determined in an effort to "weed-out" bad data points from true data scatter. Stringent criteria for screening questionable data points should be defined during the test planning phase.

THIS PAGE INTENTIONALLY LEFT BLANK

LIST OF ACRONYMS

α	Angle of Attack
deg	Degrees
K_α	Angle of Attack Feedback Gain
K_q	Pitch Rate Feedback Gain
θ_{task}	Pitch angle commanded by the tracking task
θ_{act}	Actual aircraft pitch angle
q	Pitch Rate
rad	Radian
sec	Second
$\omega_{n_{sp}}$	Short Period Natural Frequency
ζ_{sp}	Short Period Damping
AFB	Air Force Base
AFFTC	Air Force Flight Test Center
AFIT/ENY	Air Force Institute of Technology, Aeronautics Department
EP	Evaluation Pilot
FCS	Flight Control System
HQ	Handling Qualities
HQDT	Handling Qualities During Tracking
HUD	Head's-Up Display
ID	Identification
JON	Job Order Number
KIAS	Knots Indicated Airspeed
LAMARS	Large Amplitude Multimode Aerospace Research Simulator
OLOP	Open Loop Onset Point
PA	Pressure Altitude
PIO	Pilot-Induced Oscillation
PIOR	Pilot-Induced Oscillation Tendency Rating
RTO	Responsible Test Organization
SP	Safety Pilot
TIM	Technical Information Memorandum
TM	Telemetry
TMP	Test Management Project

TPS	Test Pilot School
USAF	United States Air Force
VISTA	Variable Stability In-Flight Simulator Test Aircraft
VSS	VISTA Simulation System

DISTRIBUTION

Distribution	No.	Distribution	No.
412 TW/ENTL Attn: Mrs. Lamb 307 E. Popson Ave, Bldg 1400, Rm 110 Edwards AFB CA 93524-6630	3	AFRL/VACD Attn: Mr. Curt Clark 2180 Eighth Street Rm.202, Bldg. 145, Area B WPAFB, Ohio 45433-7505	1
TPS/EDT Attn: Mr. Gary Aldrich 220 South Wolfe Ave, Bldg 1220 Edwards AFB CA 93524-6485	2	Det 1, 46 OG Attn: Maj Joel Witte 320 Tully St, Bldg 90343 Hurlburt Field, FL 32544-5446	1
USAF TPS/EDC Attn: Ms Dottie Meyer 220 S Wolfe Ave, Bldg 1220 Edwards AFB CA 93524-6485	2	Capt Svend Erik Monsen Test Pilot NDLO/AIR Luftforsvarets Forsynings Kommando PB10 2027 Kjeller Norway	1
AFFTC/HO 305 E Popson Ave, Bldg 1405 Edwards AFB CA 93523-6595	1	40 th FTS Attn: Capt Thomas Washington 505 Choctawhatchee Ave, Bldg 64 Eglin AFB, FL 32542	1
Defense Information Systems Agency DTIC 8725 John J. Kingman Rd, Ste 0944 ATTN: Willis Smith (DTIC-OCA) Fort Belvoir, VA 22060-6218	1	Capt Karl K. Cowart 1261 Roth St Edwards AFB, CA 93523	1
AFIT/ENY Attn: Dr. Brad Liebst Bldg 640 2950 P St Wright-Patterson AFB OH 45433-7521	1	Capt Richard Salasovich 1261 Roth St Edwards AFB, CA 93523	1
Advanced Engineering Systems Inc. Attn: Mr. Andrew R. Markofski 150 North Airport Drive Buffalo, New York 14225-1436	1		

TOTAL COPIES: 17